

Doctoral Thesis

Sensitization with allogeneic MHC class I molecule H-2K^d induces anti-tumor immunity in the context of PD-1 blockade

Komang Alit Paramitasari

Nara Institute of Science and Technology
Division of Biological Science

Laboratory of Functional Genomics and Medicine
(Associate Prof. Yasumasa Ishida, M.D. Ph.D.)

2022/03/17

Laboratory (Supervisor)	Functional Genomics and Medicine (Associate Prof. Yasumasa Ishida M.D. Ph.D.)		
Name	Komang Alit Paramitasari	Date	March 17, 2022
Title	Sensitization with allogeneic MHC class I molecule H-2K ^d induces anti-tumor immunity in the context of PD-1 blockade		
<p>Immune checkpoint blockade has provided remarkable outcomes to unleash the immune defense against tumors. It is well-understood that antitumor immunity is induced upon recognition of antigen-bound major histocompatibility complex class I (MHC-I) by the T cell receptor (TCR). However, the immune response against tumors may be hindered by the inhibitory mechanism. Programmed death-1 (PD-1) as one of the inhibitory receptors, promotes its expression by T cell activation and suppresses the activity of cytotoxic T lymphocyte (CTL) upon engagement with its ligand (PD-L1) expressed on tumor cells. This negative modulation of immune response can be blocked by administration of the anti-PD-1 antibody which has been demonstrated durable responses. However, the majority of patients were unable to receive the benefits from the PD-1 therapy and some patients acquired resistance after a period of the initial response, leading to disease recurrence. Thus, it is indispensable to improve the success rate of PD-1 blockade in a wide variety of cancer. Furthermore, combination therapy has been widely accepted as one of the most striking strategies to overcome resistance to immunotherapy. More importantly, tumor cells may develop immune evasion mechanisms due to failure in the antigen-presenting machinery. The introduction of exogenous MHC-I in combination with PD-1 therapy may enhance the tumor-antigen recognition and thereby provide complete tumor regression.</p> <p>To investigate the effect of MHC-I overexpression to augment immune sensitivity, I have generated an expression vector harboring cDNA of allogeneic mouse MHC-I cell surface molecule, namely H-2K^d. Upon completion of vector construction, <i>in vitro</i> experiment was performed to verify the expression level of MHC-I on the murine colorectal carcinoma (MC38) model (H-2^b). Flow cytometric analysis of the stably transfected MC38 clones confirmed the high expression levels of allogeneic H-2K^d. Next, the tumorigenicity of unmodified parental cells (MC38 PT) and MC38 H-2K^d was tested <i>in vivo</i> by subcutaneous injection into the flank of PD-1 knockout and wild-type mice in a C57BL/6 genetic background (H-2^b haplotype). MC38 PT cells readily formed tumors and grew progressively in both PD-1 KO and WT mice. The speed of MC38 PT tumor growth was appeared to be slower in PD-1 KO mice. In contrast, MC38 H-2K^d-modified cancers provided full protection to both naïve PD-1 KO and WT mice, indicated by spontaneous tumor regression.</p> <p>Next, I sought to determine the extent to which H-2K^d-overexpressing tumors could protect the mice against unmodified cancers. PD-1 KO mice were sensitized for the challenge of unresponsive MC38 PT cells by administering the highly immunogenic MC38 H-2K^d inoculums. Intriguingly, all PD-1 KO mice gained immunity against the aggressive MC38 tumor and became tumor-free. Most notably, sensitizing PD-1 KO mice with growth-arrested (MMC-treated) and debris of MC38 H-2K^d tumors also provided full protection from the growth of secondary MC38 PT tumors. This finding implied that MC38 H-2K^d cells</p>			

retained their high immunogenicity.

To assess long-term immunity, about 5 months following the sensitization, all PD-1 KO mice that had survived the first tumor injection were subjected to a second tumor challenge on the same inoculation site. Surprisingly, sensitization with cell debris of MC38 H-2K^d evidently showed the strongest protective anti-tumor immunity against the re-challenged MC38 PT cells thus conferring the highest survivability. This finding profoundly revealed that a single dose of MC38 H-2K^d cell debris was potent to immunize the mice for a long period of time.

To determine the requirements for efficient immunity in MC38 H-2K^d-sensitized mice, the sensitization experiment was then employed in WT mice in which the PD-1/PD-L1 axis functions normally. Sensitized WT mice failed to gain immunity against the challenged MC38 PT and experienced rapid tumor growth. In addition, the highly immunogenic sensitization regimen using H-2K^d cell debris was failed to trigger effective immunity in all WT mice. These findings suggested that PD-1 blockade was evidently a prerequisite to elicit protective anti-tumor immunity against aggressive carcinoma.

Furthermore, I have successfully confirmed that specific immunity against tumor antigens is mandatory to elicit antitumor immunity. Here, I established a criss-cross tumor injection between MCA-205 (murine sarcoma) and MC38 cell lines. In this fashion, the mice received administration of secondary tumor inoculation that was different from the preexistent primary tumor (*e.g.* MC38 as primary tumor and MCA-205 as secondary tumor or vice versa). Previously, it was found that the parental MC38 grew robustly but not when the PD-1 KO mice were firstly sensitized by MC38 H-2K^d. In contrast, PD-1 KO mice that had received MCA-205 H-2K^d cells as a primary tumor were not protected against subsequent MC38 tumor challenge in the distant site, indicating that the triggered immune reaction was due to MC38-specific tumor immunity.

Altogether, these findings evidently strengthen the hypothesis that allogeneic H-2K^d successfully converted the aggressive tumors into highly immunogenic tumors. Furthermore, sensitization of PD-1 KO mice with MC38 H-2K^d cell debris showed the most effective long-lasting immunity. These findings raised a possibility for the potential application of H-2K^d cell debris in a prophylactic setting, especially in combination with PD-1 blockade. The outcomes from this study may raise a possibility to overcome resistance to cancer immunotherapy.

TABLE OF CONTENTS

INTRODUCTION.....	6
Cancer immunotherapy mediated by PD-1	6
Obstacles in PD-1 therapy	7
Cancer immune evasion	8
MHC-I as the whistleblower of anti-tumor immune response	9
Cancer therapy in combination with PD-1 checkpoint blockade	11
MATERIALS AND METHODS.....	14
PLASMID CONSTRUCTION.....	14
Generation of the pCAGGS vector with a new multiple cloning site	14
Generation of the MHC-I expression vectors	15
Construction of the P2A-linked bi-cistronic vector	15
IN VITRO STUDY	17
Tumor cell lines.....	17
Stable transfection	17
Flow cytometry (FACS) analysis of stable clones	17
Limiting dilution cloning	18
IN VIVO STUDY	18
Animals	18
Allogeneic tumor studies.....	19
Bilateral tumor model.....	19
Sensitization of live cells.....	20
Sensitization of growth-arrested cells	20
Sensitization of cells debris.....	21
Criss-cross tumor model.....	21
Assessment of tumor-infiltrating lymphocytes (TILs).....	21
Flow cytometry of lymphocytes.....	22
Matrigel-embedded cancer cells study	22
Hematoxylin and eosin (HE) staining	23

Immunohistochemistry	23
Statistical analysis	24
RESULTS.....	25
ESTABLISHMENT OF EXPRESSION VECTORS FOR MOUSE ALLOGENEIC MHC CLASS I MOLECULES	25
Construction of the MHC-I expression vectors.....	25
Generation of the P2A-linked bi-cistronic cassette.....	27
IN VITRO STUDY	29
Transfer of the allogeneic H-2K ^d gene to MC38 and MCA-205 cancer cells	29
Interferon-gamma (IFN γ) stimulation profoundly elevates the cell-surface expression of PD-L1 and MHC-I.....	33
IN VIVO STUDY	35
MCA-205 tumor is sensitive to PD-1 absence but MC38 showed resistance.....	35
Polyclonal H-2K ^d -expressing MC38 and MCA-205 lines reveal distinct immunogenicity ..	36
Ectopic H-2K ^d overexpression in MC38 provides complete tumor regression	38
MCA-205 H-2K ^d tumors spontaneously regress even in the presence of PD-1	40
Allogeneic H-2K ^k negatively influences immune responses to MC38 H-2K ^d tumors	41
Delayed growth of the mixed MC38 H-2K ^d : PT tumors in vivo.....	43
Sensitizing PD-1 KO mice with immunogenic H-2K ^d tumors results in protection against parental MC38 challenge	44
MC38 PT cell debris fails to induce protective immunity	46
Sensitization with MC38 H-2K ^d cells debris provides long-term immunological memory against MC38 carcinoma.....	48
PD-1 blockade is evidently required for successful rejection of challenged MC38 PT	50
Increased PD-1 expression in CD8 ⁺ T cells alleviates anti-tumor immune responses	52
The specific immunity against tumor antigens is required to elicit antitumor responses	53
Infiltration of CD11c ⁺ and CD8 ⁺ cells is observed in the injection sites of MC38 H-2K ^d	55
DISCUSSION	59
ACKNOWLEDGEMENTS.....	64
REFERENCES	65

INTRODUCTION

The immune system has been associated with the pathogenesis of cancer due to its impressive ability to recognize and respond to the cancer antigens. It has been well understood that cancer cells are derived from rogue normal cells that divide robustly because of the rapid accumulation of mutations and genetic instability. As a rule of thumb, normal somatic cells in our body are licensed as the ‘self’ components which would not provoke immune reactions. However, cancer cells as the abnormal cells express “non-self” neoantigens, alarming the immune system to initiate an attack on cancer.

Immune response to cancer is induced upon recognition of antigen-bound major histocompatibility complex class I (MHC-I) by the T-cell receptor (TCR), along with a co-stimulatory signal of the B7/CD28 pathway which is essential to fully activate naïve T cells. Following the killing activity of T cells towards cancer cells, the inhibitory receptors, such as programmed death-1 (PD-1) and cytotoxic T-lymphocytes-associated protein (CTLA-4) are expressed on the surface of activated T cells. The normal functions of PD-1/CTLA-4 checkpoint inhibitors are to recognize host self-antigens thus preventing autoimmune response. However, these immune checkpoint pathways can be coopted by cancer cells in order to escape the antitumor immune response. More recently, the field of cancer immunotherapy has been harnessing the PD-1/CTLA-4 pathways to re-stimulate the host immune response to cancer antigens with remarkable outcomes. My research focuses on the striking feature of the PD-1 inhibitory receptor to enhance antitumor immunity.

Cancer immunotherapy mediated by PD-1

PD-1 is a transmembrane protein, and its expression is strongly elevated upon antigenic stimulation of T cells. The PD-1 gene was discovered in 1992 by exploiting the subtractive-hybridization technique (1). Several years later, the basic function of PD-1 was elucidated by a group led by Tasuku Honjo who was awarded the Nobel Prize in Physiology or Medicine in 2018, together with James P. Allison who discovered the CTLA-4 roles in the field of immunology. Observation of PD-1 deficient mice revealed that PD-1 negatively regulates immune responses (2). PD-1 has two ligands, namely PD-L1 (B7-H1) and PD-L2 (B7-DC). The PD-L1 ligand is expressed on a wide variety of hematopoietic and non-hematopoietic cell types, whereas the expression PD-L2 is restricted on dendritic cells (DCs) and macrophages. The PD-1

cytoplasmic region has two tyrosine residues in the immunoreceptor tyrosine-based inhibitory motif (ITIM) and the immunoreceptor tyrosine-based switch motif (ITSM), which is essential for the PD-1 activity. Upon engagement of PD-1 with its ligand, the tyrosine residue in ITSM is phosphorylated and further recruits the SHP-2 tyrosine phosphatase. Consequently, the SHP-2 activity on PD-1 suppresses T cell receptor signaling and T cell-mediated immune responses (3-8).

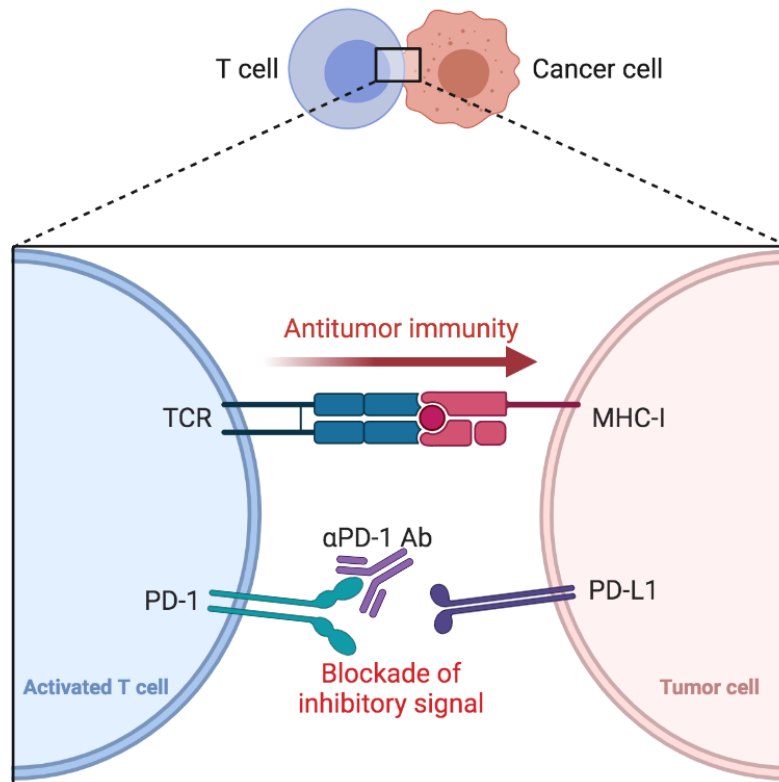


Figure 1. The basic antitumor immunity mechanism shows the engagement of TCR with tumor-derived peptide bound to MHC-I. Along with costimulatory signal (not depicted), this interaction leads to T-cell activation but further induces PD-1 expression on the surface of activated T cells. Administration of anti-PD-1 antibody functions to block PD-1 binding to its ligand, PD-L1, hence antitumor immunity can be restored (created with BioRender.com).

Obstacles in PD-1 therapy

In recent years, the PD-1–PD-L1 pathway has shed some light on the improvement of antitumor immunity (9). PD-1 is expressed on activated T cells and further dampens down the cytotoxic T lymphocyte (CTL) activity upon ligation with PD-L1 expressed on tumor cells. By inhibiting the PD-1/PD-L1 pathway through the administration of the anti-PD-1 monoclonal

antibody, the T cell could be reactivated and gain cytotoxic activity against tumor cells (Fig. 1). This finding led to the first clinical study of anti-PD-1 antibodies in 2006 which was associated with antitumor immunity for several solid tumors (10). Furthermore, the therapeutic antitumor immunity targeting the PD-1/PD-L1 checkpoint pathway has been attributed to durable response towards multiple types of cancers including non-small cell lung cancer (NSCLC), renal cell carcinoma (RCC), bladder carcinoma, melanoma, and Hodgkin's lymphoma (10-23).

The prominent results from clinical studies of PD-1 blockade have attracted scientists' interest to exploit the PD-1 molecules in the targeted therapies. Cancer immunotherapy mediated by PD-1/PD-L1 checkpoint inhibition (notably that using Nivolumab or Pembrolizumab) has received much attention in recent years due to its effectiveness to eliminate tumors. Treatment using the such fully human anti-PD-1 antibody has been demonstrated significant outcomes with durable, long-lasting responses (24), even in patients that have discontinued the immunotherapy. However, subsets of patients are refractory to the benefits of PD-1 therapy. Hence, the responses to the PD-1 blockade still vary among different types of cancer cells and patients. One of the major obstacles in cancer immunotherapy is the heterogeneity of tumors. Not all tumors appear to respond to cancer immunotherapy (9, 25, 26). These findings show significant implications that particular cancer may exhibit immune escape mechanisms.

Cancer immune evasion

The biggest conundrum of cancer is its ability to evade immune destruction. Initially, the immune system was thought to protect the host against cancer, a process that has been called cancer immunosurveillance. However, after decades of research on cancer regulation, researchers have learned the more complex duality of immune system in not only preventing tumor growth but also in sculpting selective pressures that shape survival of less immunogenic tumors, a process well-known as cancer immunoediting. The three Es of cancer immunoediting process are Elimination, Equilibrium, and Escape. The elimination phase or the so-called cancer immunosurveillance performed by innate and adaptive immunity to detect tumors at a lower burden. Equilibrium corresponds to the phase wherein the immune system selectively maintains the outgrowth of the surviving tumors for a long time. These latent tumors with reduced immunogenicity gain abilities to survive the immune attacks and eventually enter the Escape

phase where they grow uncontrollably and emerge as the major cause of tumor recurrence or metastasis in cancer patients (27, 28).

The most common tumor escape mechanism is demonstrated in tumors with a lack of antigenic expression and loss of MHC-I proteins where they cannot be recognized by T cells and become invisible to the immune system (Fig. 2). In parallel, cancer cells can exploit distinct immune evasion mechanisms by opting the PD-1/PD-L1 inhibitory pathway. It has been described that tumors with poor immunogenicity acquired resistance to PD-1 blockade due to defects in antigen-presenting machinery, failing the recognition of tumor antigens (9, 29-31).

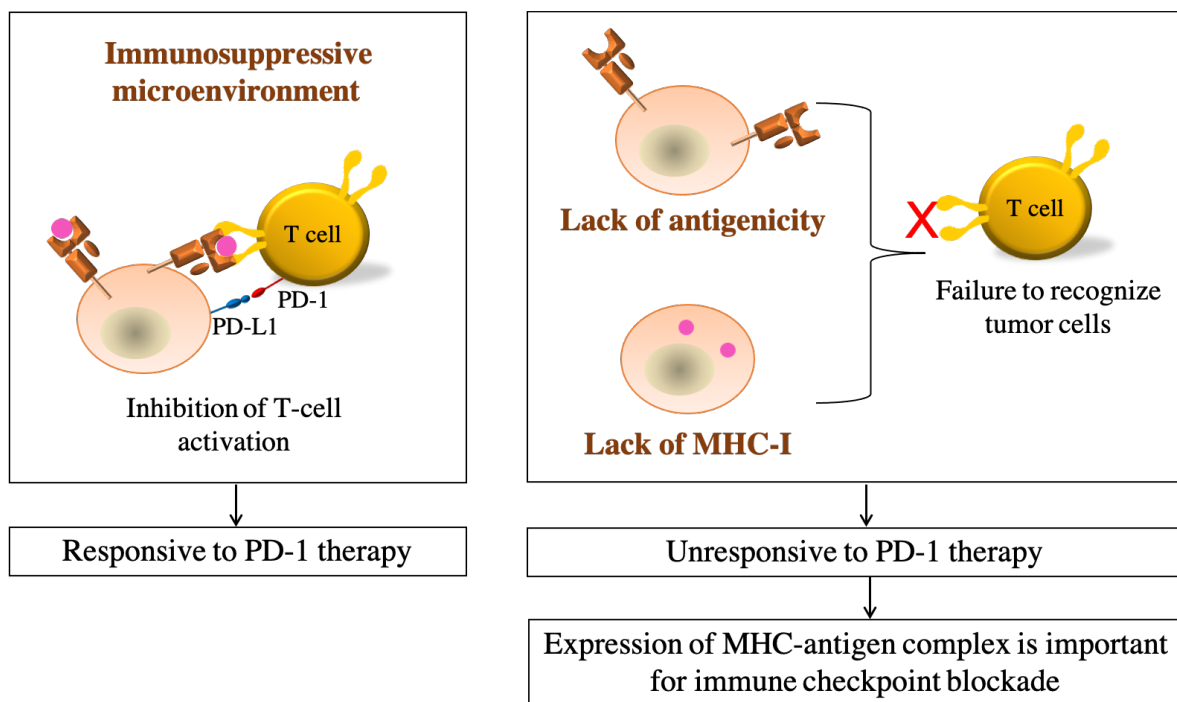


Figure 2. Tumor cells might escape from the attack of CTLs due to the immunosuppressive microenvironment exhibited by PD-1/PD-L1 engagement. In other cases, T cells failed to recognize the malignant cells with a lack of antigenic expression and disrupted MHC-I presentation. Anti-tumor immunity is initiated when T cells recognize tumor cells which further leads to T-cell activation, supporting the notion that PD-1 therapy will be beneficial to restore the activity of these T cells. In contrast, without prior recognition of tumor antigens by T cells, reinvigoration of immune cells mediated by PD-1 blockade might be ineffective.

MHC-I as the whistleblower of anti-tumor immune response

The MHC locus contains the highly polymorphic class I and class II MHC genes. Class I MHC molecules present peptides to CD8⁺ T cells, the subset of T cells which differentiate into

effector tumor-killing CTLs. Furthermore, class II MHC molecules display peptides to CD4⁺ T cells, the subtype of T lymphocytes that have multiple functions in providing help for the mediation of anti-tumor immunity by CD8⁺ CTLs as well as activation of innate immune cells.

In humans, the MHC locus is located on chromosome 6 and consisted of three MHC-I genes called Human Leukocyte Antigens, HLA-A, HLA-B, and HLA-C. The mouse MHC is located on chromosome 17, harboring three MHC-I genes called H-2K, H-2D, and H-2L (Fig. 3A). Every homozygous inbred mouse strain has an MHC haplotype, a set of MHC alleles present on each chromosome (32-36). For instance, the haplotype of MHC-I genes of the BALB/c mouse strain with d allele (H-2^d) is H-2K^d, H-2L^d, H-2D^d. Similar nomenclature is used for other mouse strains, with a precaution of the possibility of null allele caused by a genetic mutation, for example in the C57BL/6 (H-2^b) mouse strain with null H-2L allele resulted in H-2K^b and H-2D^b as its class I MHC haplotype.

Class I MHC molecules are constitutively expressed on almost all nucleated cells. Biological structure of MHC-I molecules is composed of a polymorphic α chain (or heavy chain) non-covalently linked to the β_2 -microglobulin (32). The $\alpha 1$ and $\alpha 2$ domains are the highly polymorphic residues where they function to provide variations in peptide binding and T-cell recognition (Fig. 3B). Accordingly, the expression of MHC-I molecules provides an important display system for tumor antigens (32-37).

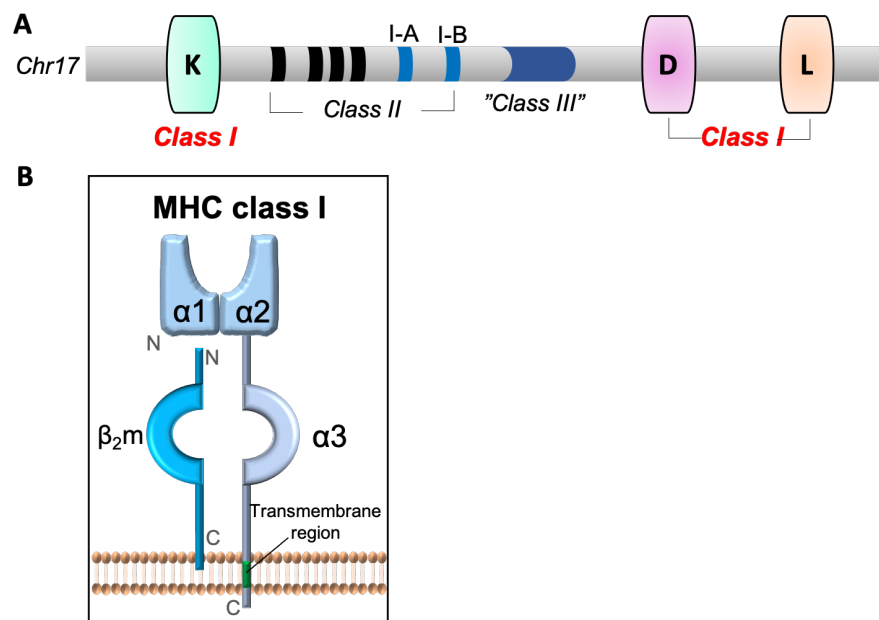


Figure 3. Mouse major histocompatibility complex (H-2). **(A)** Schematic diagram of H-2 loci. **(B)** Structure of a class I MHC molecule as described in the text.

It is generally accepted that the presentation of tumor antigens by MHC-I is required for the successful PD-1/PD-L1 blockade. In support of this point, initial attempts focusing on the induction of MHC-I expression have been shown potential outcomes to enhance the tumor-specific immune response (38-40). In addition, the transfer of an allogeneic mouse MHC-I gene was proven to significantly enhance the immunogenic property of resistant cancer cells. In this report, immunization of mice with melanoma cells stably transfected with a cytokine gene alone, or particularly in combination with an allogeneic mouse MHC-I gene, was reported to stimulate CTL responses and attain a higher survival rate in immunized mice (41).

It is well established that the MHC alloantigens provoke very strong CTL-restricted immune responses, thus resulting in rapid graft rejection after transplantation (42). This suggests that the recipient T cells are capable of recognizing the peptide-allogeneic MHC complexes, an immune mechanism well known as allorecognition or alloreactivity. Recognition of alloantigens by alloreactive T cells falls into two categories: direct and indirect recognition (32). In the direct pathway, the intact MHC molecules are recognized through TCRs of recipient T cells. Despite the conventional allorecognition of peptide-MHC complexes by TCR, some models propose that the TCR may interact either with the peptide portions or the MHC molecules alone (43). This implies that both MHC and peptides play central roles in activating T cells.

On the other hand, indirect recognition presumed the allogeneic MHC molecules are engulfed and processed by the recipient antigen-presenting cells (APC). Hence, the resulting peptides derived from allogeneic MHC are bound and presented by the host (self) MHC for the further cross-priming of T cells. This leads to the conventional immune response towards foreign antigens. Moreover, the engulfment of allogeneic MHC molecules through endocytic vesicles may end up in the MHC class II pathway that would also lead to the allorecognition by CD4⁺ T cells. It has been confirmed that the CD4⁺ T-cell responses are also beneficial for tumor elimination (44-50).

Cancer therapy in combination with PD-1 checkpoint blockade

A myriad of reports have shown that the combination therapies with the PD-1 blockade are more effective than a single treatment (3, 25, 51-53). However, little evidence is available to elucidate the function of allogeneic MHC-I in overcoming resistance to PD-1 therapy. Indeed, the study to address the effect of the PD-1/PD-L1 checkpoint inhibition in combination with the

enhancement of MHC-I expression has become urgent to be accomplished. Interestingly, the combination of radiotherapy with immune checkpoint blockade has demonstrated a synergistic effect to improve the abscopal effect (Fig. 4), a rare phenomenon of tumor regression that is located not only at the primary irradiated sites but also in the non-irradiated, distant sites (54-60). Investigation of the abscopal effect as the results of PD-1 therapy combined with other immune adjuvants has gained attention in the immuno-oncology field.

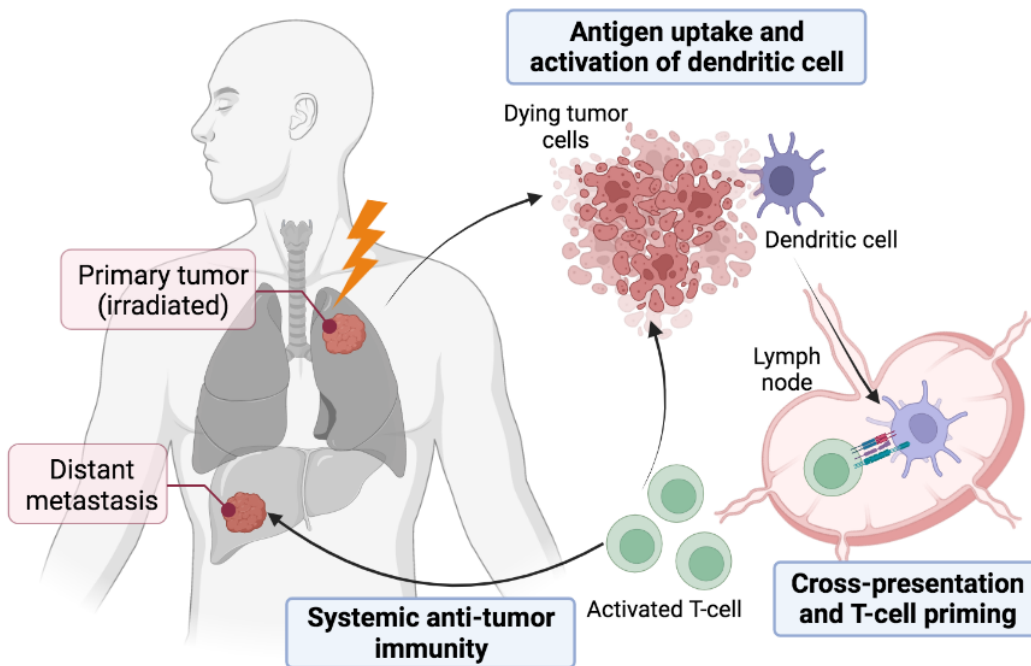


Figure 4. Schematic of the abscopal effect mechanism induced by radiotherapy. The eradication of irradiated primary tumors affected the regression of the non-irradiated distant metastatic tumors. The proposed mechanism responsible for the abscopal effect is thought to be initiated by the engulfment of dying irradiated tumor cells by DCs. The tumor antigens are then processed and cross-presented by DCs to naïve T cells in a tumor-draining lymph node. Eventually, systemic antitumor immunity towards the distant tumor is elicited by activated T cells (created with BioRender.com).

The objective of this study is to address a possible experimental system for the enhancement of tumor immunity in the context of PD-1/PD-L1 blockade. Tumor cells may develop immune evasion mechanisms due to failure in the antigen-presenting machinery. The introduction of exogenous MHC-I in combination with PD-1 immune checkpoint blockade may augment the tumor-antigen recognition and thereby provide antitumor responses. In this present

study, expression vectors harboring one of the mouse MHC-I genes (H-2Ks) consisting of allogeneic H-2K^d and H-2K^k were constructed. Moreover, the established constructs were then stably introduced into murine cancer cells with a C57BL/6 genetic background (H-2^b) in the presence (WT mice) or absence of the PD-1 gene (PD-1 knockout [KO] mice). The modified cancer cells were harnessed in order to investigate the immune reaction towards alloantigens on the basis of PD-1 checkpoint inhibition. My hypothesis is that combination therapy will augment the tumor immune response and induce an abscopal effect, resulting in a robust global anti-tumor response.

MATERIALS AND METHODS

Table 1. List of primers used in this study

Primers used for generation of P2A-linked bi-cistronic vector	
pCAGGS_Seq_F	5'-GGCTTCTGGCGTGTGACCGGC-3'
pCAGGS_Seq_R	5'-CAGAGGGAAAAAGATCTCAGTGG-3'
H-2K ^k _P2A- <i>Aat</i> II_F	5'-CTGAAGCAGGCTGGAGACGTCGAGGAGAACCCTGGACCTATGGCA CCCTGCATGCTGCTC-3'
H-2K ^d _P2A- <i>Aat</i> II_R	5'-GTTCTCCTCGACGTCTCCAGCCTGCTTCAGCAGGCTGAAGTTAGTAGC TCCGCTTCCCGCTAGAGAATGAGGGTCATGAAC-3'
Primers used to verify the H-2K^d_P2A_H-2K^k sequence	
P2A_H-2K ^k check_F	5'-AGGAGAACCCTGGACCTATG-3'
H-2K ^d end_P2A check_F	5'-CTCTCACCTGAGATGGAAG-3'
H-2K ^d end_P2A check_R	5'-CTCCATCTCAGGGT GAGAG-3'

Table 2. List of oligonucleotides used in this study

Oligonucleotides used to generate pCAGGS_Modified MCS	
Modified MCS_pCAGGS_F	5'-TTCAGAGAGGCTAGCTGTGCTCGAGAGAGGCGGCCGCTGTGGATATC-3'
Modified MCS_pCAGGS_R	5'-TTGATATCCACAGCGGCCGCTCTCTCGAGCACAGCTAGCCTCTCTG-3'

Plasmid Construction

Generation of the pCAGGS vector with a new multiple cloning site

The pCAGGS-creT plasmid (kindly provided by Professor Yasumasa Ishida) was digested by *Eco*RI to excise the creT cDNA. The digested pCAGGS plasmid was subjected to partial fill-in of 5' overhangs using DNA Polymerase I Klenow fragment (Toyobo) in 10x Ligation Buffer (1 M Tris pH 7.5, 500 mM MgCl₂, 10 ng/ml BSA) supplemented with 0.7 M KCl, 0.1 M DTT, 2 mM dATP, and Klenow (2 units/μl per microgram DNA) at 14 °C for 3 minutes. The DNA reactant was subjected to phenol-chloroform extraction and ethanol precipitation for purification.

The pCAGGS plasmid was modified to add the new restriction endonucleases sequences or multiple cloning site (MCS) into the empty pCAGGS vector (Fig. 5A). For this purpose, the complementary pairs of oligonucleotides containing *Eco*RI, *Nhe*I, *Xho*I, *Not*I, and *Eco*RV sites were annealed in equimolar concentrations at 95 °C for 5 minutes, and then the temperature was

set to gradually decrease to room temperature. By using the annealed oligonucleotides as insert and Klenow-treated pCAGGS plasmid as vector backbone, the ligation was performed using T4 DNA Ligase (Takara) in 10 μ l reaction volume. Orientation of inserted new MCS was verified by sequencing. This modified vector was designated as pCAGGS-Modified MCS (Fig. 5B).

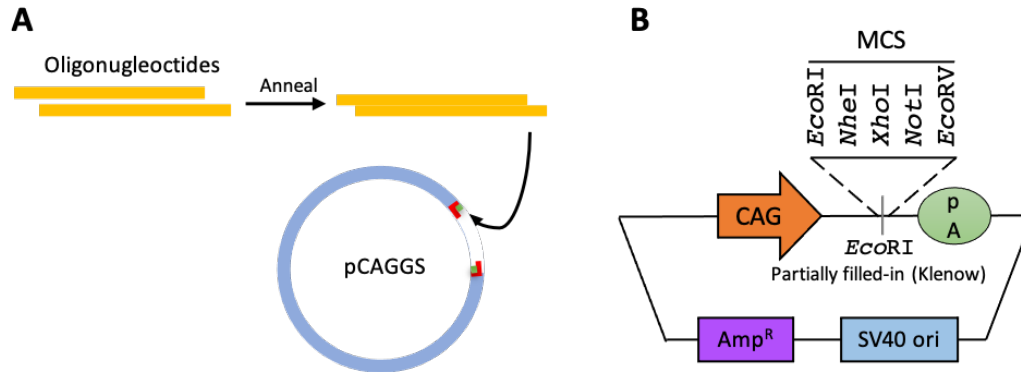


Figure 5. (A) The *EcoRI*-digested pCAGGS was modified by partially filling in the 5' overhang by Klenow fragment and adding a new multiple cloning site (MCS). (B) Schematic structures of pCAGGS-Modified MCS vector. CAG, hybrid promoter consisted of CMV-IE, cytomegalovirus-immediate early enhancer and chicken β -actin; pA, rabbit β -globin polyadenylation signal; Amp^R, ampicillin resistance gen; SV40 ori, replication of origin.

Generation of the MHC-I expression vectors

The allogeneic (H-K^d and H-2K^k) MHC-I cDNAs (kindly provided by Phan Thi Thanh Huyen) were recovered from pcDNA3.1(+) plasmid by *EcoRI* and *EcoRV* digestion (for H-2K^k) and by *EcoRI* and *XhoI* digestion (for H-K^d). The purified cDNAs were cloned into pCAGGS-Modified MCS plasmid and the successful insertion was examined by diagnostic digestion with *HindIII* (H-2K^d) and *NotI* (H-2K^k) restriction enzymes.

Construction of the P2A-linked bi-cistronic vector

The construct was produced by PCR using the primers and cloning scheme outlined in Figure 6. The primers (H-2K^k_P2A-*AatII*_F and H-2K^d_P2A-*AatII*_R, see Table 1) were designed to incorporate the P2A sequences with silent substitution to introduce the unique *AatII* recognition site. The bi-cistronic vector was constructed in two steps. First, separated PCR mixtures (KOD-Plus-Neo, Toyobo) were performed in a reaction volume of 50 μ l. The PCR conditions were as follows: (i) 94 °C, 2 min, (ii) 2x (98 °C, 10 sec; 58 °C, 30 sec), (iii) 33x (98 °C, 10 sec; 66 °C, 30 sec) and (iv) 68 °C, 7 min. Second, the amplified products were then purified,

digested, and cloned into the pCAGGS vector. *NotI* and *SphI* digestion were initially used to confirm the identity of positive clones. The inserted fragments were then verified by sequence analysis.

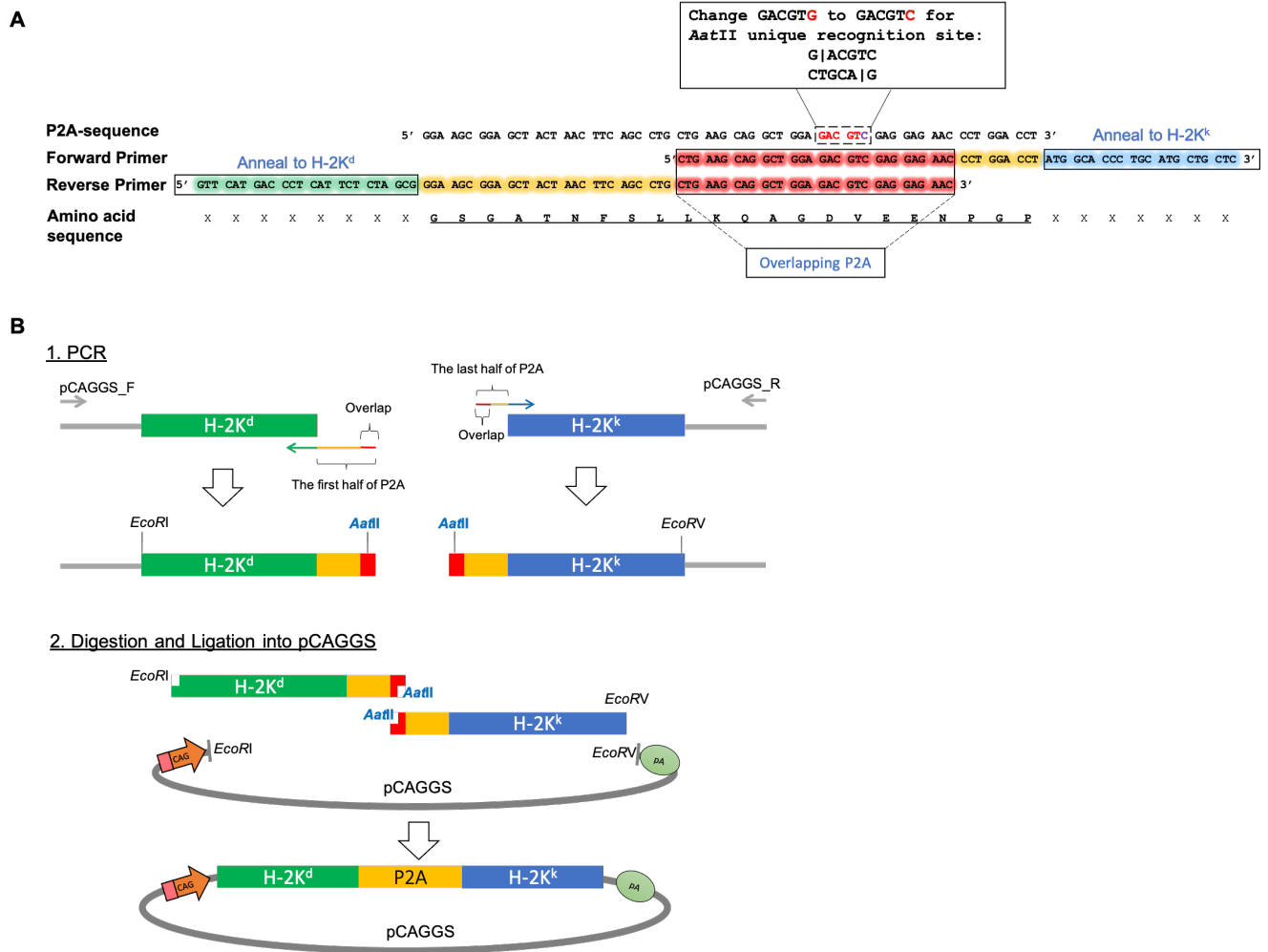


Figure 6. Schematic representation to construct a bi-cistronic expression vector for allogeneic MHC-I cDNAs via a P2A peptide. **(A)** Primer design strategy for the incorporation of P2A sequences. A set of primers containing overlapping sequences (30 nucleotides in length) was used to generate the construct. An *AatII* site was introduced within the overlap sequence by altering G to C nucleotide without amino acid substitution. The 5' region of reverse primer was designed to anneal to the end of H-2K^d sequence without a stop codon. **(B)** Cloning strategy to generate bi-cistronic vector. Each construct was produced by the separated PCR mixtures to incorporate the P2A sequence. The flanking primers (pCAGSS_F and pCAGGS_R) complementary to the vector portions were used to prevent the possibility of recombination between the homologous sequences of H-2K^d and H-2K^k. The fragments were then cloned into the pCAGGS vector by employing 3-piece ligation.

***In vitro* Study**

Tumor cell lines

MC38 and MCA-205 cell lines (generous gifts from Hideaki Tahara, Osaka International Cancer Institute) were cultured in High-Glucose Dulbecco's-modified Eagle's medium (Sigma Aldrich) supplemented with 10% (v/v) of heat-inactivated fetal bovine serum (FBS), 2 mM L-glutamine (Gibco), and antibiotics (100 µg/ml streptomycin and 100 U/ml penicillin, Gibco). Cells were grown inside a 37 °C tissue culture incubator maintained at 5% CO₂. All cells used in this study were tested free for mycoplasma contamination, confirmed with e-Myco Mycoplasma PCR Detection Kit ver.2.0 (LiliF Diagnostic) according to the manufacture's protocols.

Stable transfection

One day prior to transfection, 5×10^4 MC38 or MCA-205 cells were seeded on a 24-well dish in the growth medium without the presence of antibiotics. Transfections were performed in a total volume of 550 µl of growth medium containing 3 µg/µl of Polyethylenimine (PEI-Max) and a mixture of 1 µg of *SaII*-linearized plasmid DNA encoding mouse allogeneic MHC-I genes and 100 ng of *ScaI*-linearized KT3NP4 plasmid harboring neomycin-resistant gene (Neo^R). After 24 h, transfected cells were replated in 10 ml of complete growth medium containing 500 µg/ml of G418 (Sigma Aldrich) as the selection medium. The G418-containing medium was replaced every 2 days to maintain the selective pressure. After 10-12 days, the single-isolated Neo^R colonies were harvested using stainless steel cloning cylinder sealed with sterile silicone grease and transferred into a 24-well dish. Each colony was screened through flow cytometric analysis to detect the expression of transgenes.

Flow cytometry (FACS) analysis of stable clones

Once satisfactory confluency (80-90%) of isolated cells in a 24-well dish was reached, the old-growth medium was discarded. Each well was rinsed twice with 1X PBS and 100 µl of 0.25% Trypsin-EDTA (Gibco) was added into the cells. When the cells have begun to round up and detached from the dish bottom, 400 µl of growth medium was added to quench the trypsin. Each cell in the well was transferred into 1.5 ml tubes and spun down at 1,000 x g for 5 minutes at 4 °C. The supernatant was aspirated without disturbing the cell pellet. The centrifugation and

aspiration steps were repeated twice to ensure the complete removal of growth medium traces. In the final washing step, the cells were suspended in a 100 μ l of FACS staining buffer (1% FBS and 10mM EDTA in 1X PBS). All cells were stained for 30 min on ice with the indicated fluorochrome-conjugated antibodies; anti-H-2K^d PE (clone SF1-1.1.1, eBioscience), anti-H-2K^b APC (clone AF6-88.5.5.3, eBioscience), biotinylated anti-H-2K^k (clone AF3.12.1.3, eBioscience) indirectly conjugated with Streptavidin-APC. Stained cells were detected by BD Accuri C6 flow cytometry and the data was acquired using CFlow software.

Limiting dilution cloning

For the limiting dilution cloning, an average density of 0.5 cells/well of stably transfected MC38 or MCA-205 tumor cells were cultured in a 96-well dish. Cells were grown in a conditioned medium (0.2 μ m sterile-filtered old medium derived from cells 24 h post-culture). The cells were incubated (37 °C, 5% CO₂) for 14-21 days until the colonies were observed. Colonies derived from single cells representing a monoclonal population were harvested and cultured in a 24-well dish. Isolated monoclonal cells were subjected to flow cytometry to screen the allogeneic MHC-I surface expression. Clones that expressed the highest allogeneic MHC-I were expanded in a 10-cm dish and cryopreserved for the sequential *in vivo* experiments.

***In vivo* Study**

Animals

All experiments were conducted in accordance with the animal experimentation guidelines of the Nara Institute of Science and Technology that comply with the National Institute of Health Guide for the Care and Use of Laboratory Animals. All efforts were made to minimize the number of animals used and their suffering. PD-1 KO and WT mice in a C57BL/6N genetic background were bred and maintained in a specific pathogen-free environment and climate/light cycle controlled animal room at a constant temperature of 23-24 °C, 50-70% humidity with *ad libitum* access to pellet diet and water. Female BALB/c^{nu/nu} immunodeficient mice were purchased from CLEA Japan and used between 8-9 weeks of age. Humane endpoints were applied to prevent unalleviated pain according to guidelines. Tumor volume was measured with digital calipers and animals were euthanized before tumor size reached the maximum allowed or

if the tumor displayed a sign of ulceration. Euthanasia was performed according to guidelines for animal cervical dislocation.

Allogeneic tumor studies

In vivo tumor studies were performed as follows: age-matched 8-12 week-old male/female PD-1 KO and/or WT mice were inoculated subcutaneously in the unilateral or bilateral flank with allogeneic MHC-I-expressing tumor cells. Tumor injections were prepared at 5×10^6 cells/ml concentration suspended in Dulbecco's PBS(-) (Nacalai Tesque) inside a 1ml syringe with a 27G needle (Terumo). Mice were anesthetized using continuous isoflurane gas followed by subcutaneous inoculation of cancer cells in the dorsal flank region. Each tumor injection had a volume of 100 μ l containing 5×10^5 cells. Palpable tumors were measured starting day 5-6 post-inoculation and each 2 days thereafter until the endpoint of the experiment. Tumor volume was calculated using the formula: $0.5 \times \text{length} \times \text{width}^2$, where the length represents the largest tumor diameter and width represents the perpendicular tumor diameter.

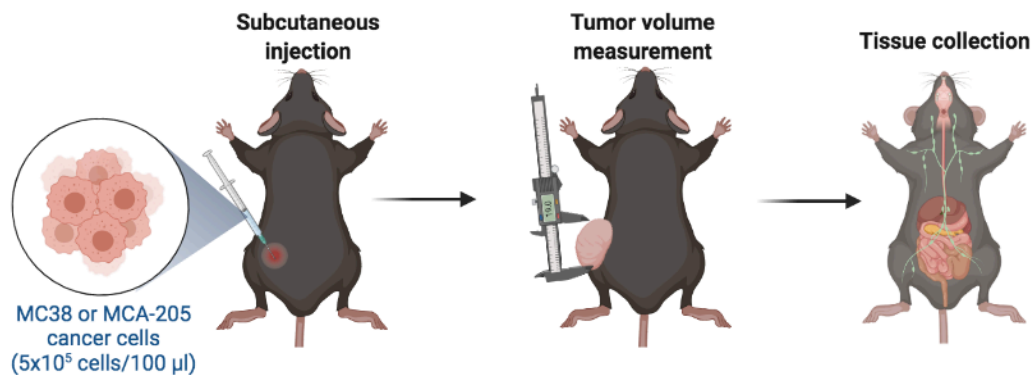


Figure 7. The general experimental design of *in vivo* study. Cancer cells (unmodified or allogeneic MHC-I transfectants) were inoculated into the flank of WT and/or PD-1 KO mice. The rate of tumor growth was monitored by measuring tumor volume every two days. Mice were sacrificed when tumors became ulcerated or reached the endpoint of the experiment. Tumor, spleen, and draining lymph nodes (inguinal and axillary) were collected for downstream analysis.

Bilateral tumor model

Bilateral tumor studies were carried out with the objective to achieve the abscopal effect. The same number of unmodified or parental (PT) and H-2K^d cells were administered subcutaneously in both flanks. Strategies used in this study are illustrated in Figure 8.

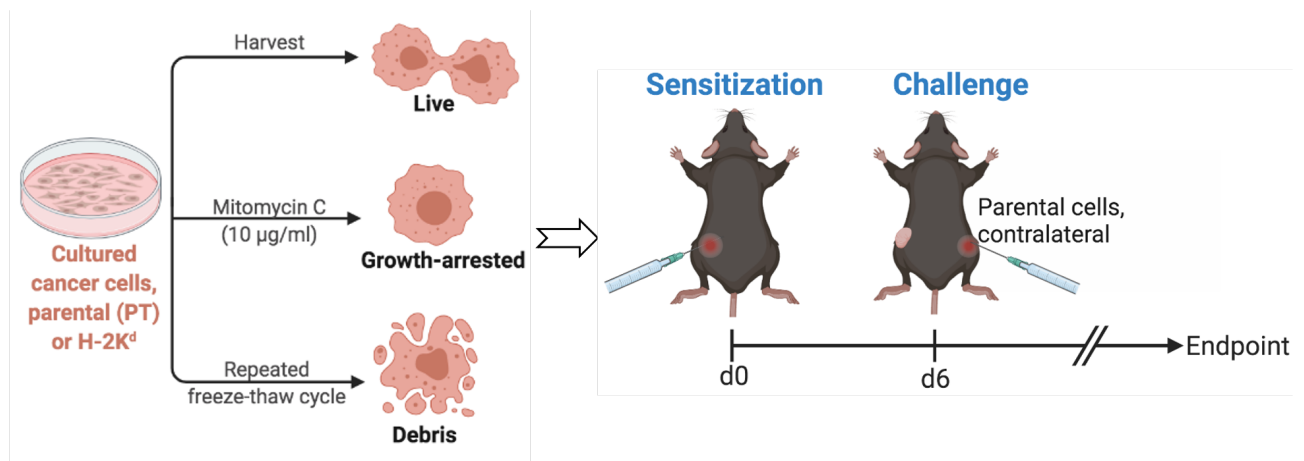


Figure 8. Timeline of sensitization experiments. PD-1 KO mice were inoculated by immunogenic MC38 H-2K^d-expressing cells or parental/unmodified cancer cells (MC38 PT) on day 0. The sensitized mice were then challenged by MC38 PT cells on the contralateral side on day 6. Tumor growth was measured every other day and tumor-bearing mice were analyzed once tumor size reached maximum allowed or showed signs of ulceration.

Sensitization of live cells

A total of 5×10^5 cells expressing MC38 H-2K^d in 100 μ l of D-PBS(-) suspension were inoculated into the left flank of PD-1 KO mice. Mice were challenged with 5×10^5 parental cells in the contralateral flank after six days.

Sensitization of growth-arrested cells

The MC38 H-2K^d stable clones were seeded one day prior to Mitomycin C (Fujifilm Wako) treatment and grown in humidified culture incubator until they reached 70% confluency on the next day. A total concentration of 10 μ g/ml of Mitomycin C (MMC) reconstituted in sterile D-PBS(-) was administered into the culture medium and the cells were incubated for 3 h. The culture medium containing MMC was replaced with pre-warmed complete medium after washing the cells with 1X PBS two times. The growth-arrested cells were harvested on the next day for s.c. injection (5×10^5) into the left flank of mice. On day 6 the mice were given the same dose of injection of parental unmodified cells in the right flank.

Sensitization of cells debris

MC38 H-2K^d-harboring cells were aseptically collected and adjusted to reach the concentration of 5×10^6 cells in 1 ml of D-PBS(-) and then transferred into cryogenic vials. The vials were submerged into liquid nitrogen for 5 minutes and immediately transferred into prewarmed water at a temperature of 37 °C until the entire cells were completely thawed. These freeze-thaw steps were repeated 5 times and then mixed vigorously to prevent cell aggregation. Complete cell death was assessed by trypan blue exclusion. Cell debris was injected into the left flank and marked as day 0. On day 6, the same mice were implanted with 5×10^5 parental cells in the right flank.

Criss-cross tumor model

To examine the specific immunity between MC38 and MCA-205 tumors, the criss-cross experiment was performed in which the mice were subsequently challenged with secondary tumors disparate from the pre-established parental tumors. WT mice were given 5×10^5 of MC38 H-2K^d tumor cells as a primary tumor in the left flank. After six days, the MCA-205 PT cells were implanted in the right flank as the secondary tumor. On the other hand, 6 days after the establishment of subcutaneous MCA-205 H-2K^d tumors, PD-1 KO mice were challenged with MC38 PT in the opposite flank.

Assessment of tumor-infiltrating lymphocytes (TILs)

MC38 or MCA-205 tumors were resected from euthanized tumor-bearing mice. Bulk tumors were prepared by cutting tumors with scalpel blades, followed by enzymatic digestion with 0.13 Wünsch units of Liberase TL (Roche) in 10 ml of RPMI-1640 (Fujifilm Wako) for 45 minutes at 37 °C with gentle agitation (30 r/min). The digested tumor was passed through a 40 µm cells strainer (Falcon) and washed with 1X PBS (containing 2% FBS and 10mM EDTA to stop the enzymatic reaction) and spun down at 1,000 x g for 10 min at 4 °C.

The tumor was undergone density separation using a discontinuous isotonic Percoll gradient (GE Healthcare Life Sciences) to remove debris and necrotic cells. One part of 1.5 M NaCl was added to 9 parts of Percoll (1.130 g/ml) to create 100% Percoll solution, which was then diluted to 80%, 40%, and 20% solutions with 0.15 M NaCl. The filtered cell suspension was washed and suspended in 4 ml of 80% Percoll, which was subsequently overlaid with 4 ml of

40% Percoll, and then 3 ml of 20% Percoll above it. Tubes were centrifuged at 1,000 x g for 30 min at room temperature. The resulting interfacial layer between the 80% and 40% layers was collected for flow cytometric analysis.

Flow cytometry of lymphocytes

Splenocytes were extracted by removing the spleen aseptically and crushed with cover glasses. The cell suspension was passed through 40 µm nylon mesh and subjected to erythrocytes lysis by using HybriMax Red Blood Cell Lysis (Sigma Aldrich) at room temperature for 3 minutes. The cells were washed twice with 1X PBS and spun down at 1,000 x g for 3 min at 4°C. Inguinal and axillary lymph nodes on both sides of the mouse body were collected and crushed in the suspension of FACS Staining Buffer (1% heat-activated FBS and 10mM EDTA in 1X PBS) and filtered through 40 µm nylon mesh. The cells were washed twice with FACS Staining buffer and centrifuged at 1,000 x g for 3 min at 4°C.

Isolated lymphocytes derived from spleen, lymph nodes, and tumors were incubated with purified rat anti-mouse CD16/CD32 (FCγIII/II Receptor, clone 2.4G2, BD Pharmingen) for 10 min and directly stained with APC-conjugated anti-mouse CD45 (clone 30-F11, BD Pharmingen) to specifically stained leukocytes. Cells were stained for other surface markers: CD3ε (clone 145-2C11, eBioscience), CD4 (clone GK1.5, eBioscience), CD8α (clone 53-6.7, eBioscience), PD-1 (clone RMPI-30, eBioscience). Dead cells were stained with Propidium Iodide (eBioscience) incubation for 30 min without further washing step. Cells were analyzed on the BD Accuri C6 and data were processed using CFlow software.

Matrigel-embedded cancer cells study

PD-1 KO mice were subcutaneously injected with a mixture of MC38 cells and Growth Factor Reduced Matrigel Matrix phenol red-free (Corning). A total of 5×10^5 MC38 parental or H-2K^d-transfected cells (live or debris) was suspended in 700 µl of ice-cold Matrigel and kept on ice until injection. All equipment (syringe, tips, needles) and reagents should be chilled at all times to prevent the polymerization of Matrigel matrix. Before injection, mice were anesthetized with continuous isoflurane gas. The cells-Matrigel mixtures were loaded into a chilled syringe and the needle was injected all the way to the end in order to reduce leaking. The syringe was

held in place for at least 30 second to allow the gelling to begin. A bump will appear at the injection site (the size will reduce due to absorption and partial degradation of Matrigel *in vivo*).

Hematoxylin and eosin (HE) staining

At the endpoint of the Matrigel-related experiment (day 7), the Matrigel plugs were removed by wide excision of the flank subcutaneous tissue. Each plug was embedded in Tissue-Tek OCT compound (Sakura), immediately snap-frozen on liquid nitrogen vapors, and cut into 8- μ m sections using a cryostat. Frozen tissue sections were air-dried overnight and fixed with acetone for 5 minutes at room temperature. All of the following steps for HE staining were performed at room temperature. Cryosections were rehydrated in distilled water for 5 minutes and nuclei were stained with Mayer's Hematoxylin Solution (Fujifilm Wako) for 5 minutes and then rinsed with running tap water. Sections were stained with eosin and dehydrated consecutively in 80%, 90%, and absolute ethanol, then further bathed with xylene three times before mounting with PathoMount (Fujifilm Wako).

Immunohistochemistry

For immunostaining, upon acetone fixation, sections were incubated for 1 hour at RT with D-PBS(-) + 5% Normal Goat Serum (Abcam) to block nonspecific binding sites and then incubated overnight at 4°C with primary antibodies diluted in D-PBS(-). Following primary antibody staining, sections were washed three times with 1XPBS and incubated with fluorochrome-conjugated secondary antibodies diluted in D-PBS(-) for 1 hour at RT. Secondary antibodies were then washed with 1XPBS three times and the nuclei were stained with DAPI (4',6-diamidino-2-phenylindole). Slides were finally mounted with Immunoselect Antifading Mounting Medium (DNV Dianova). Immunostaining was performed using the following primary antibodies: mouse anti-rat CD8 α (clone 53-6.7, eBioscience) and mouse anti-Armenian hamster CD11c (clone N418, BioLegend). CD8 α primary staining signal was further amplified using an anti-rat secondary antibody conjugated to Alexa Fluor (AF) 555. An anti-Armenian hamster AF647 antibody was used in combination with CD11c primary antibody. Samples were imaged using a confocal laser scanning microscope LSM 710 (Carl Zeiss) and images were processed using ImageJ (National Institute of Health).

Statistical analysis

Statistical analysis was performed using Prism 9.0 (GraphPad Software). Differences between 2 groups were evaluated using unpaired Student's *t*-test with Welch's correction unless otherwise stated. Kaplan-Meier survival curves were analyzed with log-rank (Mantel-Cox) test. The level of significance was set at * $p < 0.05$, ** $p < 0.01$, and *** $p < 0.001$.

RESULTS

Establishment of expression vectors for mouse allogeneic MHC class I molecules

Construction of the MHC-I expression vectors

The pCAGGS mammalian expression vector contains a strong promoter CAG derived from the chicken β -actin gene (AG) connected with the cytomegalovirus enhancer sequences (61). Single digestion by *EcoRI* to acquire the empty pCAGGS plasmid might lead to self-ligation and multimerization of inserts after ligation. These problems were prevented by exploiting the DNA polymerizing activity of the Klenow fragment (62) by partial filling-in of the 3' overhangs of DNA fragments without generating blunt ends. Another advantage of this approach is that vector dephosphorylation is not required for the prevention of self-ligation because the partially filled-in overhangs are incompatible to ligate to each other.

Due to the limited availability of cloning sites in the pCAGGS plasmid, I expanded the MCS by the addition of oligonucleotides containing the desired restriction sites into the Klenow-treated plasmid. Furthermore, the inserted oligonucleotides were verified by sequencing after confirmation of correct digestion patterns of successfully ligated clones. The linearized 4,827 bp bands indicated the successful clones after ligation (Fig. 9A). Results of the nucleotide sequencing revealed the presence and correct orientation of the MCS (Fig. 9B), confirming the generation of pCAGGS_Modified MCS.

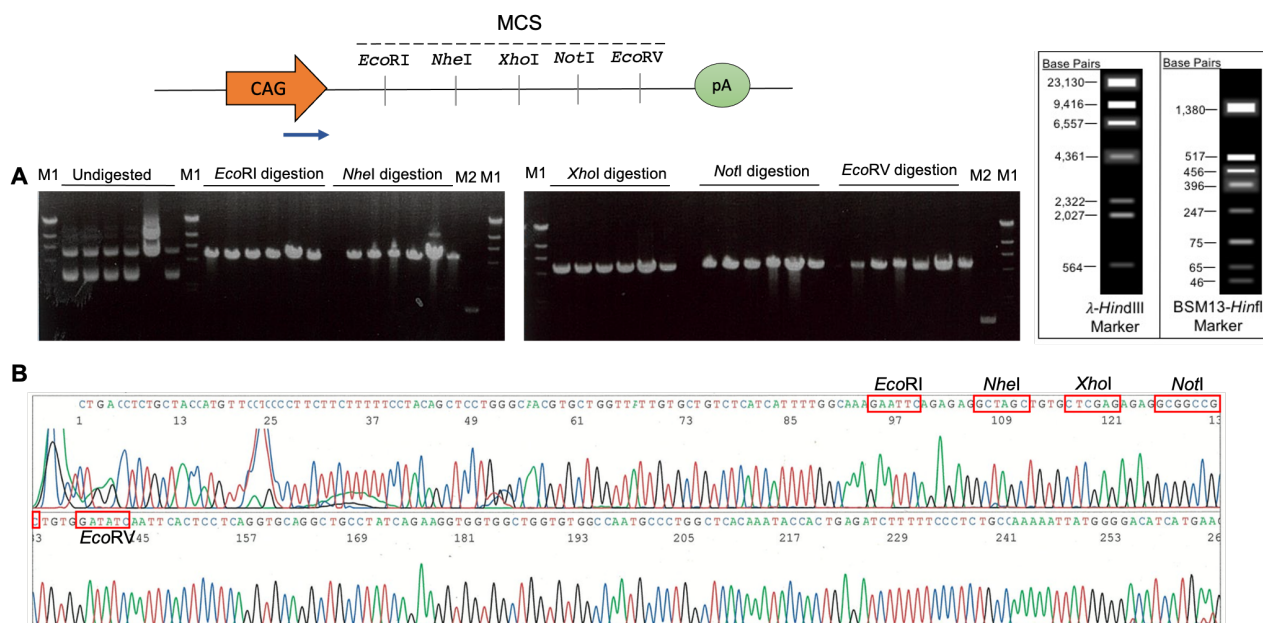


Figure 9. Confirmation of the pCAGGS_Modified MCS plasmid identity. Blue arrow represents sequencing primer to check MCS orientation. **(A)** Restriction enzyme mapping by diagnostic digests to confirm the unique presence of the inserted MCS. M1: λ -*HindIII*, M2: BSM13 *HinfI* marker. **(B)** Verification of MCS orientation by sequence analysis. Several random base pairs (spacer) were added between each recognition site for restriction enzyme cleavage efficiency.

The cDNAs of mouse MHC-I molecules (H-2K^d and H-2K^k) composing of the signaling, extracellular, transmembrane, and cytoplasmic sequences were originally amplified using the primers containing the Kozak consensus sequence and restriction sites for cloning. The established MCS downstream of the CAG promoter permits the insertion of each MHC-I gene in the appropriate orientation. The *EcoRI*, *EcoRV*, and *XhoI* sites are especially beneficial in this respect. Patterns of restriction mapping of the pCAGGS-based constructs were confirmed to be correct as shown in Figure 10A and 10B. Restriction digests by excising the insert from the plasmid backbone (Fig. 10A) resulted in a correct lower band representing the full size of each cDNA insert. Furthermore, the linearized bands (5,881 bp) were generated after *NotI* digestion of the H-2K^k-carrying plasmid, whereas *HindIII* (H-2K^d) digestion gave rise to two bands with the size of 5,134 and 793 bp (Fig. 10B).

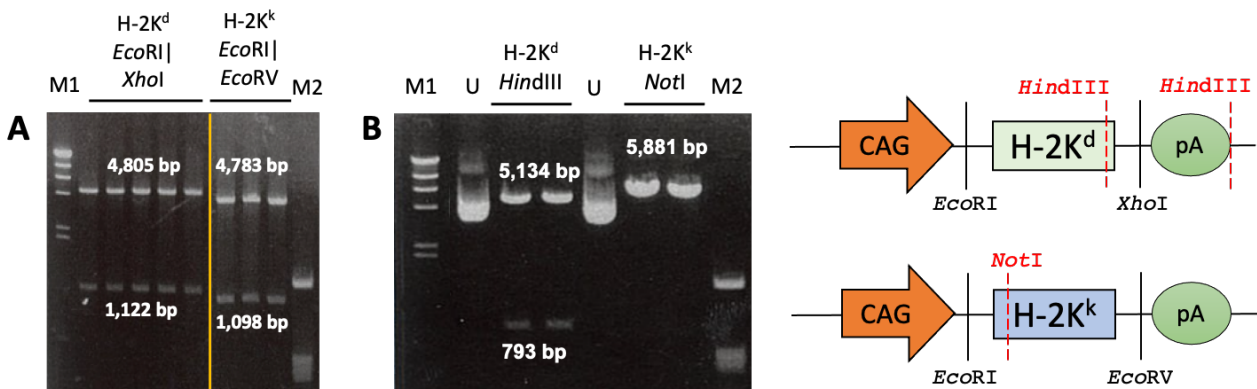


Figure 10. Diagnostic restriction digests to confirm the identity of pCAGGS comprising MHC-I cDNA. The right pictures illustrate the position of restriction sites used to determine the correct digestion pattern. **(A)** Restriction enzyme mapping with cut sites (black letters) that flank the cDNA insert. The pCAGGS_H-2K^k has a 1,098 bp cDNA insert (lower band). The pCAGGS_H-2K^d has a 1,122 bp cDNA insert. **(B)** Results of diagnostic digestion with enzymes indicated with red letters. U: undigested plasmid, M1: λ -*HindIII*, M2: BSM13 *HinfI* marker.

Generation of the P2A-linked bi-cistronic cassette

In order to express MHC-I molecules that are allogeneic to the H-2^b haplotype of the PD-1 KO mice (C57BL/6 genetic background), I constructed a bi-cistronic vector containing the H-2K^d and H-2K^k cDNAs connected via a P2A peptide. Although recombinant PCR was initially used to join both cDNAs, the high homology between H-2K^d and H-2K^k hampered this strategy. A new set of overlap primers with *Aat*II sites were then designed, and the cloning strategy was modified to amplification, digestion, and 3-piece ligation into pCAGGS plasmid. An important note to take into account is that the final cassette must have only one start codon with the Kozak sequence and one stop codon.

As indicated in Figure 11A, the amplified cDNA fragments incorporating half portion of P2A peptides were confirmed by the appearance of 1,296 bp and 1,224 bp bands for H-2K^d and H-2K^k, respectively. Moreover, the following steps of digestion and 3-piece ligation were carried out. The predicted size of the joined-construct is a linear band (7,051 bp) after cutting by *Sph*I, attributable to the presence of only one *Sph*I site at H-2K^k. I further confirmed the correct restriction map of positive clones by diagnostic digestion as shown in Figure 11B. On the basis of these results, a bi-cistronic vector carrying the two allogeneic MHC-I cDNAs was successfully generated.

To exclude the possibility of incorporation of the PCR-generated mutations, the nucleotide sequence of the established pCAGGS_H-2K^d_P2A_H-2K^k vector was verified. One silent mutation from guanine (GAG) to adenine (GAA) at the P2A sequence was found (Fig. 11C) wherein both codons conferred to glutamate. This mutation is unlikely to lead to improper function of the P2A peptide because changes in base pair composition of P2A sequences can be made on the condition that the amino acid sequence remains unmodified (63).

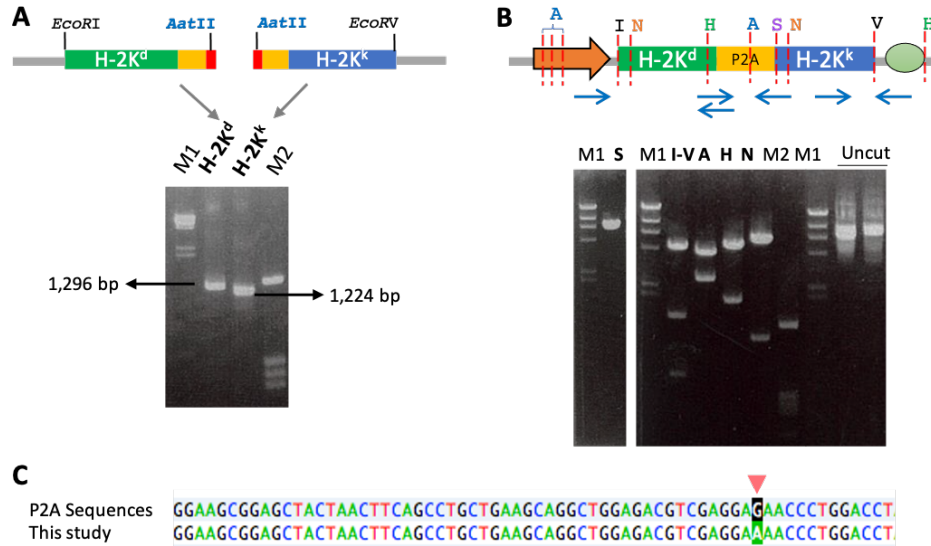


Figure 11. Confirmation of the bi-cistronic vector encoding allogeneic MHC-I, designated as pCAGGS_H-2K^d_P2A_H-2K^k. **(A)** Confirmation of successful amplification to incorporate P2A sequences resulted in a 1,296 bp band for the H-2K^d-first half P2A and a 1,224 bp band for the H-2K^k-last half P2A fragments. **(B)** Restriction pattern of the successful clone was assessed by digestions and resulted in predicted band sizes: 7,051 bp by *SphI* (S); 4,781 bp, 1,557 bp, 713 bp by *EcoRI* (I) | *EcoRV* (V) double digestion; 4,311 bp, 2,604 bp, 83 and 53 bp by *AatII* (A); 5,134 bp and 1,917 bp by *HindIII* (H); 5,881 and 1,170 bp by *NotI* (N) digestion. The blue arrows indicate sequencing primers used for DNA sequencing step. **(C)** Sequence analysis result of the bi-cistronic cassette revealed a synonymous mutation at P2A peptide. M1: λ -*HindIII*, M2: BSM13 *HinfI* marker.

The 2A peptide, also known as the ‘self-cleaving’ peptide, actually functions by making the ribosome skip the synthesis of glycine-proline peptide bond at its own carboxyl terminus, resulting in separation between the end of the 2A sequence and the downstream peptides (64). As the consequence, in my vector system, the 2A peptide residues will remain attached to the upstream cistron (H-2K^d), whereas the downstream cistron (H-2K^k) will start with the proline residue. Szymczak-Workman *et al.* reported that the presence of residual sequences will not lead to the adverse effect (63). This is likely due to the relatively small size (18-22 amino acids) of 2A peptides, leading to a lower risk of impeding the function of the co-expressed genes. Among 2A peptides reported to date, the porcine teschovirus-1 (P2A) peptide was confirmed to show the highest cleavage efficiency (64), therefore I decided to incorporate this peptide in the bi-cistronic construct. Another advantage of 2A peptide is its low immunogenicity which implies the safety for employing multi-cistronic vector harboring 2A sequences even in human gene therapy (65).

In vitro Study

Transfer of the allogeneic H-2K^d gene to MC38 and MCA-205 cancer cells

Upon completion of vector construction, I introduced each established vector into MC38 and MCA-205 cancer cells. To determine the expression of syngeneic and allogeneic class I MHC molecules from the parental and transfected cells, FACS analysis was employed using anti-mouse H-2K^b and H-2K^d monoclonal antibodies. Next, I confirmed that MC38 and MCA-205 cells constitutively expressed high basal levels of endogenous H-2K^b class I MHC (Fig. 12 and Fig. 13). In the *in vitro* study, the stably transfected MC38 and MCA-205 cells were successfully overexpressed high levels of allogeneic H-2K^d. This suggested that the transfectants became double-positive for both H-2K^b and H-2K^d expressions (Fig. 12 and Fig. 13). The expression of H-2K^d was stable after more than 5 months of continuous passage in culture.

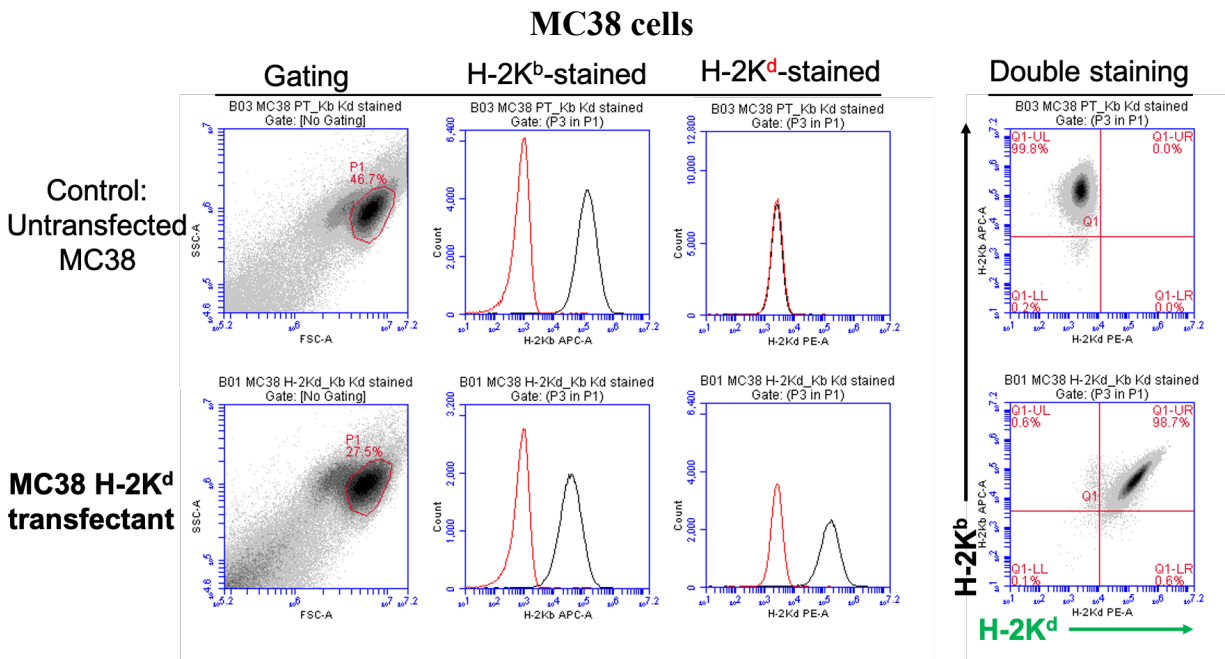


Figure 12. Flow cytometric assessment of unmodified and stable MC38 clones. The transfectant simultaneously expressed H-2K^d and H-2K^b class I MHC molecules represented by the entire shifting of histogram plot into the right side (black line) and position of the cell population into the upper right quadrant in the density plot. Unstained control is shown in the red line. Data are representative of at least five independent experiments.

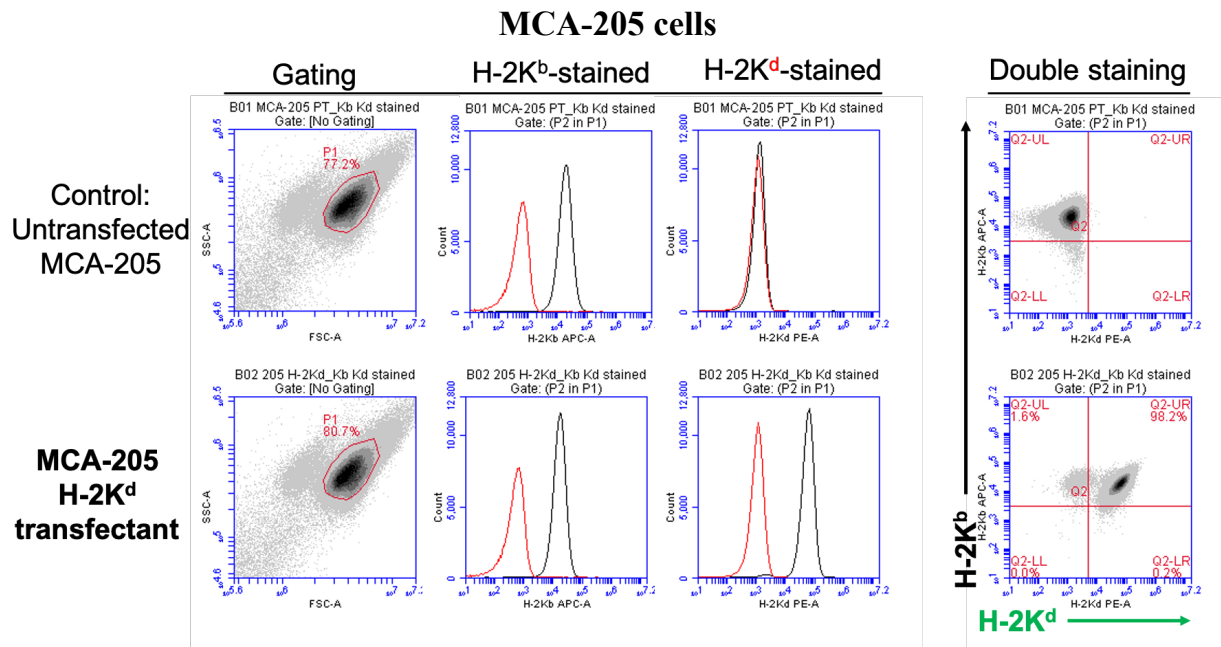


Figure 13. Original and stably-transfected MCA-205 cells were subjected to flow cytometric analysis. The transfectant simultaneously expressed H-2K^d and H-2K^b class I MHC molecules represented by the entire shifting of histogram plot into the right side (black line) and position of the cell population into the upper right quadrant in the density plot. Unstained control is shown in the red line. Data are representative of at least five independent experiments.

Furthermore, the polyclonal mass of cells harvested directly after stable transfection may contain a mixture of untransfected cells or a subpopulation of cells that are transfected with selectable marker gene (Neo^R) alone as indicated by the low to zero of H-2K^d expression amounts (Fig. 14A). Limiting dilution cloning was implemented in order to exclude such undesirable possibilities thus reassuring that a monoclonal cell population derived from the single transfected cells was being employed for the subsequent *in vivo* analysis. Detection of H-2K^d from two monoclonal MC38 populations (Fig. 14B) derived from highly-expressed polyclonal cells (>90%) rendered to the nearly uniform expression of H-2K^d (Fig. 14B-D). In contrast, when the moderate allogeneic H-2K^d expression (line #7, 70%) was subjected to limiting dilution, the resulting MCA-205 monoclonal populations were varied in the level of H-2K^d, in comparison with monoclonal population selectively grown from line #12 with the highest H-2K^d expression (Fig. 15A-D).

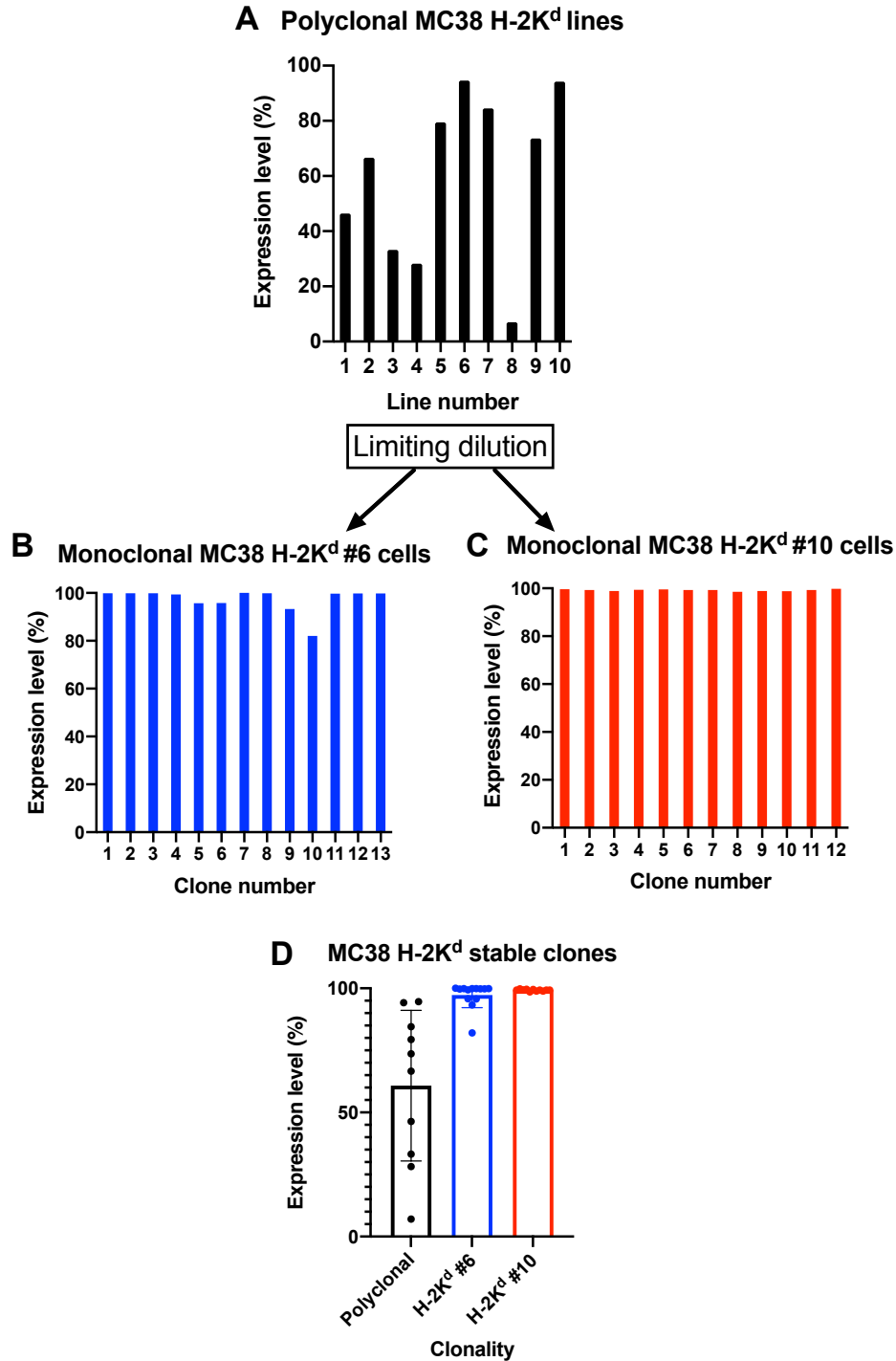


Figure 14. The expression level of H-2K^d from the stably transfected MC38 cells. **(A)** Polyclonal cells derived from isolated colonies upon stable transfection were stained by anti-mouse H-2K^d PE antibody and subjected to flow cytometric analysis. **(B)** Polyclonal MC38 H-2K^d lines #6 and #10 which conferred the best H-2K^d expression were expanded and sub-cloned to obtain a monoclonal cell population. The H-2K^d expressions were then validated from the resulting clones. **(C)** Summary of H-2K^d levels in polyclonal and monoclonal MC38 cells.

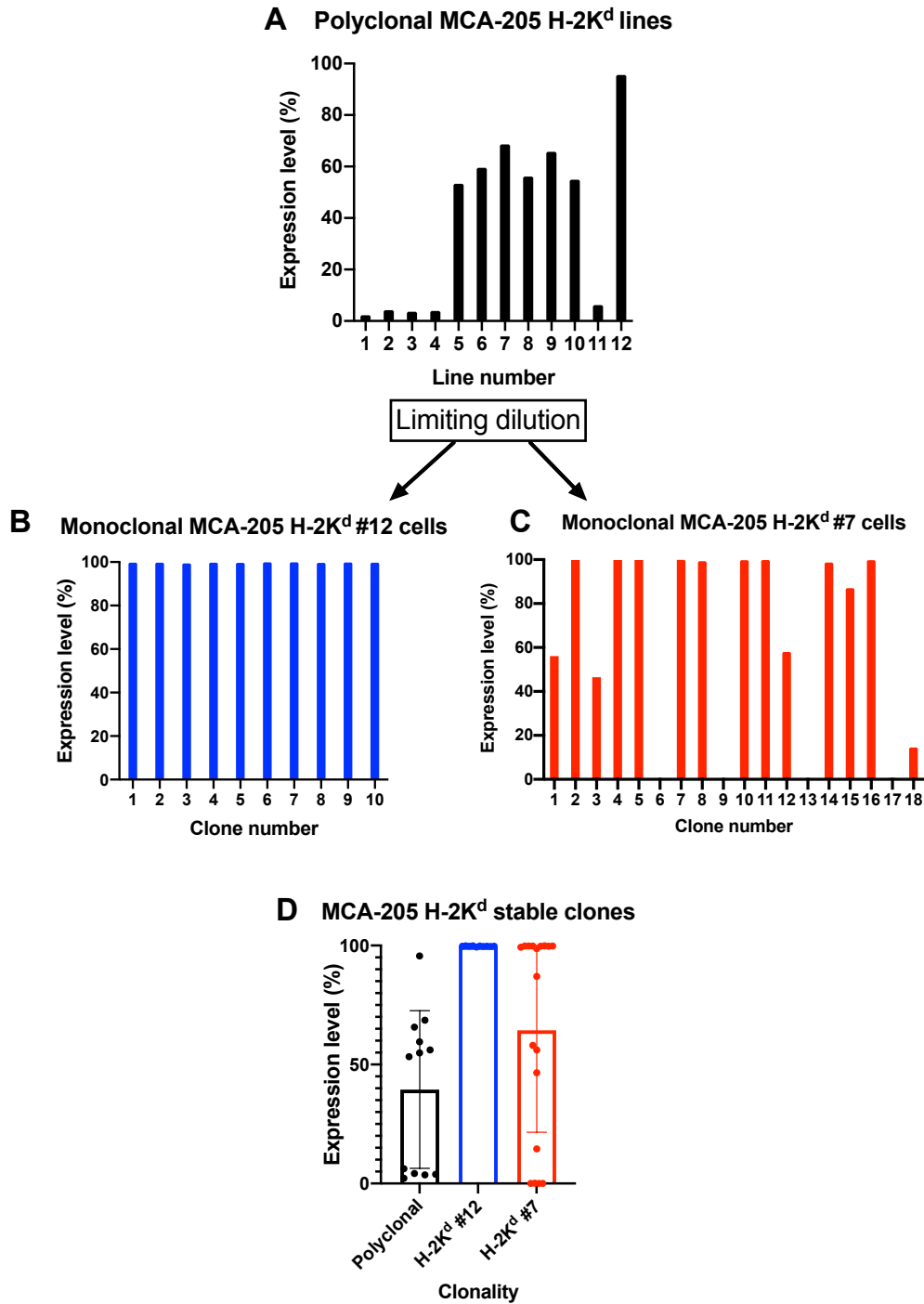


Figure 15. H-2K^d expression from stably transfected MCA-205 cells (shown in percentage). **(A)** Polyclonal cells were stained by anti-mouse H-2K^d PE antibody and subjected to flow cytometric analysis. **(B)** MCA-205 H-2K^d cell lines #12 and #7 gave the best H-2K^d expression and were strictly selected by limiting dilution to obtain monoclonal cell population. H-2K^d expressions were identified from the resulting clones. **(C)** Summary of H-2K^d levels in polyclonal and monoclonal MCA-205 cells.

Interferon-gamma (IFN γ) stimulation profoundly elevates the cell-surface expression of PD-L1 and MHC-I

Next, I asked whether the MC38 and MCA-205 cancer cells innately expressed immunoregulatory ligand PD-L1. The basal (unstimulated) level of PD-L1 in MC38 cells was moderate while MCA-205 displayed a low expression level (Fig. 16 and 17). High PD-L1 inhibitory ligand levels are usually associated with poor prognosis (66). Confirmation of enriched PD-L1 expression *in vitro* upon cytokine stimulation might be indicative for the actual condition in the tumor microenvironment whereas IFN γ is being secreted by the effector T cells.

Driven by those reasons, the original and H-2K^d-overexpressing stable clones were stimulated with 20 ng/ml IFN γ for 24 h (66) to assess the expression of PD-L1. Although the mechanism as to how the IFN γ can upregulate MHC-I and PD-L1 expression has not been elucidated in detail, it was reported that IFN γ affected post-translational regulation of genes involved in antigen-presenting machinery (67).

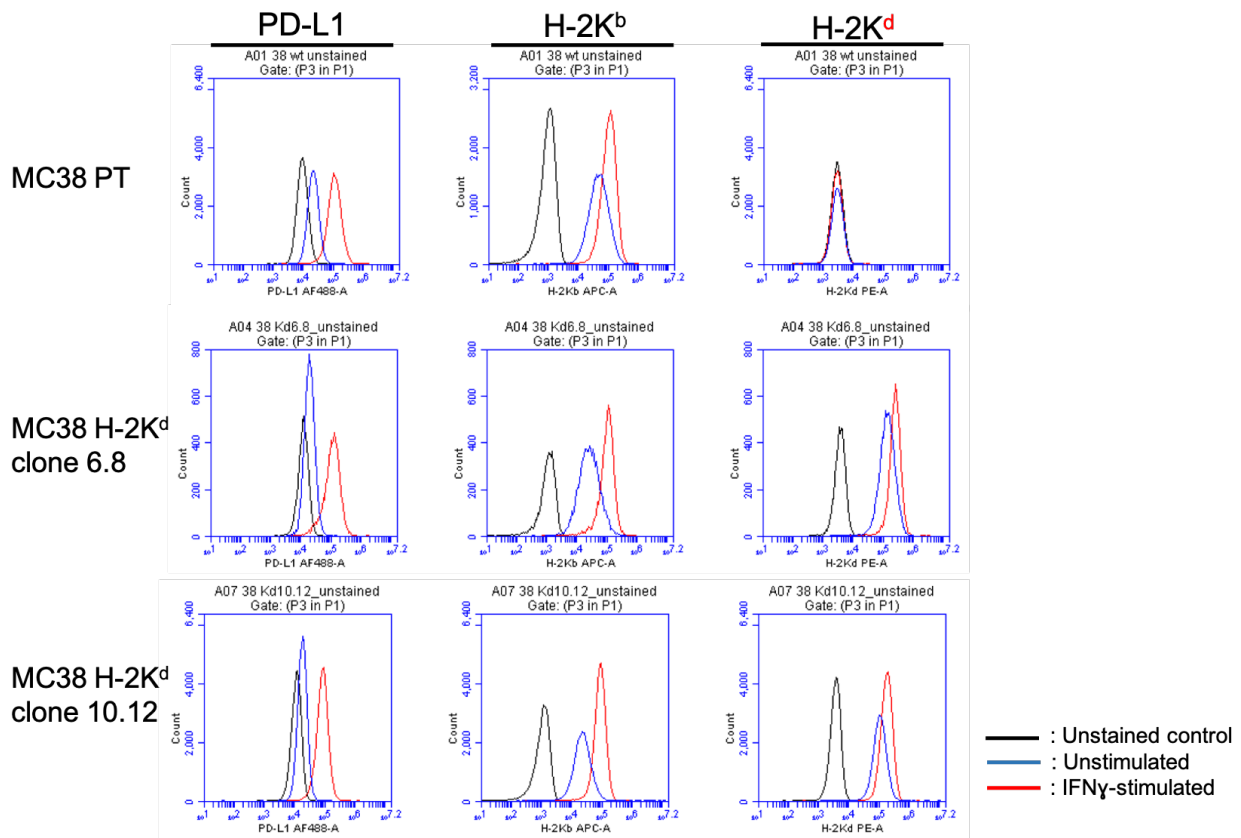


Figure 16. MC38 cells were cultured *in vitro* and stimulated with IFN- γ (20 ng/ml) for 24 h as shown in the red line. Expression of PD-L1, H-2K^b, and H-2K^d was assessed by flow cytometry. Unstained control is shown in the black line while unstimulated cells are represented in the blue line. Data are representative of two independent experiments.

IFN γ treatment evidently boosted PD-L1 expression, as well as endogenous and allogeneic MHC-I (H-2K^b and H-2K^d, respectively) in MC38 (Fig. 16) and MCA-205 cells (Fig. 17). Inducible PD-L1 expression in MC38 cancer cells was higher than that of MCA-205. These results might be considered to predict the possibility of PD-1/PD-L1-mediated antitumor immune resistance in the *in vivo* settings. The two-faced effects of IFN γ presence could be beneficial to increase MHC-I expression, while on the hostile side, could also induce inhibitory receptor signaling.

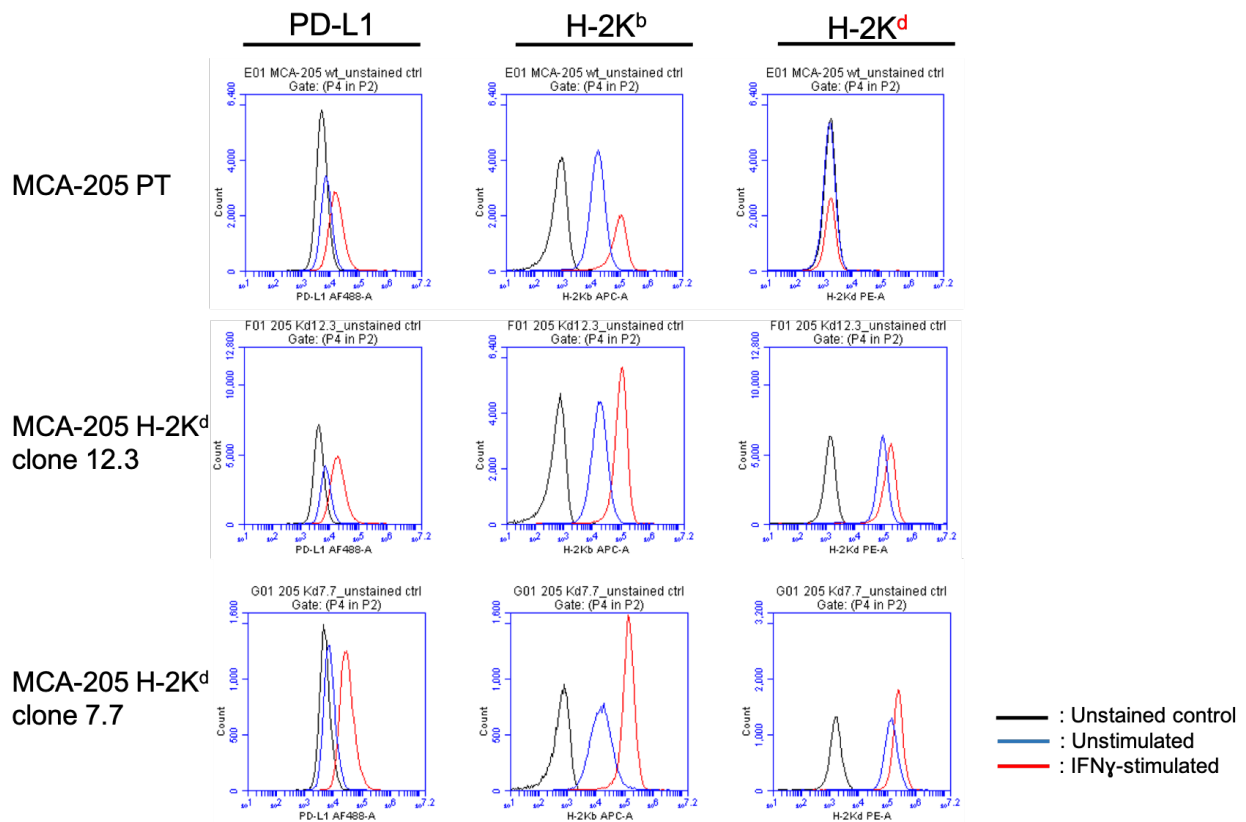


Figure 17. MCA-205 cells were cultured *in vitro* and stimulated with IFN- γ (20 ng/ml) for 24 h, represented in the red line. Expression of PD-L1, H-2K^b, and H-2K^d was assessed by flow cytometry. Unstained control is shown in the black line while unstimulated cells are represented in the blue line. Data are representative of two independent experiments.

In vivo Study

MCA-205 tumor is sensitive to PD-1 absence but MC38 shows resistance

MC38 colon adenocarcinoma cells have been previously reported as an immunogenic cancer cell line with high sensitivity to PD-1/PD-L1 axis blockade (66, 68-73). In this study, MC38 cells appeared to be partially responsive to the global absence of PD-1 in the knockout mouse model studied. Subcutaneously implanted parental MC38 cells (MC38 PT) formed tumors and grew progressively in both PD-1 KO and WT mice (Fig. 18A), but the speed of tumor growth appeared to be slower in PD-1 KO mice (Fig. 18B). Robust tumor advancement followed by ulceration within two weeks post-inoculation resulted in low survivability of tumor-bearing mice.

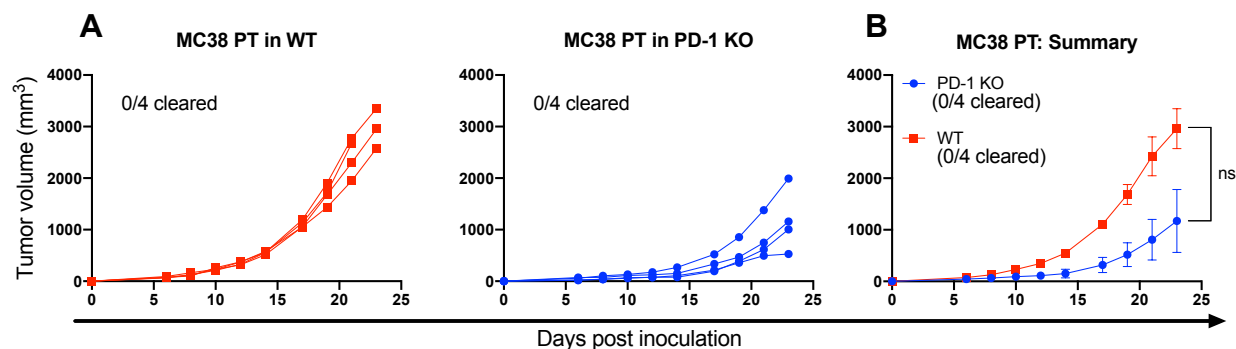


Figure 18. Subcutaneous injection results of parental (unmodified) MC38 cells into WT and PD-1 KO mice showed progressive tumor growth. **(A)** Individual tumor growth curves. **(B)** Average tumor growth curves. Data are representative of at least two independent study repeats with $n = 4$ to 5 mice per group. Statistical significance was determined by unpaired Student's t -test. Error bars depict the standard error of the mean (SEM) from the means ($p = 0.1085$).

In contrast, the methylcholanthrene (MCA)-induced murine sarcoma cell line MCA-205 was shown to be highly responsive to PD-1 blockade (Fig. 19A and 19B). The MCA-205 tumor implant was initially formed in PD-1 KO mice and then completely cleared. Tumor recurrence has never occurred for at least six months of observation and the animals became tumor-free. In contrast, no tumor regression was seen in WT mice. In this study, the unleashed antitumor immune responses supported by deficiency of PD-1 inhibitory pathway were detrimental for MCA-205, but not for MC38 cancers.

These preliminary observations demonstrated an evident likelihood of immune evasion exploited by MC38 and MCA-205 tumors. Despite the apparent fact that both tumors were competent at expressing their own endogenous H-2K^b molecules *in vitro*, the implanted tumors nevertheless escaped from immune surveillance. As previously reported, cancer cells could evade the recognition of CD8 T cells by downregulating the MHC-I antigen presentation pathway through gene mutation and epigenetic modification (37).

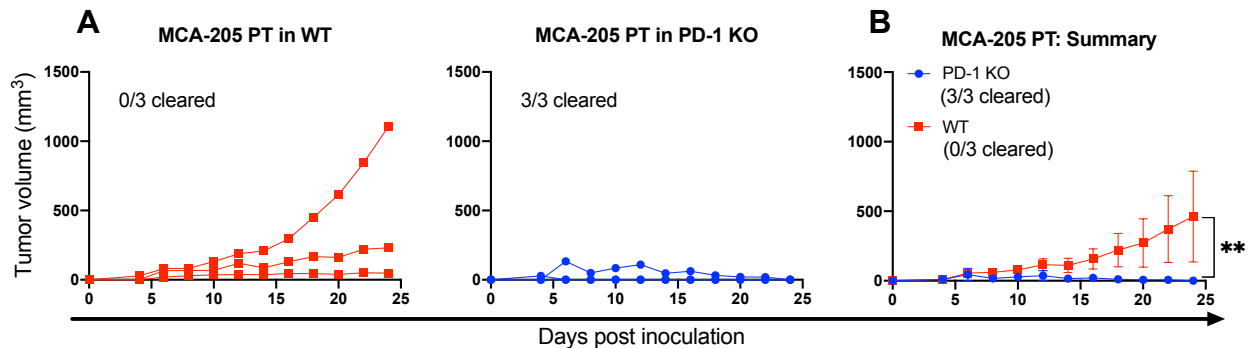


Figure 19. MCA-205 PT cells were inoculated subcutaneously into the flank of PD-1 KO and WT mice. **(A)** Individual tumor growth curves in PD-1 KO mice showed complete regression while in WT mice, tumors were growing progressively. **(B)** Summary of tumor growth curves. Shown are representative data from one of three repeated experiments with $n = 3$ mice per group. Statistical significance was determined by unpaired Student's *t*-test. Error bars depict means \pm SEM.

Polyclonal H-2K^d-expressing MC38 and MCA-205 lines reveal distinct immunogenicity

To evaluate whether the bulk H-2K^d-expressing cells could yield into heterogeneous immune response, the MC38 H-2K^d polyclonal lines were tested for their immunogenicity by transplantation into WT and PD-1 KO mice. All MC38 H-2K^d bulk cell lines (#6 and #10) were regressed spontaneously in PD-1 KO mice (Fig. 20A and 20B). In contrast, the polyclonal MC38 H-2K^d lines formed progressively growing tumors in roughly half of the WT mice, supporting the potent immunosuppressive role of PD-1 and also the importance of using a monoclonal cell population for *in vivo* study. I assumed that the Neo^R-transfected and H-2K^d non-expressing cancer cells in the polyclonal cell mixtures are capable of rendering nonimmunogenic tumors, making the H-2K^d cells to be less visible to the immune surveillance.

Interestingly, albeit the exclusion of limiting dilution step, the polyclonal MCA-205 H-2K^d line #12 displayed strong antitumor immunity, represented by 100% rejection in all tested

animals (Fig. 20C). Looking back to the *in vitro* results, MCA-205 H-2K^d cell line #12 has an equally high H-2K^d expression level after sub-cloning (Fig. 15B), suggesting low tumor heterogeneity. Contrary to that, in the case of MCA-205 H-2K^d cell line #7 with initially moderate expression of allogeneic molecules (Fig. 15C), the subcutaneous tumor was only partially rejected from the WT host (Fig. 20C), indicating the possible presence of non-transfectants or Neo^R subpopulation that ultimately outgrew the immunogenic H-2K^d cells.

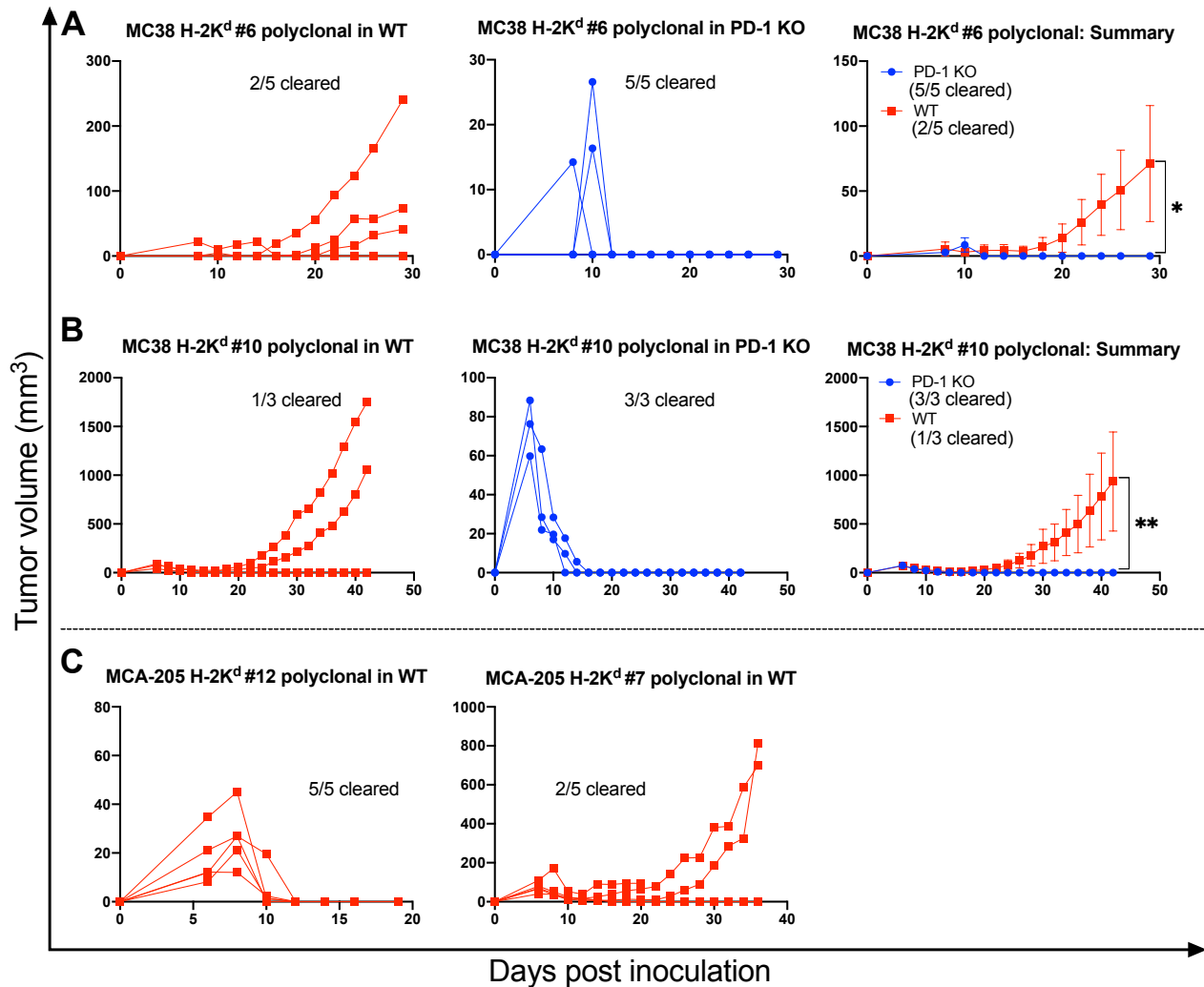


Figure 20. Polyclonal MC38 H-2K^d cells from the lines #6 (A) and #10 (B) were implanted into PD-1 KO mice and completely regressed while partial tumor rejection occurred in WT mice. (C) Individual tumor growth of bulk MCA-205 H-2K^d cell lines #12 and #7 in WT mice. Average tumor growth curves depict means \pm SEM. Statistical significance for (A) and (B) was determined by unpaired Student's *t*-test.

Ectopic H-2K^d overexpression in MC38 provides complete tumor regression

To validate that allogeneic MHC-I was attributable specifically to enhance host immunity against tumors, each MC38 H-2K^d bulk line was cloned and single-cell clones were then inoculated into the mice. Indeed, the monoclonal MC38 H-2K^d cells (clone #6.8) were completely regressed in PD-1 KO and WT mice (Fig. 21A), signifying high immunogenicity. Next, to exclude the possibility that H-2K^d-mediated tumor regression might be effective only to a particular clone, I inoculated a different clone (MC38 H-2K^d #10.12) and confirmed the growth and spontaneous regression in both WT and PD-1 KO mice (Fig. 21B). To this end, the clonal variability was not affecting the *in vivo* study. Taken together, these findings undeniably suggested that allogeneic H-2K^d involvement is required for successful tumor clearance. In addition, the regression of the MC38 H-2K^d tumor was confirmed to be PD dependent on allogeneic MHC-I itself given that the control of MC38 tumor encoding Neo^R gene alone grew progressively (Fig. 21C).

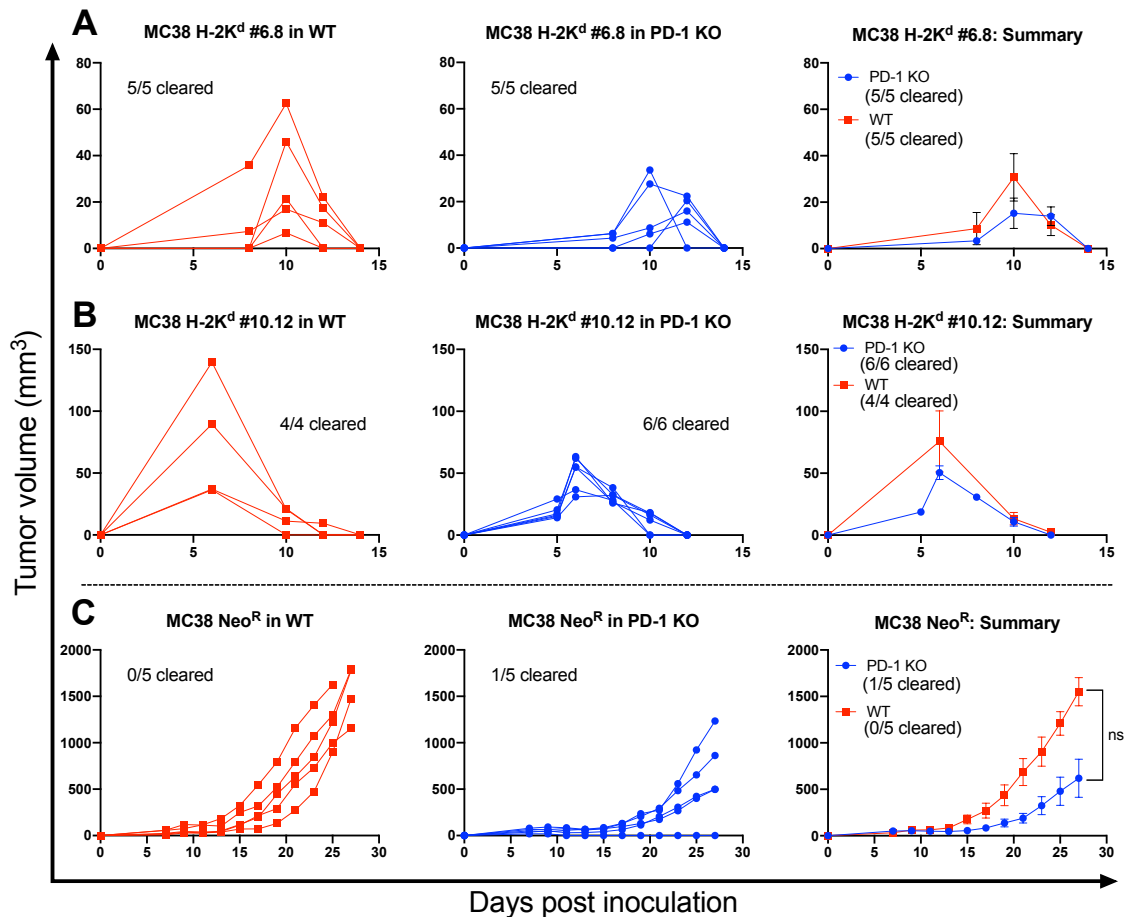


Figure 21. MC38 tumors expressing allogeneic H-2K^d were completely rejected from the PD-1 KO and WT mice. Tumor growth curves of MC38 H-2K^d from clones #6.8 (A) and #10.12 (B).

(C) MC38 Neo^R tumors were used as controls to exclude the possibility of drug resistance-mediated immunogenicity. Data shown are from two independent experiments with n = 5 mice per group (A) and from one experiment with n = 4-6 mice (B and C). Average tumor growth curves depict means ± SEM. Statistical significance was determined by unpaired Student's *t*-test (*p* = 0.1001).

Having observed a tremendous immune response demonstrated by the expression of allogeneic H-2K^d in MC38 tumors, I further asked whether this result was specifically due to H-2K^d-mediated modulation of antitumor immunity rather than the possibility of delayed tumor onset. To clarify this point, I compared the tumorigenicity of MC38 cells in an immunodeficient mouse model (Fig. 22A). BALB/c^{nu/nu} mouse lacks a thymus thus unable to produce T cells (74) which is required to fend off robust growth of implanted tumors. Notably, I found that all inoculated MC38 H-2K^d tumors grew progressively in immunodeficient BALB/c^{nu/nu} mice (Fig. 22B), eliminating the possibility of a loss of tumorigenicity. These data strongly validated that the MC38 H-2K^d tumors are inherently capable of *in vivo* growth. Moreover, spontaneous MC38 H-2K^d tumor regression in C57BL/6N PD-1 KO and WT mice was confirmed to be specifically induced by the presence of allogeneic class I MHC.

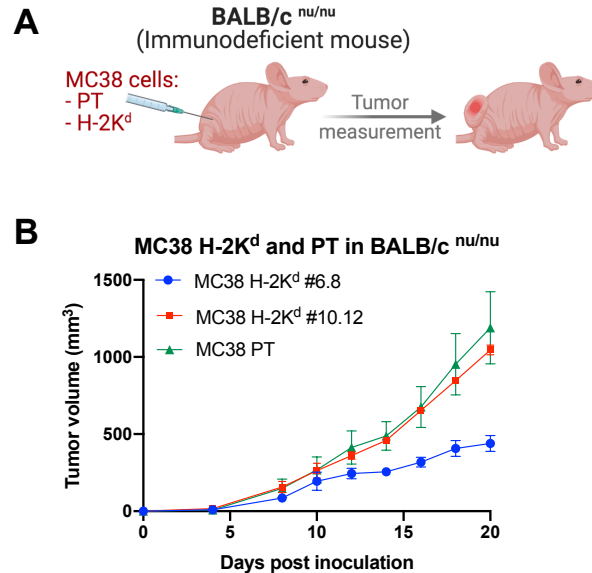


Figure 22. Injection of MC38 tumors in BALB/c^{nu/nu} immunodeficient mice to validate the tumorigenicity of inoculated cells used in this study. (A) Schematic diagram of tumor injection is shown. MC38 PT and MC38 H-2K^d stable clones were injected into BALB/c^{nu/nu} mice followed by observation of palpable tumor. (B) Kinetics of tumor growth is shown for MC38 PT, H-2K^d clone #6.8, and H-2K^d clone #10.12 tumor-bearing hosts. Data represent the means ± SEM of three mice for each group.

MCA-205 H-2K^d tumors spontaneously regress even in the presence of PD-1

Having established that unmodified MCA-205 cells spontaneously regressed when injected into PD-1 KO animals (Fig. 19A and 19B), I focused on the investigation of MCA-205 H-2K^d clones in the WT mice model. Similar to the MC38 study, the MCA-205 H-2K^d clone #12.3 was completely regressed (Fig. 23A). Consistently, a different clone of H-2K^d-overexpressing MCA-205 cancer cells (clone #7.7) also displayed strong antitumor immunity represented by 100% rejection in the WT host (Fig. 23B). These remarkable results were confirmed to be achieved through the H-2K^d-mediated immunity, but not due to the possible immunogenicity of Neo^R gene. The MCA-205 Neo^R tumors were less visible to the immune cells, resulting in robust growth in the WT animals (Fig. 23C). In addition, the possibility of late tumor progression was excluded in this study as the MCA-205 H-2K^d-tumor-bearing host did not exhibit any tumor regrowing for about 7 months of observation. Altogether, these data evidently strengthen the hypothesis that allogeneic H-2K^d successfully converted the aggressive tumors into highly immunogenic tumors, even in the WT mice without any blocking of PD-1/PD-L1 inhibitory receptors.

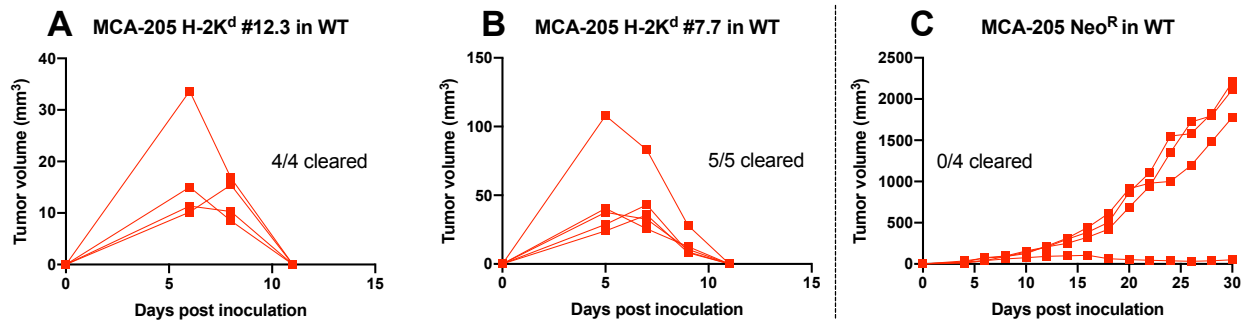


Figure 23. Growth curves of MCA-205 H-2K^d tumors indicated spontaneous regression in WT mice. Individual tumor growth of monoclonal MCA-205 H-2K^d #12.3 (A) and #7.7 (B). (C) MCA-205 cells stably transfected with the Neo^R gene were used as a control to assess drug resistance-mediated immunogenicity. Data shown are from one experiment, n = 4-5 mice per group.

Allogeneic H-2K^k negatively influences immune responses to MC38 H-2K^d tumors

To provide a comparison with another mouse MHC-I H-2K allele, I have established MC38 cells overexpressing the H-2K^k gene. The level of H-2K^k molecules from the stably-transfected monoclonal MC38 was confirmed to be sufficiently high (Fig. 24A). Next, I tested the tumorigenicity of MC38 H-2K^k cells in PD-1 KO and WT mice. Unexpectedly, the monoclonal MC38 H-2K^k tumors were not rejected in roughly half of the inoculated mice (Fig. 24B), contrary to the complete prevention of H-2K^d tumor growth in 100% of the mice.

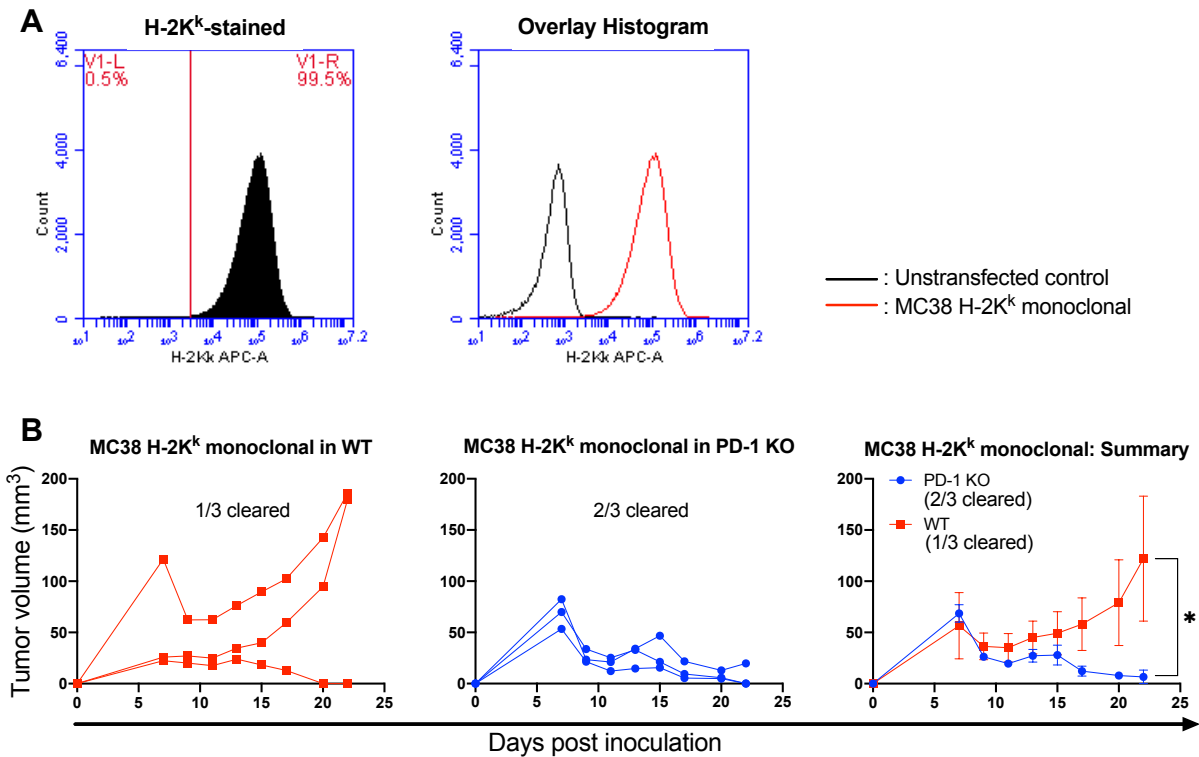


Figure 24. (A) Flow cytometric analysis of monoclonal MC38 H-2K^k cells. The high expression level of H-2K^k was confirmed by the total shifting of the cell population to the right side of the histogram (shown in the red line of overlay histogram). (B) Inoculation of MC38 H-2K^k cells into PD-1 KO and WT mice indicated partial tumor regression. Data shown are representative of two independent experiments, $n = 3$ mice per group. Average tumor growth curves depict means \pm SEM. Statistical significance was determined by unpaired Student's t -test.

In addition, I also constructed a bi-cistronic vector linked by the P2A peptide in order to co-express both allogeneic H-2K^d and H-2K^k genes. MC38 cells were stably transfected with the bi-cistronic vector and were validated for the equal expression levels of H-2K^d and H-2K^k molecules (Fig. 25A). Furthermore, the established monoclonal MC38 H-2K^d.p2A.H-2K^k cells

were then injected into the flanks of PD-1 KO and WT mice. Intriguingly, I found that the allogeneic H-2K^k showed immunodominance against the H-2K^d gene. Simultaneous cell surface expression of both d and k alleles of the H-2K gene was not effective in inducing tumor growth inhibition (Fig. 25B). All WT animals experienced rapid tumor growth while half of the PD-1 KO mice could not survive from the high tumor burden.

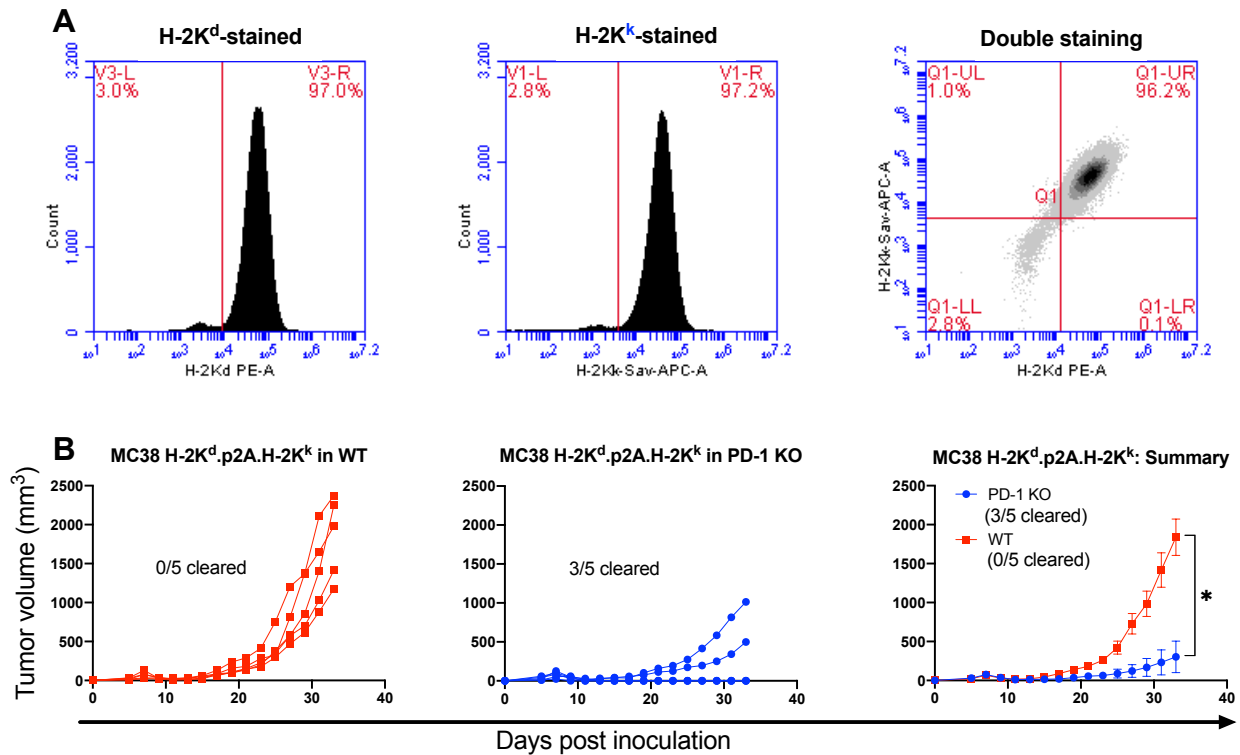


Figure 25. (A) Flow cytometric analysis of monoclonal bi-cistronic MC38 H-2K^d.p2A.H-2K^k cells. The simultaneous and equal expression levels of both allogeneic H-2K^d and H-2K^k were shown in the histogram and density plot (double-positive cell population at the upper right quadrant). (B) MC38 H-2K^d.p2A.H-2K^k tumor growth in PD-1 KO showed partial regression but robust growth in WT mice. Data shown are from one experiment, n = 5 mice per group. Average tumor growth curves depict means ± SEM. Statistical significance was determined by unpaired Student's *t*-test.

These findings suggested that H-2K^k molecules might compete with H-2K^d and consequently led to the decline of effector T-cell responses. Previously, it has been reported that particular MHC-I molecules could alter the presentation of other MHC-I alleles, resulting in a severe reduction of CTL responses (75). Although the previous study was not conducted in the context of immuno-oncology, it has been reported that the H-2D^b-mediated antiviral responses

were outcompeted when H-2K^k was also present (76). This evidently suggested that H-2K^d class I molecules have the higher ability to induce a greater antitumor immune response. Hence, it is rational to further utilize H-2K^d-overexpressing tumors for the subsequent experiments in my study.

Delayed growth of the mixed MC38 H-2K^d : PT tumors *in vivo*

In the quest of achieving abscopal effect phenomenon, I next asked whether the presence of allogeneic H-2K^d cells could affect the immunogenicity against the original MC38 PT cells. To investigate this, prior to subcutaneous inoculation, I mixed an equal cell density (1:1) of MC38 H-2K^d : PT cells and implanted the mixture into either PD-1 KO or WT mice (Fig. 26A). The growth of transplanted tumor-mixture was significantly delayed in both mice (Fig. 26B and 26C), contrary to the progressive growth of MC38 PT cell alone. Nevertheless, the speed of *in vivo* growth in WT mice was faster compared to that of PD-1 KO mice. Indeed, the inhibition of immunosuppressive PD-1/PD-L1 signal highly contributed to slow tumor progression in PD-1 KO animals, validating the importance of immune checkpoint blockade. This finding showed that in the pooled mixture of aggressive MC38 PT and immunogenic MC38 H-2K^d cells, trans-acting cross-immunity might have occurred against the poorly immunogenic parental cells, which is evidently mediated by the allogeneic H-2K^d.

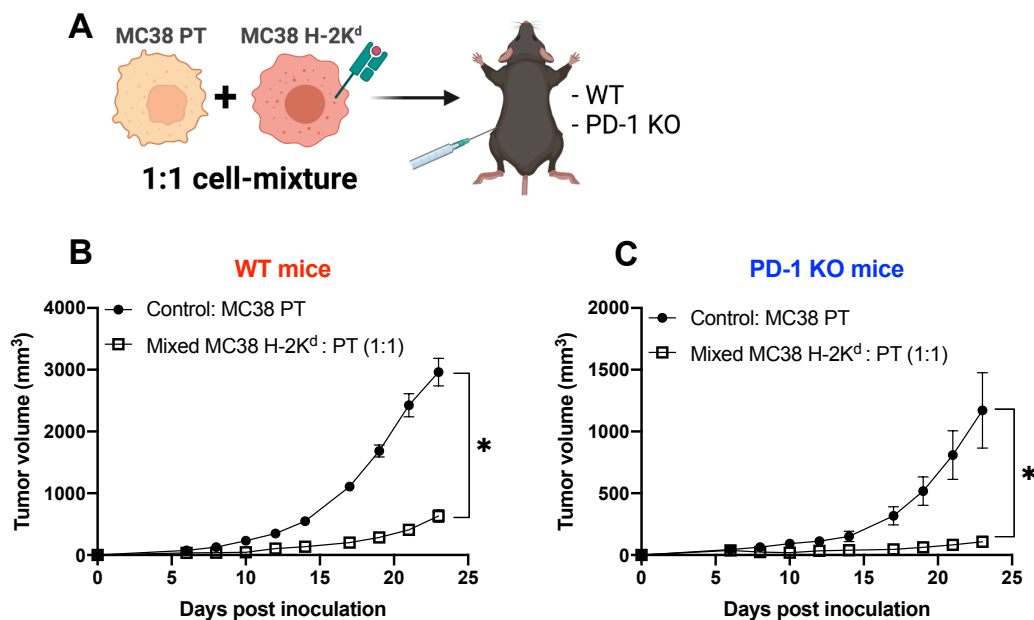


Figure 26. (A) Experimental design: prior to injection into PD-1 KO and WT mice, the equal numbers of MC38 PT cells (5×10^5 cells/100 μ l) and MC38 H-2K^d clone #6.8 (5×10^5 cells/100 μ l)

were counted and mixed, totaling the final cell concentration to 5×10^5 cells/100 μ l per inoculation. As a control, MC38 PT cells (5×10^5 cells/100 μ l) were injected into both mice. Palpable tumors growth was then measured once every 2 days. The mixed-tumor growth in WT mice (**B**) and in PD-1 KO mice (**C**) showed delayed progression compared with MC38 PT tumor inoculated with similar total cell density. Data shown are from one experiment, $n = 4-5$ mice per group. Average tumor growth curves depict means \pm SEM. Some error bars are shorter than the size of the symbol hence cannot be shown. Statistical significance was determined by unpaired Student's *t*-test.

Sensitizing PD-1 KO mice with immunogenic H-2K^d tumors results in protection against parental MC38 challenge

Next, I sought to determine the extent to which H-2K^d-overexpressing tumors could protect the mice against unmodified cancers. The MC38 H-2K^d clone was further investigated in the settings of concomitant tumor immunity and the possibilities of eliciting the abscopal effect. Concomitant tumor immunity is a phenomenon in which a tumor-bearing host is resistant to the growth of similar secondary tumor implants at the distant site (77). To test this, I developed sensitization strategies by inoculating MC38 H-2K^d tumors (clone #6.8) into the flank of PD-1 KO mice followed by challenging them with parental cells on the contralateral side after 6 days (Fig. 27A). Surprisingly, the sensitization treatment provided complete protection against the unmodified MC38 tumor challenge with all mice rejecting the tumor inoculums (Fig. 27B). Reproducibly, inoculating a different clone of MC38 H-2K^d tumors (clone #10.12) resulted in parental tumor rejection in all tested PD-1 KO mice (Fig. 27C). Collectively, these data showed that rejection of parental MC38 is an H-2K^d-dependent phenomenon.

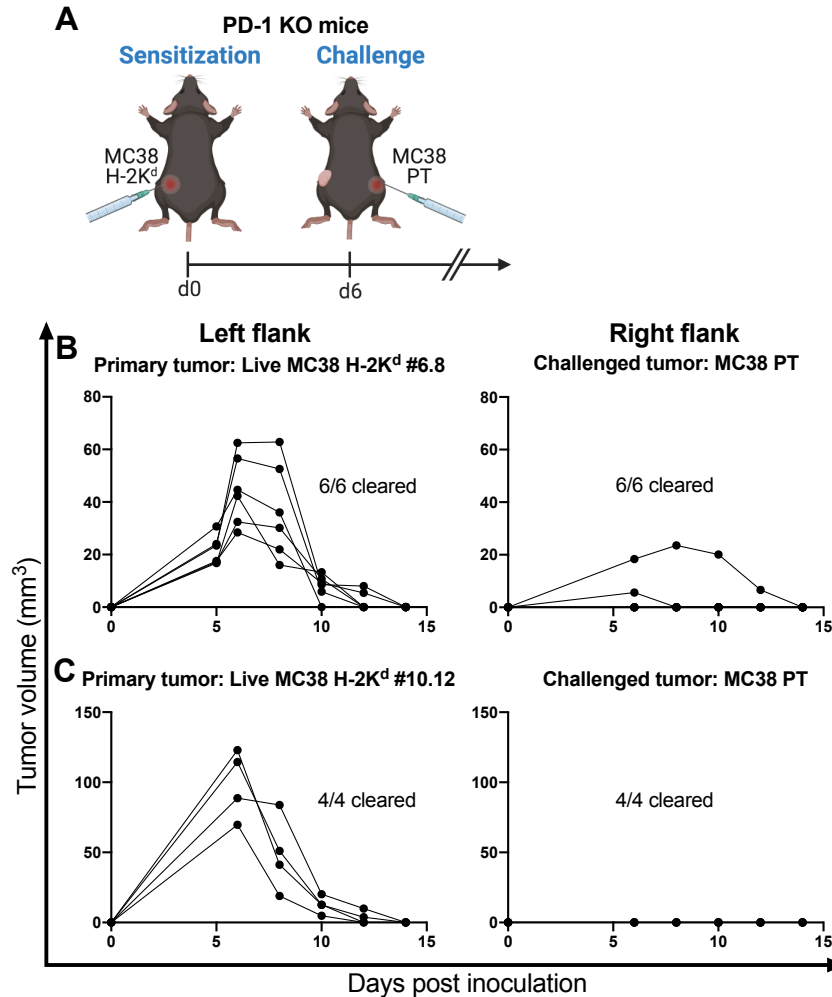


Figure 27. MC38 H-2K^d induces protective immunity against parental cell challenge. **(A)** Experimental design: PD-1 KO mice were implanted with MC38 H-2K^d on the left flank followed by challenge on the contralateral side with parental MC38 PT on day 6. **(B)** Individual growth curves of primary and secondary tumors of MC38 H-2K^d #6.8-sensitized mice. **(C)** Another clone of MC38 H-2K^d (clone #10.12) was tested in a similar fashion. Data are representative of two independent study repeats with n = 4-6 mice per group.

Remarkably, sensitizing PD-1 KO mice with growth-arrested (MMC-treated) cells or debris of both clones of MC38 H-2K^d tumors provided full protection from the encounter of secondary unmodified tumors (Fig. 28A-C). This finding implied that MC38 H-2K^d retained high immunogenicity regardless of their compromised growing capacity and dead/alive status. Most interestingly, sensitized animals immediately gained immunity against the challenge of secondary parental tumors at the distant site even without employing any additional immune adjuvants. This implies that H-2K^d itself could act as an adjuvant to boost antitumor immunity.

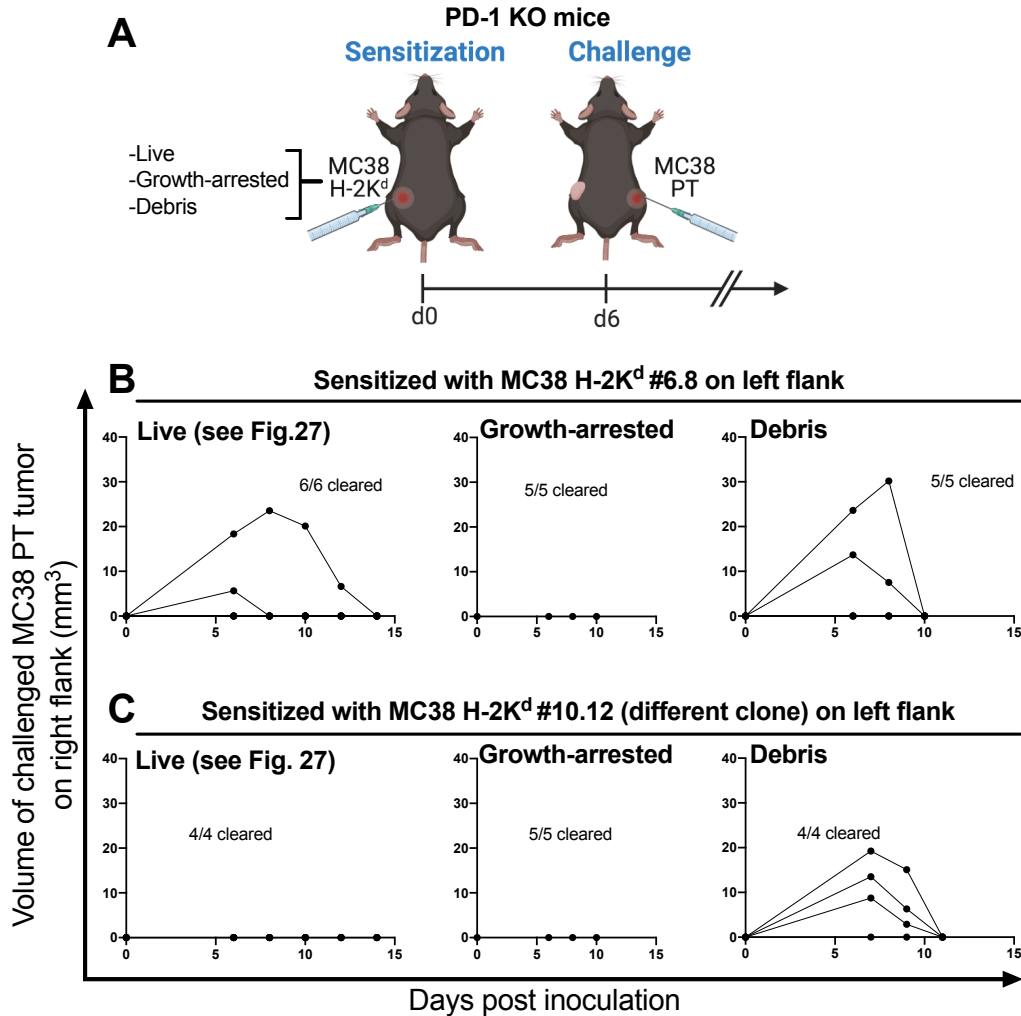


Figure 28. Kinetics of the secondary tumor growth (MC38 PT) in PD-1 KO mice sensitized with MC38 H-2K^d. **(A)** Experimental design: three different conditions of immunogenic MC38 H-2K^d tumors; live, growth-arrested (Mitomycin C-treated), and debris (frozen-thawed cells) were inoculated in the sensitization experiment settings, and on day 6, MC38 PT cells were injected subcutaneously on the contralateral side. Individual tumor growth curves of the challenged MC38 PT tumors in PD-1 KO sensitized with live, growth-arrested, and debris of MC38 H-2K^d clones #6.8 **(B)** and #10.12 **(C)**. Data shown are from two experiment with n = 4-6 mice per group.

MC38 PT cell debris fails to induce protective immunity

Having established an effective sensitization treatment with MC38 H-2K^d in PD-1 KO mice, I further asked whether this phenomenon was specifically due to the H-2K^d-mediated immune modulation rather than the general effects of the MC38 cell itself. To clarify this point, I pre-sensitized PD-1 KO mice with MC38 PT cells (live, growth-arrested, and debris) followed by

observation of challenged MC38 PT tumor growth in the distant site (MC38 PT vs. MC38 PT, as shown in Fig. 29A).

Sensitization with growth-arrested MC38 PT cells provoked antitumor immunity wherein all mice rejected inoculums in both flanks effectively (Fig. 29B). Moreover, concomitant immunity occurred when PD-1 KO mice received primary inoculation of live MC38 PT, indicated by a complete rejection of equivalent live MC38 PT tumor. However, due to the robust growth of primary tumor (Fig. 29C), the subjected mouse condition was deteriorated rapidly and ultimately resulted in a faster endpoint of the experiment, in comparison with the long-term tumor-free status of animals sensitized with the highly immunogenic H-2K^d tumor (Fig. 27).

Most excitingly, I found that sensitization with cell debris of MC38 PT failed to prevent tumor growth, evidently displayed by the progressive growth of live parental cells (Fig. 29B). These findings further highlight the ability of H-2K^d cells debris, but not MC38 PT debris, to mount a markedly effective immunity, particularly in the absence of PD-1 activity.

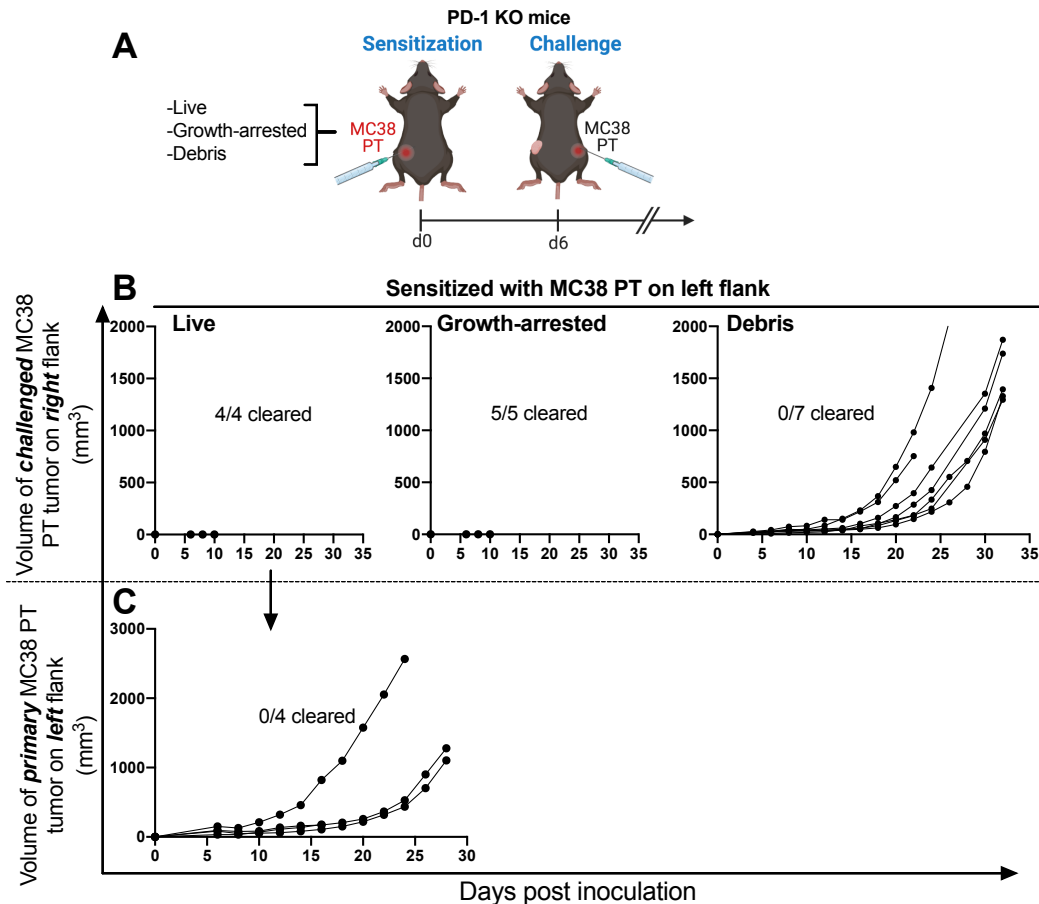


Figure 29. (A) MC38 PT tumors were treated (live, growth-arrested, and debris) and inoculated into PD-1 KO mice as a sensitization regimen. Mice were challenged six days later with the same

MC38 PT cell line. **(B)** Summaries of the challenged MC38 PT tumor growth. Representative data are shown as individual tumor growth curves. Data for sensitization with MC38 PT cell debris are pooled from two independent experiments. **(C)** Live MC38 PT cells were implanted as the primary tumor in order to sensitize PD-1 KO mice. Data shown as individual tumor growth curves from one independent experiment with $n = 4$.

Sensitization with MC38 H-2K^d cells debris provides long-term immunological memory against MC38 carcinoma

When taking into account that sensitizing PD-1 KO mice with MC38 H-2K^d prompted a strong anti-tumor immunity, I next sought to validate whether this treatment could be sufficient to protect sensitized mice from subsequent tumor rechallenge in a long period of time. To more deeply assess long-term protective immunity, about 5 months following the sensitization, all mice that had survived the first tumor (MC38 PT) inoculation were rechallenged with MC38 PT on the same site as the first injection (Fig. 30A). Observation of palpable tumor formation was conducted for a period lasting more than 8 weeks to exclude the possibility of delayed onset of tumor growth.

PD-1 KO mice that were sensitized with the debris of MC38 H-2K^d cells showed the strongest immune response, with 80% (MC38 H-2K^d #6.8–sensitized) and 100% (MC38 H-2K^d #10.12–sensitized) of the mice surviving the second tumor challenge (Fig. 30B and 30C). In contrast, rejection rates of growth-arrested–sensitized mice from both H-2K^d clones reproducibly showed the lowest survival, indicating failure to induce long-term immunity (Fig. 31). Furthermore, treatment with live MC38 H-2K^d cells also showed durable memory response with more than 60% of rechallenged mice eliminated the tumors, however, in the practical settings, administrating live tumor cells as prophylaxis is ethically impossible. Taken together, these data put an emphasis that the greater and durable immune responses were significantly induced by MC38 H-2K^d cell debris, particularly in the absence of PD-1 activity.

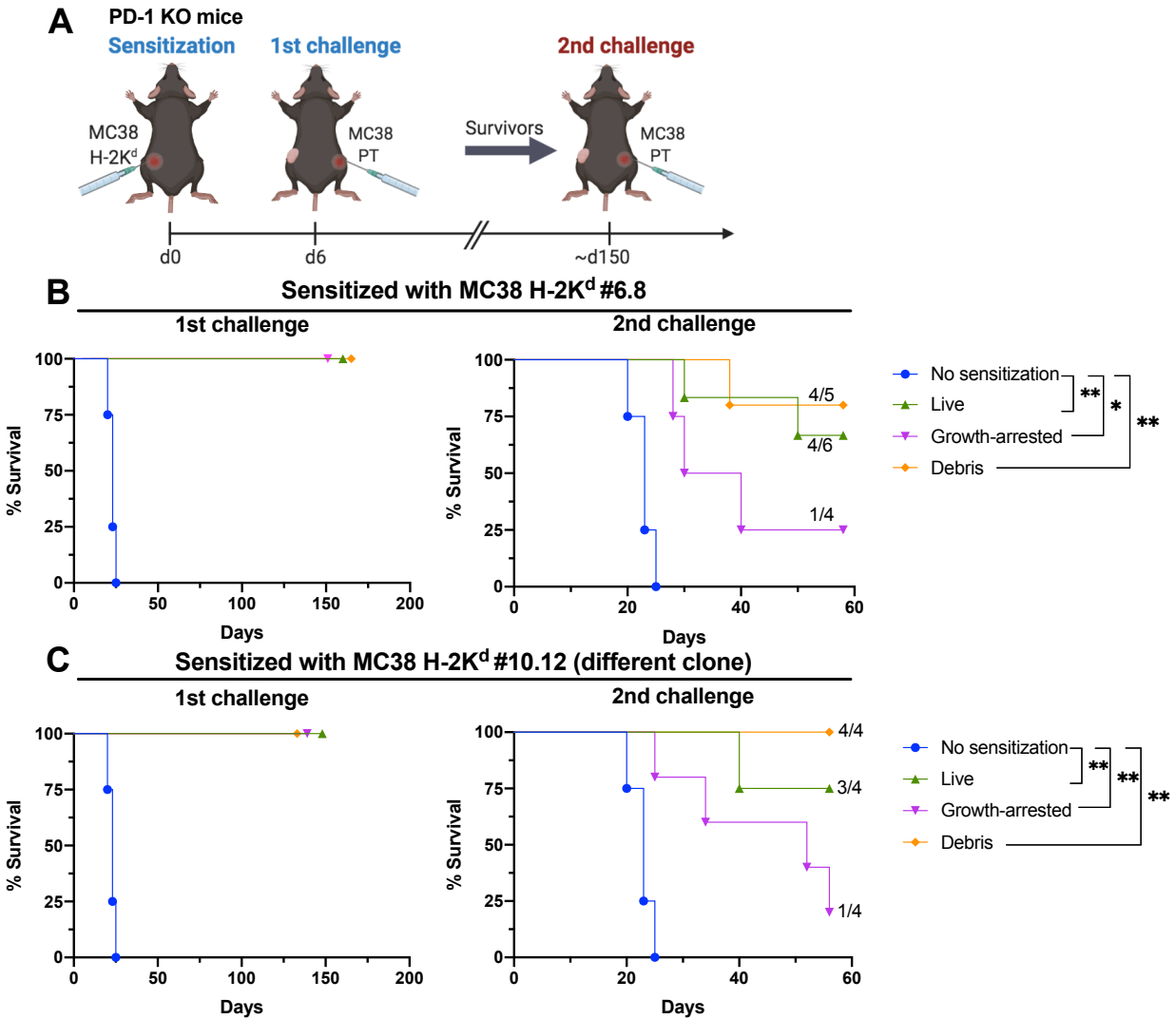


Figure 30. (A) Experimental design: PD-1 KO mice were sensitized on the left flank with each clone of MC38 H-2K^d cells (live, growth-arrested, and debris) and on day 6, MC38 PT were injected subcutaneously on the contralateral side. Upon the first challenge, tumor growth was recorded and mice that rejected tumors were rechallenged around 150 days later with MC38 PT. **(B and C)** Kaplan-Meier survival curves following the first and second tumor challenges in PD-1 KO mice pre-sensitized with MC38 H-2K^d #6.8 (B) and MC38 H-2K^d #10.12 tumors (C). Naïve PD-1 KO mice were used as positive controls for tumor growth (no sensitization). Endpoint defined as tumor volume > 1000mm³. Data shown are from one experiment, n = 4 to 6 mice per group. Statistical significance was determined by log-rank (Mantel-Cox) test.

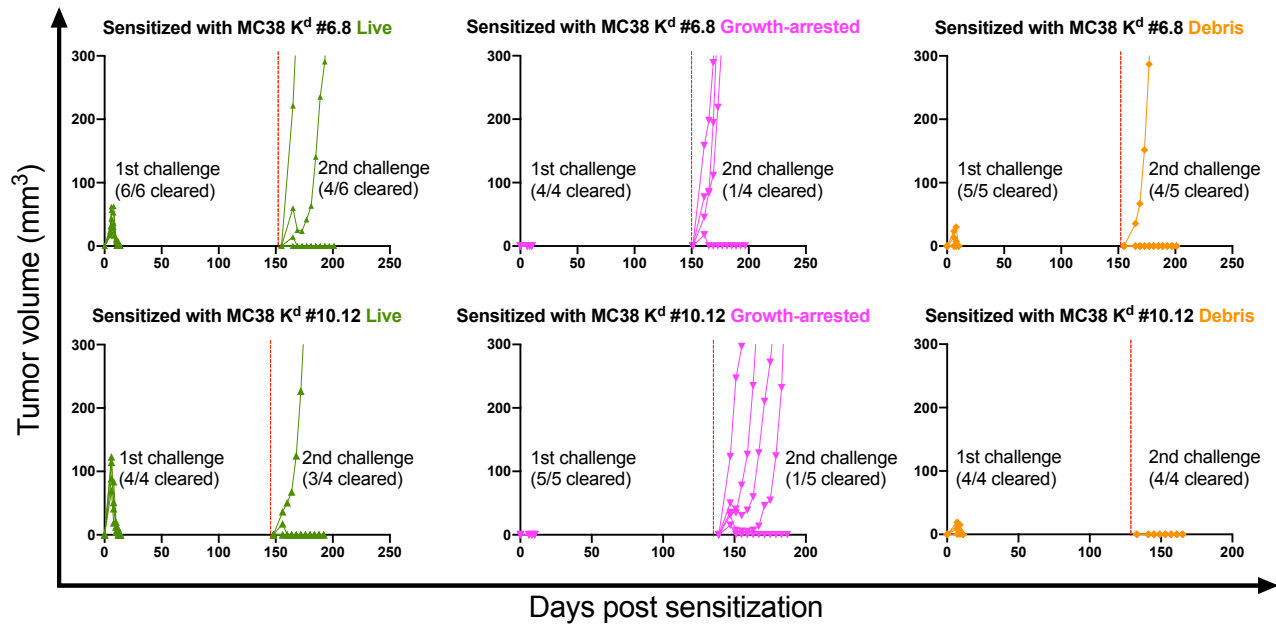


Figure 31. PD-1 KO mice were implanted with live (green), growth-arrested (magenta), and cell debris (orange) of MC38 H-2K^d clone #6.8 or clone #10.12 tumor followed by the first challenge with MC38 PT. All survivors were rechallenged (red dashed line) 5 months later with MC38 PT cell line at the same site as the first challenge. Representative data are shown as individual tumor growth curves.

PD-1 blockade is evidently required for successful rejection of challenged MC38 PT

Having elucidated the potent induction of anti-tumor immunity in PD-1 KO mice, I asked whether MC38 H-2K^d cells could also sensitize WT mice for the protection against challenged MC38 PT tumor *in vivo*. To formally address this question, the sensitization regimen was then tested in WT mice in which the PD-1/PD-L1 axis functions normally (Fig. 32A). In the presence of the PD-1 inhibitory receptor, antitumor immunity against parental MC38 cells was diminished as indicated by the robust tumor growth (Fig. 32B, right flank). Furthermore, the unanticipated finding was unveiled by the regrowing of MC38 H-2K^d tumor in WT mice (Fig. 32B, left flank), necessitating the importance of PD-1 blockade to reinvigorate host immunity against tumor. Clearly, by revisiting the previous successful sensitization results in PD-KO mice wherein both H-2K^d and PT tumors were completely rejected (Fig. 32C), these findings strongly identify the synergistic effect of PD-1 blockade and allogeneic H-2K^d in the tumor niche.

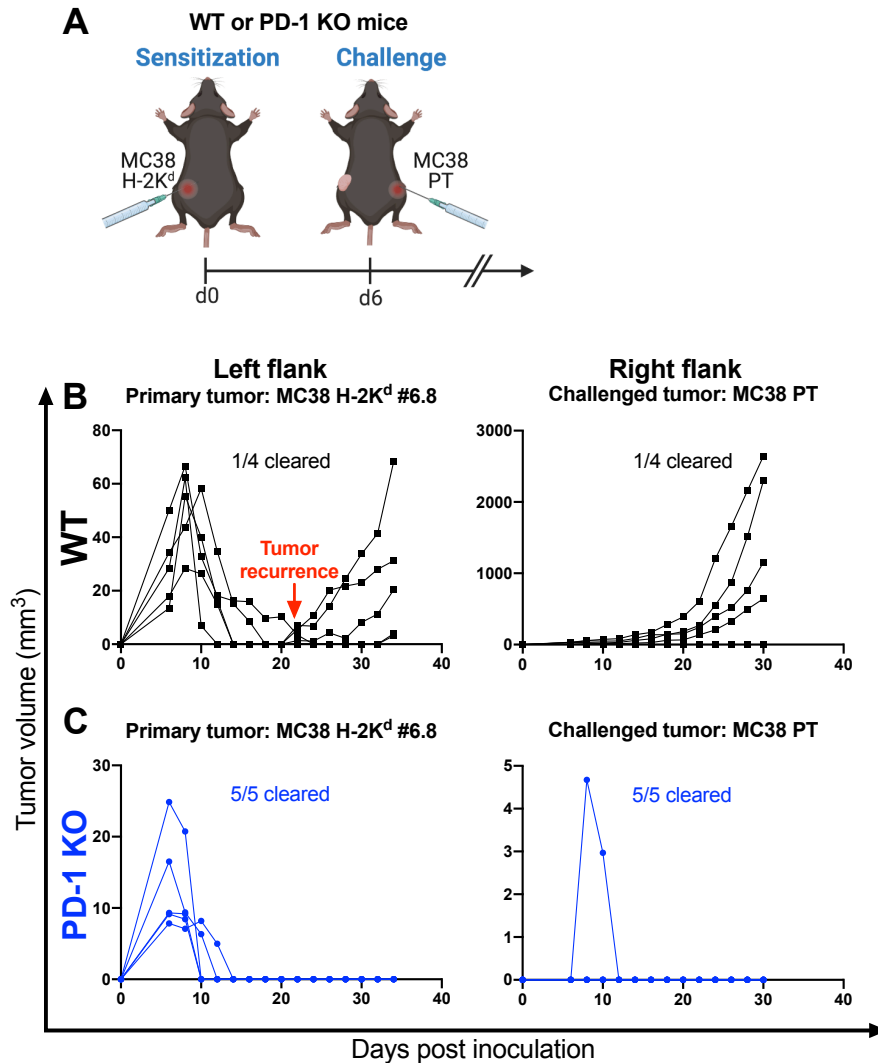


Figure 32. (A) Experimental design: WT or PD-1 KO mice were sensitized with live MC38 H-2K^d and then challenged with MC38 PT on day 6. (B) Kinetics of primary tumor growth (MC38 H-2K^d) in WT mice (black line) showed initial tumor rejection followed by recurrence, while on the opposite flank, the challenged parental line grew robustly. (C) Growth curves of individual tumors showing complete rejection of both tumors in PD-1 KO mice (blue line) as a comparison. Data shown are from two repeated experiments, n = 4-6 mice per group.

Next, to provide a proportional comparison with sensitization study in PD-1 KO mice, WT animals were also injected with inactivated or dead tumor cells ectopically expressing H-2K^d 6 days prior to parental tumor challenge (Fig. 33A). The secondary MC38 PT tumors were partially rejected in WT mice pre-sensitized with live (2/4 mice) and growth-arrested (1/4 mice) MC38 H-2K^d cells (Fig. 33B). Moreover, WT mice that received debris of MC38 H-2K^d cells as primary inoculums completely failed to acquire sensitivity to the challenged parental MC38

tumor rejection in comparison with that of PD-1 KO mice. These findings corroborated the fact that the absence of PD-1 inhibitory signal is a prerequisite to generate protective antitumor immunity against the aggressive parental cell line.

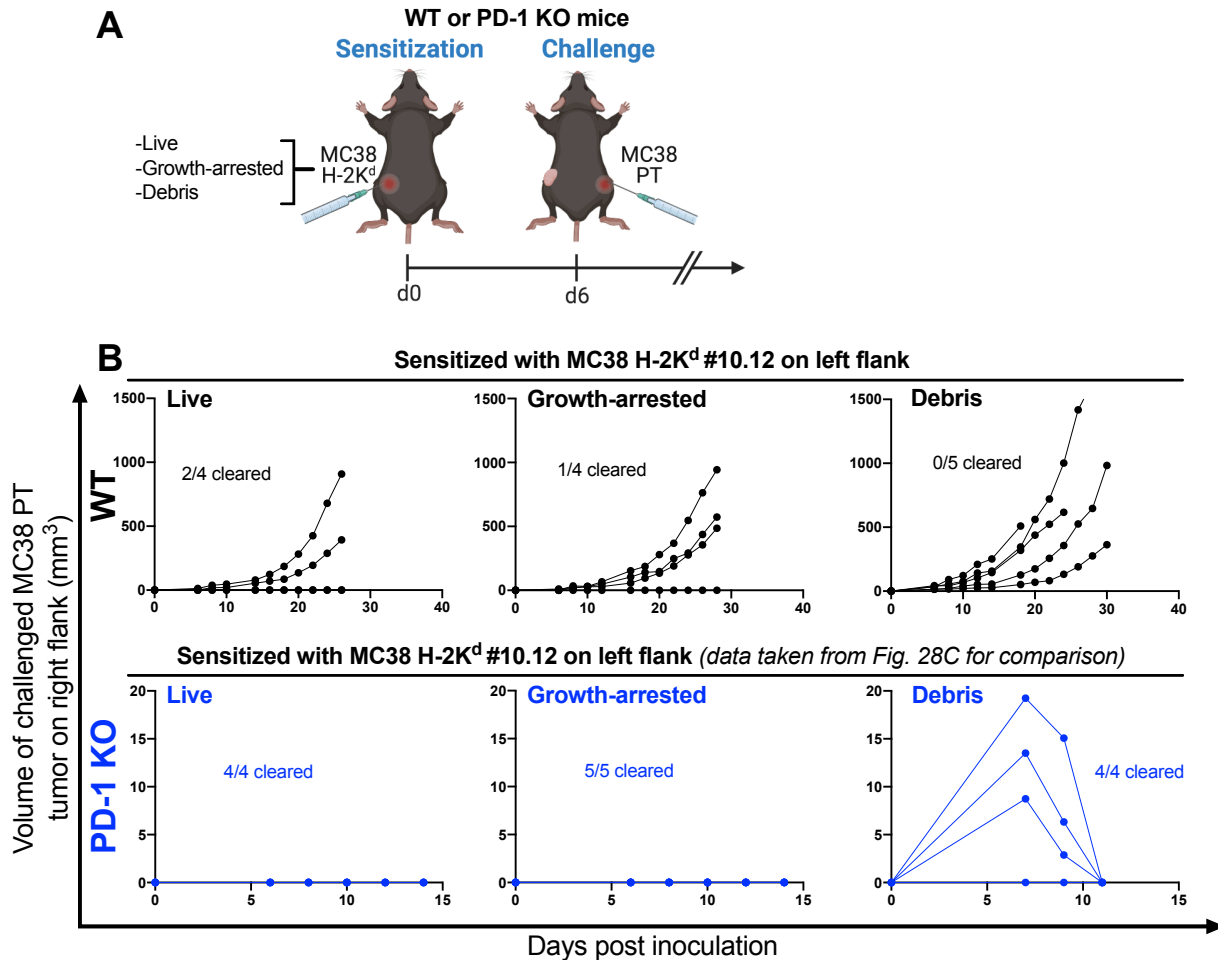


Figure 33. (A) Experimental design: WT or PD-1 KO mice were sensitized with MC38 H-2K^d (live, growth-arrested, and debris) and on day 6, MC38 PT was injected subcutaneously on the contralateral side. (B) Individual tumor growth kinetics of parental MC38 tumor in WT animals (black) versus PD-1 KO mice (blue). Complete tumor rejection was achieved in all PD-1 KO mice while WT mice failed to completely eradicate the challenged tumor.

Increased PD-1 expression in CD8⁺ T cells alleviates anti-tumor immune responses

To validate the importance of PD-1 blockade to sustain anti-tumor immunity, the tumor-infiltrating lymphocytes (TILs) were isolated from the MC38 H-2K^d-sensitized WT mice bearing the secondary MC38 PT tumor. Indeed, a marked increase in the frequencies of CD8⁺ PD-1⁺ T cells was detected (Fig. 34A). However, there was no significant difference in the percentage of

CD8⁺ PD-1⁺ T cells between sensitization treatments (Fig. 34B). High PD-1 expression within the infiltrating CD8⁺ T cells is deemed to poor prognosis (78, 79) due to the inactivation of effective tumor-killing ability. Overall, these data strengthen the importance of the immunomodulation effects of PD-1 blockade in synergizing with H-2K^d-induced antitumor immunity.

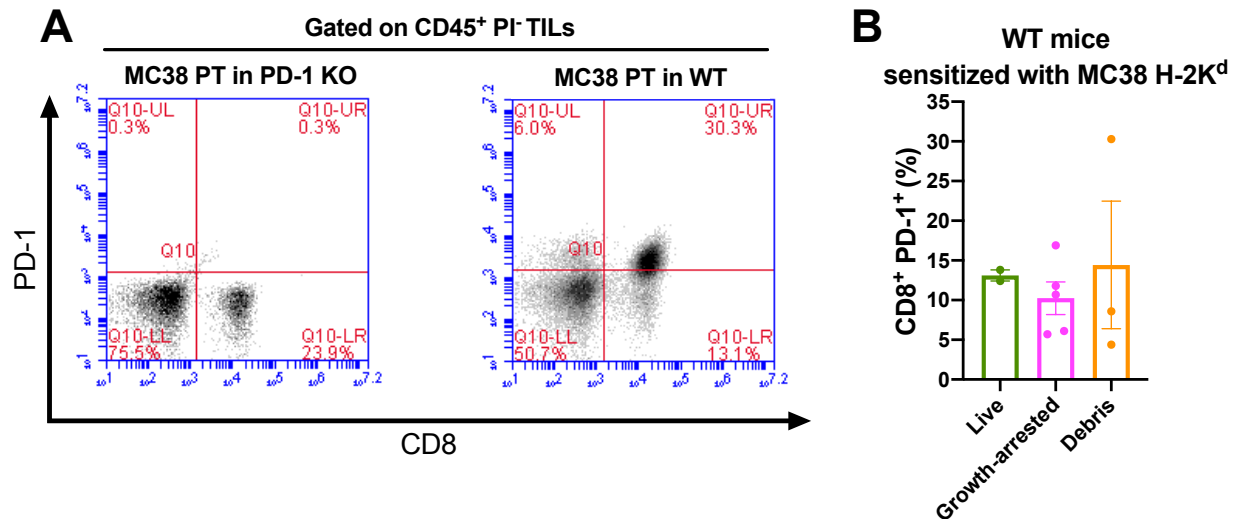


Figure 34. Elevated PD-1 expression in CD8⁺ T cells from tumor-bearing WT mice. **(A)** Representative FACS patterns of CD8⁺ PD-1⁺ cells in tumors isolated from PD-1 KO (control) and WT mice. TILs after tumor digestion were stained with anti-CD45 and propidium iodide (PI) in order to gate live lymphocytes. The established gate was then plotted to identify CD8 and PD-1 cells population. **(B)** Bar graphs of CD8⁺ PD-1⁺ frequency among TILs of MC38 H-2K^d-sensitized WT mice. No statistical significance was achieved.

The specific immunity against tumor antigens is required to elicit antitumor responses

As previously shown, the H-2K^d-harboring tumor has completely protected the animals from the challenge of unmodified tumors. Next, I asked whether the retardation of tumors is also specific to tumor antigens rather than a universal effect of allogeneic H-2K^d presentation. To assess this question, I established a concomitant immunity model between MCA-205 and MC38 cell lines. In this fashion, the mice received administration of secondary tumor inoculation that was distinct from the preexistent primary tumor (*e.g.* MC38 as primary tumor and MCA-205 as secondary tumor or vice versa).

In PD-1 KO, it was previously established that the parental MC38 grew robustly (Fig. 18) but not when the mice were firstly sensitized by MC38 overexpressing H-2K^d (Fig. 27). In

contrast, the PD-1 KO that had received MCA-205 H-2K^d cells as a primary tumor was not protected against subsequent MC38 tumor challenge in the distant site (Fig. 35A), indicating that the triggered immune reaction was due to MC38-specific tumor immunity.

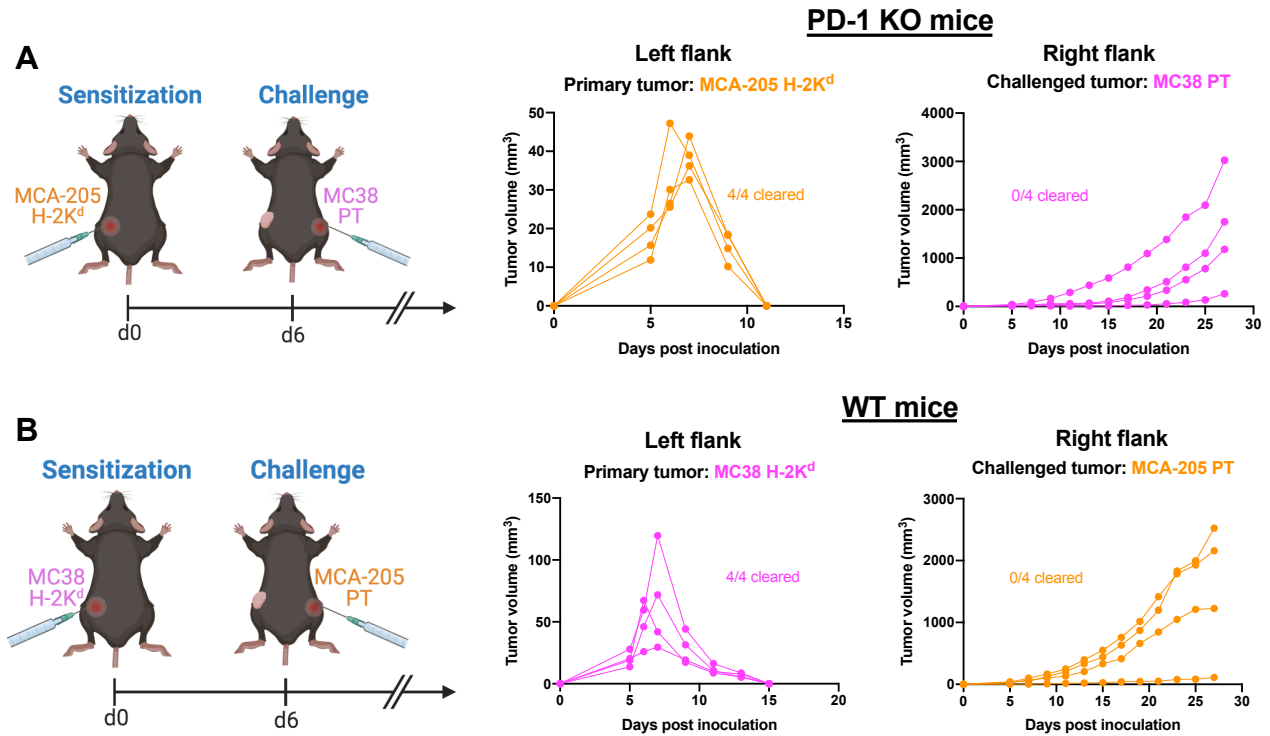


Figure 35. Individual tumor growth curves of criss-cross experiments between MC38 and MCA-205 cancer cells. **(A)** PD-1 KO mice were subcutaneously inoculated with MCA-205 H-2K^d as the primary tumor and then challenged with unmodified MC38 cells at day 6. **(B)** WT mice were injected with inoculums of MC38 H-2K^d and received a different parental line (MCA-205) as the secondary tumor. Data shown are from one experiment, n = 4 mice per group.

A similar experiment using WT mice to test the MCA-205-specific immunity was conducted. Because MCA-205 readily formed tumors in WT mice (Fig. 19), I inoculated these mice with MC38 H-2K^d tumors and sequentially challenged them with the MCA-205 parental line. As anticipated, although the immunogenic MC38 H-2K^d tumors spontaneously regressed, the inoculated mice were naïve for MCA-205-derived tumor antigens hence they could not exhibit immunity against the sarcomas (Fig. 35B). Having observed the phenomena of specific immunity, it is evident that the display of tumor-specific antigens through MHC class I is essential for successful antitumor immunity. In the context of my study, since the endogenous

MHC-I failed to be licensed by immune cells, nonetheless the cancer antigens were effectively displayed by the introduced exogenous H-2K^d thus became visible to the effector T cells.

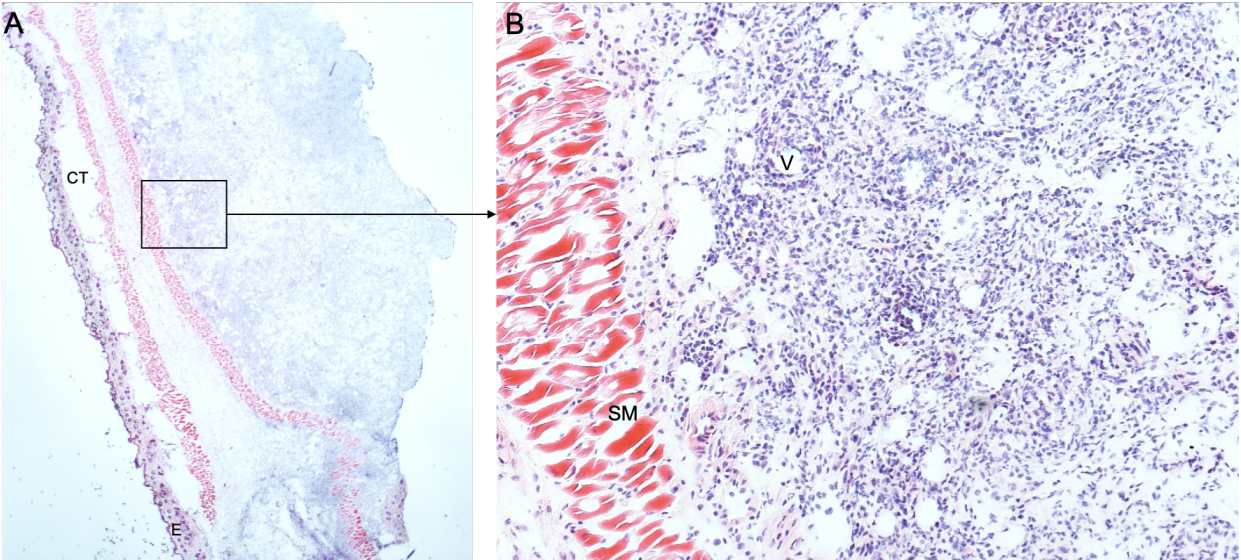
Infiltration of CD11c⁺ and CD8⁺ cells is observed in the injection sites of MC38 H-2K^d

Evaluation of infiltrating immune cells in MC38 tumors ectopically expressing H-2K^d was impractical to conduct because the tumors reached their maximum size between day 6 and 10 and spontaneously regressed thereafter (Fig. 21A and 21B). In addition, the size of palpable tumors was very small, adding constraints to isolate bulk tumors for downstream analysis. Similarly, it was impossible to locate the inoculated MC38 H-2K^d cell debris *in vivo*. Since sensitization with the debris of MC38 H-2K^d generated durable antitumor immune responses, analysis of infiltrating immune cells becomes exciting to accomplish.

To more deeply investigate the possible involvement of immune cells inside the highly immunogenic tumor microenvironment, I embedded MC38 H-2K^d tumors or their cell debris in the Matrigel basement membrane. Matrigel solidifies at body temperature, resulting in a plug that might trap the infiltrating host cells. In this study, Matrigel plugs containing MC38 H-2K^d cells (live or debris) were isolated from PD-1 KO mice on day 7 and were visualized by hematoxylin and eosin (HE) staining and immunofluorescence staining.

HE staining of Matrigel carrying live MC38 H-2K^d cells showed the massive number of nucleated cells within the plug (Fig. 36A and 36B). Possible penetration of host immune cells toward the Matrigel plug was suggested by the presence of nucleated cells nearby blood vessels at the periphery side of the plug (Fig. 36B). Furthermore, precise localization of cell debris *in vivo* after injection was made possible by embedding dead MC38 H-2K^d cells in Matrigel (Fig. 36C and 36D). Histological analysis revealed remarkably fewer nucleated cells in the MC38 H-2K^d debris-containing Matrigel plug (Fig. 36C). At day 7 after inoculation, some nucleated cells were seen trapped within the Matrigel, near to the subcutaneous tissue (Fig. 36D). This solid disparity of histological visuals between live and dead MC38 H-2K^d cells inside the Matrigel plug has validated the *de facto* situation of tumor microenvironment.

MC38 H-2K^d live



MC38 H-2K^d debris

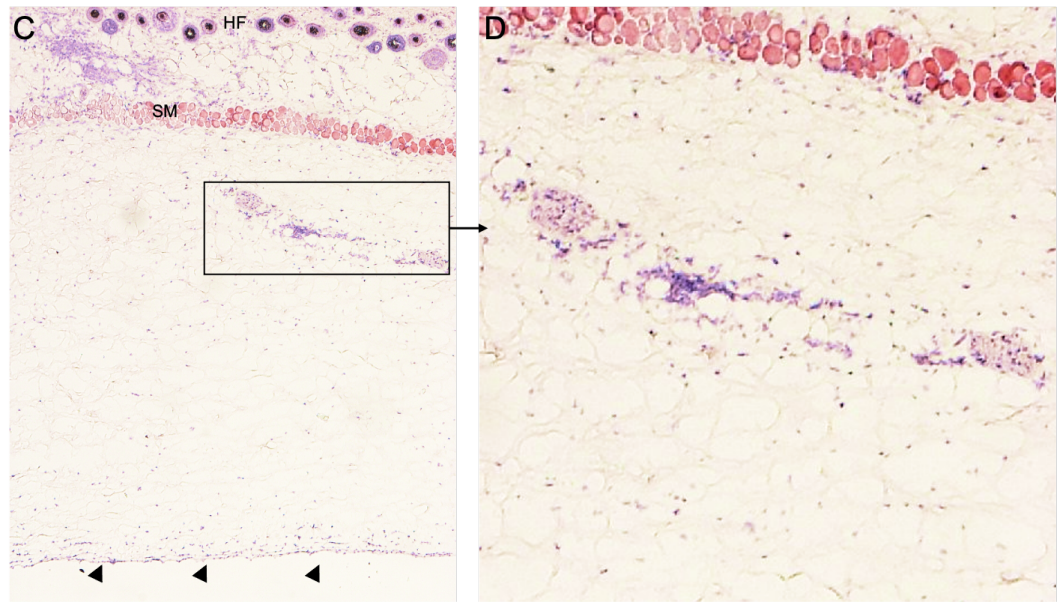


Figure 36. Representative histological images of HE-stained Matrigel plugs containing live MC38 H-2K^d cells (A and B) showing the large number of nucleated cells within the Matrigel area at 7 days after injection. (B) Higher magnification of the area in (A) shows the blood vessel and possible penetration of host cells. (C and D) Subcutaneous Matrigel plug containing MC38 H-2K^d cell debris showing the border of Matrigel plug indicated by black arrowheads (C) and a remarkably smaller number of nucleated cells within Matrigel plug (D) in comparison with that of live cells (B). CT, soft connective tissue; SM, striated muscle; E, epidermis; HF, hair follicle; V, blood vessel.

Next, in order to distinguish between tumor cell population and infiltrating host cells, the live MC38 H-2K^d cells-containing Matrigel sections were further immunostained. The nucleated cells (DAPI-stained) inside the Matrigel plug can be divided into MC38 H-2K^d tumor cells and penetrating host immune cells that were stained well with markers for cytotoxic T lymphocytes (CD8 α) and dendritic cells (CD11c) (Fig. 37A). Large numbers of CD11c⁺ and CD8⁺ host cells were seen infiltrating the Matrigel plug, of which several cells were in close contact, pinpointing the possibility of cross-presentation (Fig. 37B and 37C). Professional antigen-presenting cells (APC) such as dendritic cells have the ability to capture and to engulf tumor cells and present tumor antigens to CD8⁺ T cells, a process referred to as cross-presentation (32).

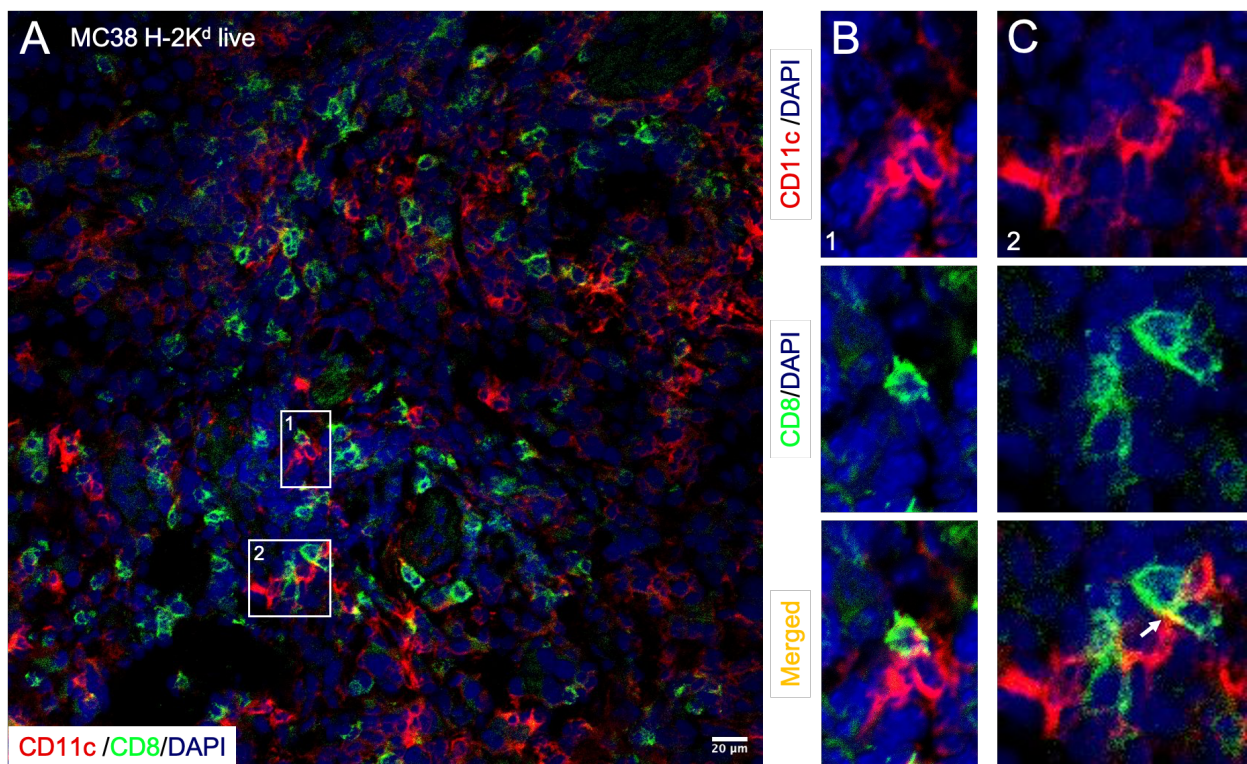


Figure 37. Infiltration of host immune cells into Matrigel plugs containing MC38 H-2K^d cells. PD-1 KO mice were injected subcutaneously in the flank with live MC38 H-2K^d cells embedded in Matrigel and plugs were isolated for immunohistochemistry 7 days after injection. (A to C) Representative images of plug sections immunostained for CD11c⁺ (dendritic cells, red) and CD8⁺ (T cells, green), and 4',6-diamidino-2-phenylindole (DAPI) (nuclei, blue). (A) Host cells expressing CD11c and CD8 are present within the Matrigel area. (B and C) Higher magnification of the area inside the region of interest marked with the white box in (A). White arrow shows possible contact between CD11c⁺ cells and CD8⁺ cells.

Last, I observed massive infiltration of CD11c⁺ cells in Matrigel plugs harboring debris of MC38 H-2K^d cells (Fig. 38A). Consistently, direct cell-cell contact between CD11c⁺ and CD8⁺ cells was also observed in Matrigel plugs containing the debris of MC38 H-2K^d cells (Fig. 38B and 38C). Apparently, the efficient uptake of tumor antigens by APC might be associated with positive anti-tumor immune responses in the sensitization (Fig. 28B-C) and the tumor rechallenge experiments (Fig. 30B-C) in this study. Therefore, the mingling of CD11c-CD8 in the tumor microenvironment might serve as an indicator for a favorable prognosis. Notably, the recruitment of host immune cells was dependent on the presence of cancer cells and not caused by the Matrigel itself since very few cells were seen infiltrating cell-free Matrigel plug (data not shown).

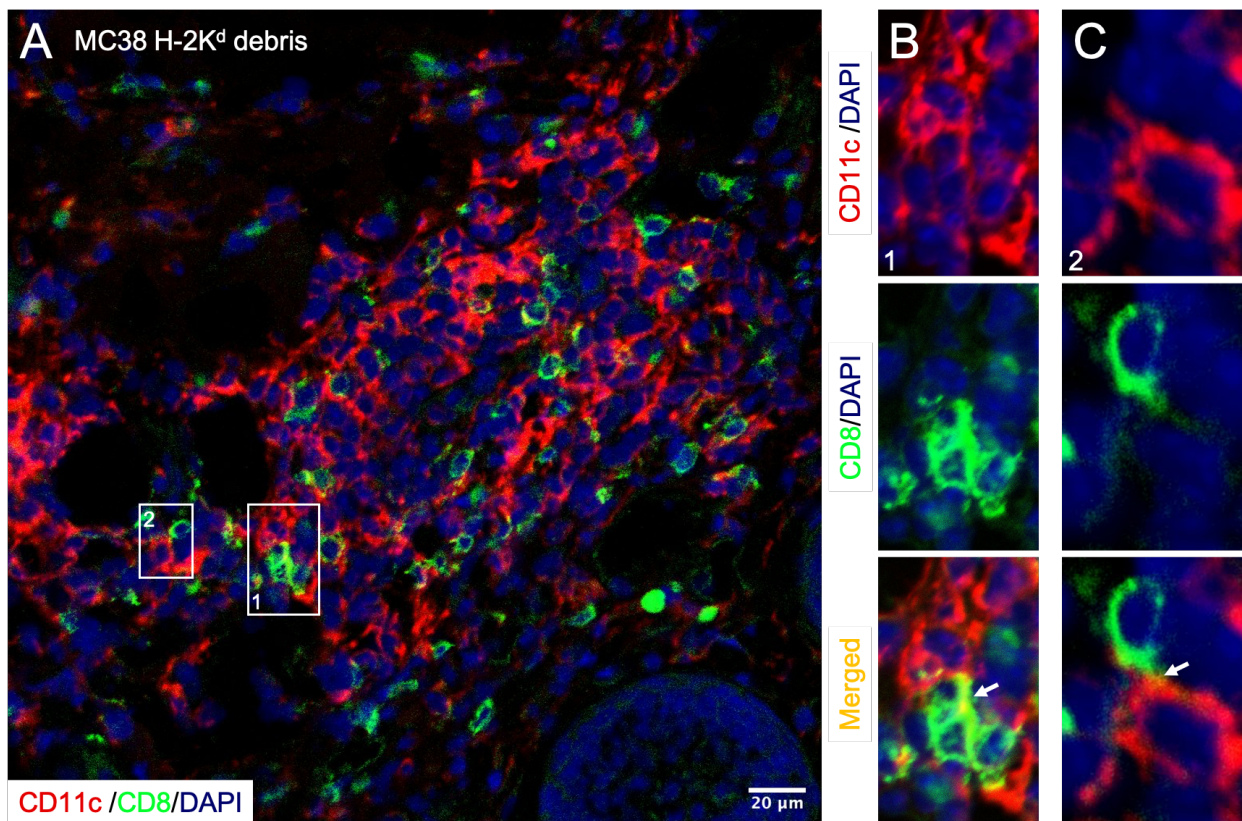


Figure 38. PD-1 KO mice were injected subcutaneously in the flank with Matrigel bearing debris of MC38 H-2K^d cells. (A to C) Representative images of plug sections at day 7 were immunostained for CD11c⁺ (dendritic cells, red) and CD8⁺ (T cells, green), and 4',6-diamidino-2-phenylindole (DAPI) (nuclei, blue). (A) Visualization of host cells infiltrating Matrigel. (B and C) Higher magnification of the area inside the region of interest marked with the white box in (A), visualizing the possibility of direct cell-cell interaction between CD11c⁺ cells and CD8⁺ cells as indicated by white arrows.

DISCUSSION

During the past few years, immune checkpoint blockade has provided remarkable outcomes to unleash the immune system against tumors. However, the majority of patients were unable to receive benefits from the PD-1 therapy (13), and some patients acquired resistance after a period of the initial response, leading to disease recurrence (9). Thus, it is indispensable to improve the success rate of PD-1 blockade in a wide variety of cancer. Furthermore, combination therapy has been widely accepted as one of the most striking strategies to overcome resistance to immunotherapy (25, 51-53). In this study, I have attempted to bolster responsiveness to PD-1 checkpoint inhibitors by exploiting exogenous murine MHC-I genes.

The downregulation of MHC-I molecules is often associated with tumor immune evasion (31, 34). Intriguingly, the presence of tumor antigen-bound MHC is evidently important to improve the efficacy of PD-1 therapy (80). Theoretically, the introduction of allogeneic MHC-I-overexpressing vectors might improve the MHC-I-restricted immune responses mediated by cytotoxic T cells (*i.e.*, direct alloantigen recognition). The expression of MHC molecules may further help to direct immune cells to the site of antigen presentation. On the other hand, to initiate an immune response, antigen-presenting cells (APCs) such as dendritic cells must display antigens through MHC. Therefore, the uptake of allogeneic MHC by APC in the host cells may help to accelerate immune response (*i.e.*, indirect alloantigen recognition). Most notably, the presentation of allogeneic MHC-I by APCs is extremely important to aid the recruitment of immune cells to the tumor sites.

Little attention has been given to the impact of tumor MHC-I expression in the studies of immune checkpoint blockade. Thus, in the present study, I have generated mouse MHC class I-encoding vectors to be further exploited and combined with the PD-1/PD-L1 blockade in cell lines and mouse models. In this study, I used the allogeneic MHC-I genes (H-2Ks) aiming to trigger the immune system and augment the tumor immunity. The mammalian expression vectors carrying MHC-I cDNAs flanked by a strong CAG promoter and poly(A) signals from the pCAGGS vector were successfully constructed (Fig. 10). The established expression vectors were well integrated into the genome of MC38 and MCA-205 cancer cells. Murine tumor models in this study could highly express their endogenous H-2K^b along with the exogenous H-2K^d as the alloantigen (Fig. 12 and Fig. 13).

Paradoxically, although both cancer cell lines used in this study expressed high amounts of endogenous H-2K^b molecules, however, the parental tumors were not rejected in tested animals. This finding emphasizes that there is a threshold required for the induction of effective anti-tumoral immunity. It has been reported that even cancer cells that are capable of efficiently expressing their neoantigens through class I MHC still failed to be recognized and killed by T cells specific for this particular tumor, pointing out the presence of non-functional tumor antigens (81) and immune escape mechanism.

While the T lymphocyte response elicited by progressive tumors is typically insufficient to achieve tumor rejection, defects have been described in several stages of the immune response in the tumor-bearing host including failure in antigen-presenting machinery (30, 31, 37, 40). Transfer of MHC-I genes into tumor cells could lead to enhancement of antigen presentation and tumor elimination. I thus attempted to evaluate the therapeutic effect of allogeneic MHC-I-expressing tumors *in vivo*. Satisfactory results were achieved by the MC38 H-2K^d and MCA-205 H-2K^d tumor models. MC38 carcinomas were previously shown to be partially resistant to the chronic absence of PD-1 (Fig. 18). Remarkably, MC38 H-2K^d-modified cancers provided full protection to both naïve PD-1 KO and WT mice, represented by spontaneous tumor regression (Fig. 21). In the MCA-205 tumor model which conferred high responsiveness to PD-1 blockade, the challenged mice were completely benefited by H-2K^d-mediated anti-tumor immunity, even without any blockade of PD-1/PD-L1 pathway (in WT mice). Notably, the expression of cell surface H-2K^d successfully converted non-responders into responders.

In contrast to the expectation of delivering both H-2K^d and H-2K^k allogeneic MHC-I to induce stronger alloimmunity against transfected cancer cells *in vivo*, this study demonstrated possible competition between the two H-2K genes which led to compromised antitumor immune response (Fig. 25B). H-2K^d class I MHC evidently elicited a more robust immune response in comparison with H-2K^k molecules (Fig. 21 and 24). The reason as to why the presence of H-2K^k appeared to be immunodominant is still inconclusive. However, these results gave a critical hint to further investigate the potency of H-2K^d-mediated immunity against cancers in the following studies.

Furthermore, in the context of concomitant tumor immunity, PD-1 KO mice were prophylactically prepared for the challenge of unresponsive parental cancer cells by administering the highly immunogenic MC38 H-2K^d inoculums. Intriguingly, all PD-1 KO mice

gained immunity against the aggressive MC38 tumor and became tumor-free (Fig. 27). This finding leads to another open question regarding in what kind of fashion the effector immune cells could recognize the allogeneic H-2K^d molecules. To test this, the sensitization experiment was elaborated into distinct approaches in which the growth-arrested and dead MC38 H-2K^d tumors were employed. The compromised MC38 H-2K^d tumors never grew in PD-1 KO mice, validating the efficacy of Mitomycin C and freeze-thaw treatment. More importantly, regardless of the cancer cells treatments prior to inoculation, I found that all tested PD-1 KO animals became immune to the challenge of original MC38 cells in the distant site (Fig. 28). Interestingly, the successful sensitization was proven to be reliant on PD-1 blockade and tumor-specific immunity (Fig. 32-35).

Consistently, I have demonstrated that the sensitization regimen elicits an efficient tumor rejection and persistent, long-lasting immunity. Specifically, the debris of MC38 H-2K^d cells was capable of providing durable anti-tumor immunity (Fig. 30A and 30B). This unanticipated yet surprising finding of optimum anti-tumor immune response mediated by allogeneic H-2K^d-containing cell debris has sparked a potential provision for immunogenic cell death. Intriguingly, this result was accomplished exclusively in the context of PD-1 blockade in combination with allogeneic H-2K^d, whereas similar treatment repeated in WT animals, or by employing MC38 PT tumors, were crestfallen (Table 3).

Table 3. Induction of tumor immunity against MC38 cells

Mouse	Sensitization	Rejection of challenged MC38 PT cells	
PD-1 KO	MC38 PT	Live cells	Yes*
		Growth-arrested cells	Yes
		Cell debris	No
	MC38 H-2K ^d	Live cells	Yes
		Growth-arrested cells	Yes
		Cell debris	Yes
WT	MC38 H-2K ^d	Live cells	No
		Growth-arrested cells	No
		Cell debris	No

*Deaths due to progressive growth of primary tumor (MC38 PT).

Rationally, findings in this study raised a possibility for the potential application of H-2K^d cell debris for immunization, especially in combination with PD-1 blockade therapy. A major advantage of using cells debris is its safety and feasibility as a tumor-targeting approach to

provide accessible immunogenic materials. Generally, there is no established common consent for how tumors from patients should be prepared as a cancer vaccine. The long interval time between the tedious processing of tumors until they are available as cancer vaccine might eventually result in decrement of vaccine efficacy as the progressively growing tumors accumulated a much higher burden (82). Allogeneic cancer vaccines may then serve as potent prophylaxis, a readily available option to administer before tumors reach a more advanced stage and become overwhelming.

Moreover, the strong immunity induced by allogeneic H-2K^d molecules in combination with global PD-1 blockade leads to spontaneous tumor rejection in the MC38 cancer cell model. This finding showcases that antitumor immune responses were activated before tumors were completely rejected. Consequently, characterization of the early immune cell infiltration becomes the next interesting point to investigate. A clever strategy to study the immunological events at the nascent tumor site was achieved by embedding the inoculated tumor cells in Matrigel. Matrigel is a soluble basement membrane that is extracted from Engelbreth-Holm-Swarm (EHS) mouse sarcoma, a tumor rich in extracellular matrix membrane proteins (laminin, collagen IV, heparan sulfate, proteoglycan, and entactin) (83). Accordingly, Matrigel represents a natural tumor microenvironment and is also permissive for host cells penetration.

In this study, the Matrigel plugs containing live MC38 H-2K^d cells were heavily infiltrated by CD11c⁺ and CD8⁺ lymphocytes. Several possibilities of intratumoral cell-cell interaction between CD11c⁺ and CD8⁺ T cells were particularly found in both live and dead MC38 H-2K^d-containing Matrigel plugs (Fig. 37-38). Tumor-associated DCs are assumed to endocytose cellular debris and transport tumor antigens to the draining lymph node where they are primed with T cells and induce T cell activation (84-87). Furthermore, cross-talk between DCs and CD8 T cells in the tumor niche and tumor-draining lymph nodes has been associated with improved efficacy of tumor-killing activity (88-90). Although this study does not rule out that other cell subsets expressing CD11c and CD8 might exist, the initial attempt by immunostaining suggested that the injection sites were massively infiltrated by cell types associated with APCs and tumor-killing T cells.

Most excitingly, my results provide compelling evidence for the potential augmentation of antitumor immune response mediated by allogeneic mouse MHC class I. Prior to the H-2K^d gene introduction, cancer models used in this study were growing robustly, leading to zero survival

rate of tumor-bearing mice. By appreciating the fact that the presence of H-2K^d alone could positively reverse the outcomes of tumor progression suggested that this approach appears to be effective. However, some limitations are worth noting. The unproved tenet of cancer treatment is that the earlier the tumor is found, particularly at the lower burden, the more likely the cancer immunotherapy is to be successful. Sensitization with the allogeneic molecule in this study preferably leaning towards the prophylactic setting. More in-depth studies will be needed to evaluate the therapeutic potential of H-2K^d cell debris in combination with anti-PD-1 antibody-mediated checkpoint blockade. Future works should therefore investigate the intricate roles of host-immune cells in recognizing and choreographing the H-2K^d-mediated immune response. Nevertheless, the empirically grounded findings in this study reveal an exciting development to enhance the benefit of PD-1 therapy.

ACKNOWLEDGEMENTS

First and foremost, I would like to convey my deepest and humble gratitude to God for blessing me and guiding me in the process of widening my horizons of knowledge.

I would like to express my profound gratitude to my supervisor, Associate Professor Yasumasa Ishida, for welcoming me into his lab and for giving me an opportunity to grow as a budding scientist. I am thankful for his continuous support, insightful advice, and constructive feedback on my research in the best possible way.

I also want to take a moment to thank the Advisory Committee members, Professor Yasumasa Bessho and Associate Professor Ayako Isotani, as well as to Professor Taro Kawai and Professor Jun-ya Kato for providing valuable feedback and helping me to see the big picture of my research.

My sincerest gratitude to Dr. Takahashi Akazawa and Dr. Yu Mizote from Osaka International Cancer Institute (OICI) for their terrific support through the stimulating scientific discussion and wonderful ideas to enhance the depth and quality of this study.

My hearty thanks to Assistant Professor Chio Oka, Assistant Professor Eishou Matsuda, and Mrs. Mayumi Ishida. I am thankful to Iida-san and Professor Yasumasa Bessho for letting me to stay at Ayameike Dormitory during my extended period of study. I greatly appreciate the faculty members at NAIST and the staff at Animal Facility who have given me support and kind assistance. I am grateful to all of those with whom I have had the pleasure to work during this project and other opportunities. Particularly, I am forever grateful to Dr. Satoko Maki for her genuine and incredible support.

Furthermore, I would like to thank the Japanese Ministry of Education, Culture, Sports, Science and Technology for providing financial support through the MEXT scholarship.

To my long-time friends, thank you for sticking by my side even though we live a few thousand miles apart. I am deeply thankful to the heartwarming people I have met here and became friends with, especially to Ila, a good friend with a heart of gold.

Last but not least, a very special gratitude to my family for believing in me, praying for me, and showering me with endless moral and emotional supports in my life, particularly during my journey as a student in a foreign country.

To my father, I hope I have made you proud. You are always in my heart.

REFERENCES

1. Ishida, Y., Agata, Y., Shibahara, K. & Honjo, T. (1992). Induced expression of PD-1, a novel member of the immunoglobulin gene superfamily, upon programmed cell death. *EMBO J* 11, 3887–95.
2. Nishimura, H., Nose, M., Hiai, H., Minato, N. & Honjo, T. (1999). Development of lupus-like autoimmune diseases by disruption of the PD-1 gene encoding an ITIM motif carrying immunoreceptor. *Immunity* 11, 141–151.
3. Jin H.T., Ahmed R., & Okazaki T. (2010). Role of PD-1 in Regulating T-Cell Immunity. In: Negative Co-Receptors and Ligands. Current Topics in Microbiology and Immunology R. Ahmed, T. Honjo T, eds. (Berlin, Heidelberg: Springer) 350, pp.17-37.
4. Dong, H., Zhu, G., Tamada, K., & Chen, L. (1999). B7-H1, a third member of the B7 family, co-stimulates T-cell proliferation and interleukin-10 secretion. *Nat Med*, 5:1365-1369.
5. Freeman, G.J., Long, A.J., Iwai, Y., Bourque, K., Chernova, T., Nishimura, H., Fitz, L.J., Malenkovich, N., Okazaki, T., Byrne, M.C. and Horton, H.F. (2000). Engagement of the PD-1 immunoinhibitory receptor by a novel B7 family member leads to negative regulation of lymphocyte activation. *J Exp Med*, 192:1027-1034.
6. Dong, H., Strome, S.E., Salomao, D.R., Tamura, H., Hirano, F., Flies, D.B., Roche, P.C., Lu, J., Zhu, G., Tamada, K. and Lennon, V.A. (2002). Tumor-associated B7-H1 promotes T-cell apoptosis: a potential mechanism of immune evasion. *Nat Med*, 8:793-800[Erratum, *Nat Med* 2002;8:1039.]
7. Topalian, S. L., Drake, C. G., & Pardoll, D. M. (2012). Targeting the PD-1/B7-H1 (PD-L1) pathway to activate anti-tumor immunity. *Curr Opin Immunol* , 24(2), 207-212.
8. Iwai, Y., Ishida, M., Tanaka, Y., Okazaki, T., Honjo, T., & Minato, N. (2002). Involvement of PD-L1 on tumor cells in the escape from host immune system and tumor immunotherapy by PD-L1 blockade. *Proc Natl Acad Sci*, 99(19), 12293-12297.
9. Sharma, P., Hu-Lieskovan, S., Wargo, J. A., & Ribas, A. (2017). Primary, adaptive, and acquired resistance to cancer immunotherapy. *Cell*, 168(4), 707-723.
10. Brahmer, J. R., Drake, C. G., Wollner, I., Powderly, J. D., Picus, J., Sharfman, W. H., Stankevich, E., Pons, A., Salay, T.M., McMiller, T.L. & Gilson, M. M. (2010). Phase I study of single-agent anti-programmed death-1 (MDX-1106) in refractory solid tumors: safety, clinical activity, pharmacodynamics, and immunologic correlates. *J Clin Onco*, 28(19), 3167.

11. Borghaei, H., Paz-Ares, L., Horn, L., Spigel, D.R., Steins, M., Ready, N.E., Chow, L.Q., Vokes, E.E., Felip, E., Holgado, E. and Barlesi, F. Borghaei, H., Paz-Ares, L., Horn, L., Spigel, D. R., Steins, M., Ready, N. E., ... & Brahmer, J. R. (2015). Nivolumab versus docetaxel in advanced nonsquamous non–small-cell lung cancer. *N. Engl J Med*, 373(17), 1627-1639.
12. Gettinger, S.N., Horn, L., Gandhi, L., Spigel, D.R., Antonia, S.J., Rizvi, N.A., Powderly, J.D., Heist, R.S., Carvajal, R.D., Jackman, D.M. and Sequist, L.V. (2015). Overall survival and long-term safety of nivolumab (anti–programmed death 1 antibody, BMS-936558, ONO-4538) in patients with previously treated advanced non–small-cell lung cancer. *J Clin Onco*, 33(18), 2004.
13. Topalian, S.L., Hodi, F.S., Brahmer, J.R., Gettinger, S.N., Smith, D.C., McDermott, D.F., Powderly, J.D., Carvajal, R.D., Sosman, J.A., Atkins, M.B. & Leming, P.D. (2012). Safety, activity, and immune correlates of anti–PD-1 antibody in cancer. *N. Engl J Med*, 366(26), 2443-2454.
14. Brahmer, J.R., Tykodi, S.S., Chow, L.Q., Hwu, W.J., Topalian, S.L., Hwu, P., Drake, C.G., Camacho, L.H., Kauh, J., Odunsi, K. and Pitot, H.C. (2012). Safety and activity of anti–PD-L1 antibody in patients with advanced cancer. *N. Engl J Med*, 366(26), 2455-2465.
15. Wolchok J. D., Kluger H., Callahan M. K., Postow M. A., Rizvi N. A., Lesokhin A. M., Segal N. H., Ariyan C. E., Gordon R. A., Reed K., Burke M. M., Caldwell A., Kronenberg S. A., Agunwamba B. U., Zhang X., Lowy I., Inzunza H. D., Feely W., Horak C. E., Hong Q., Korman A. J., Wigginton J. M., Gupta A., Sznol M. (2013). Nivolumab plus ipilimumab in advanced melanoma. *N. Engl J Med*. 369, 122–133
16. Robert C., Ribas A., Wolchok J. D., Hodi F. S., Hamid O., Kefford R., Weber J. S., Joshua A. M., Hwu W. J., Gangadhar T. C., Patnaik A., Dronca R., Zarour H., Joseph R. W., Boasberg P., Chmielowski B., Mateus C., Postow M. A., Gergich K., Elassaiss-Schaap J., Li X. N., Iannone R., Ebbinghaus S. W., Kang S. P., Daud A. (2014). Anti-programmed-death-receptor-1 treatment with pembrolizumab in ipilimumab-refractory advanced melanoma: A randomised dose-comparison cohort of a phase 1 trial. *Lancet*, 384, 1109–1117.
17. Powles T., Eder J. P., Fine G. D., Braiteh F. S., Loriaut Y., Cruz C., Bellmunt J., Burris H. A., Petrylak D. P., Teng S. L., Shen X., Boyd Z., Hegde P. S., Chen D. S., Vogelzang N. J.

- (2014). MPDL3280A (anti-PD-L1) treatment leads to clinical activity in metastatic bladder cancer. *Nature* 515, 558–562.
18. Ansell S. M., Lesokhin A. M., Borrello I., Halwani A., Scott E. C., Gutierrez M., Schuster S. J., Millenson M. M., Cattry D., Freeman G. J., Rodig S. J., Chapuy B., Ligon A. H., Zhu L., Grosso J. F., Kim S. Y., Timmerman J. M., Shipp M. A., Armand P. (2015). PD-1 blockade with nivolumab in relapsed or refractory Hodgkin's lymphoma. *N. Engl J Med.* 372, 311–319.
 19. Garon, E. B., Gandhi, L., Rizvi, N., Hui, R., Balmanoukian, A. S., Patnaik, A., ... & Leighl, N. (2014). Anti-tumor activity of pembrolizumab (Pembro; MK-3475) and correlation with programmed death ligand 1 (PD-L1) expression in a pooled analysis of patients (pts) with advanced non-small cell lung carcinoma (NSCLC). *Ann Oncol.* 25, LBA43.
 20. Chow, L. Q. M., Haddad, R., Gupta, S., Mahipal, A., Mehra, R., Tahara, M., et al. (2016). Antitumor activity of pembrolizumab in biomarker-unselected patients with recurrent and/or metastatic head and neck squamous cell carcinoma: results from the phase Ib KEYNOTE-012 expansion cohort. *J. Clin. Oncol.* 34, 3838–3845.
 21. Chung, H. C., Ros, W., Delord, J. P., Perets, R., Italiano, A., Shapira-Frommer, R., et al. (2019). Efficacy and safety of pembrolizumab in previously treated advanced cervical cancer: results from the phase II KEYNOTE-158 study. *J. Clin. Oncol.* 37, 1470–1478.
 22. Carbone, D. P., Reck, M., Paz-Ares, L., Creelan, B., Horn, L., Steins, M., et al. (2017). First-line nivolumab in stage IV or recurrent non-small-cell lung cancer. *N. Engl. J. Med.* 376, 2415–2426.
 23. Bellmunt, J., de Wit, R., Vaughn, D. J., Fradet, Y., Lee, J. L., Fong, L., et al. (2017). Pembrolizumab as second-line therapy for advanced urothelial carcinoma. *N. Engl. J. Med.* 376, 1015–1026.
 24. McDermott, D., Lebbé, C., Hodi, F. S., Maio, M., Weber, J. S., Wolchok, J. D., Thompson, J.A. & Balch, C. M. (2014). Durable benefit and the potential for long-term survival with immunotherapy in advanced melanoma. *Cancer Treat Rev*, 40(9), 1056-1064.
 25. Patel, S. A., & Minn, A. J. (2018). Combination cancer therapy with immune checkpoint blockade: mechanisms and strategies. *Immunity*, 48(3), 417-433.

26. Sharma, P., Wagner, K., Wolchok, J. D., & Allison, J. P. (2011). Novel cancer immunotherapy agents with survival benefit: recent successes and next steps. *Nature Reviews Cancer*, 11(11), 805-812.
27. Dunn, G. P., Bruce, A. T., Ikeda, H., Old, L. J., & Schreiber, R. D. (2002). Cancer immunoediting: from immunosurveillance to tumor escape. *Nature immunology*, 3(11), 991–998.
28. Schreiber, R. D., Old, L. J., & Smyth, M. J. (2011). Cancer immunoediting: integrating immunity's roles in cancer suppression and promotion. *Science*, 331(6024), 1565-1570.
29. Zaretsky, J. M., Garcia-Diaz, A., Shin, D. S., Escuin-Ordinas, H., Hugo, W., Hu-Lieskovan, S., Torrejon, D.Y., Abril-Rodriguez, G., Sandoval, S., Barthly, L. & Saco, J. (2016). Mutations associated with acquired resistance to PD-1 blockade in melanoma. *N Engl J Med*, 375(9), 819-829.
30. Šmahel, M. (2017). PD-1/PD-L1 blockade therapy for tumors with downregulated MHC class I expression. *Int J Mol Sci*, 18(6), 1331.
31. Garrido, F., Aptsiauri, N., Doorduijn, E. M., Lora, A. M. G., & van Hall, T. (2016). The urgent need to recover MHC class I in cancers for effective immunotherapy. *Curr Opin Immunol*, 39, 44-51.
32. Abbas, A. K., Lichtman, A. H., & Pillai, S. (2014). Cellular and Molecular Immunology 8th Edition. (Philadelphia: Elsevier Saunders).
33. Hatina, J. (2008). Major Histocompatibility Complex Genes: Mouse H². *eLS*.
34. Leone, P., Shin, E. C., Perosa, F., Vacca, A., Dammacco, F., & Racanelli, V. (2013). MHC class I antigen processing and presenting machinery: organization, function, and defects in tumor cells. *J Natl Cancer Inst*, 105(16), 1172-1187.
35. Neefjes, J., Jongmsa, M. L., Paul, P., & Bakke, O. (2011). Towards a systems understanding of MHC class I and MHC class II antigen presentation. *Nat Rev Immunol*, 11(12), 823-836.
36. Rock, K. L., Reits, E., & Neefjes, J. (2016). Present yourself! By MHC class I and MHC class II molecules. *Trends in immunology*, 37(11), 724-737.
37. Dhatchinamoorthy, K., Colbert, J. D., & Rock, K. L. (2021). Cancer Immune Evasion Through Loss of MHC Class I Antigen Presentation. *Front. Immunol.*, 12, 469.
38. Nabel, G. J., Gordon, D., Bishop, D. K., Nickoloff, B. J., Yang, Z. Y., Aruga, A., Cameron, M.J., Nabel, E.G. & Chang, A. E. (1996). Immune response in human melanoma after

- transfer of an allogeneic class I major histocompatibility complex gene with DNA–liposome complexes. *Proc Natl Acad Sci*, 93(26), 15388-15393.
39. Curti, A., Parenza, M., & Colombo, M. P. (2003). Autologous and MHC class I–negative allogeneic tumor cells secreting IL-12 together cure disseminated A20 lymphoma. *Blood*, 101(2), 568-575.
 40. Gettinger, S., Choi, J., Hastings, K., Truini, A., Datar, I., Sowell, R., ... & Politi, K. (2017). Impaired HLA class I antigen processing and presentation as a mechanism of acquired resistance to immune checkpoint inhibitors in lung cancer. *Cancer discovery*, 7(12), 1420-1435.
 41. Lim, Y. S., Kang, B. Y., Kim, E. J., Kim, S. H., Hwang, S. Y., & Kim, T. S. (1998). Augmentation of therapeutic antitumor immunity by B16F10 melanoma cells transfected by interferon-gamma and allogeneic MHC class I cDNAs. *Mol Cells*, 8(5), 629-636.
 42. Lindahl, K. F., & Wilson, D. B. (1977). Histocompatibility antigen-activated cytotoxic T lymphocytes. II. Estimates of the frequency and specificity of precursors. *J Exp Med*, 145(3), 508-522.
 43. Felix, N. J., & Allen, P. M. (2007). Specificity of T-cell alloreactivity. *Nat Rev Immunol*, 7(12), nri2200.
 44. Mumberg, D., Monach, P. A., Wanderling, S., Philip, M., Toledano, A. Y., Schreiber, R. D., & Schreiber, H. (1999). CD4+ T cells eliminate MHC class II-negative cancer cells in vivo by indirect effects of IFN- γ . *Proc Natl Acad Sci*, 96(15), 8633-8638.
 45. Alspach, E., Lussier, D.M., Miceli, A.P., Kizhvatov, I., DuPage, M., Luoma, A.M., Meng, W., Lichti, C.F., Esaulova, E., Vomund, A.N. and Runci, D. (2019). MHC-II neoantigens shape tumour immunity and response to immunotherapy. *Nature*, 574(7780), pp.696-701.
 46. Dobrzanski, M. J. (2013). Expanding roles for CD4 T cells and their subpopulations in tumor immunity and therapy. *Frontiers in oncology*, 3, 63.
 47. Tran, E., Turcotte, S., Gros, A., Robbins, P.F., Lu, Y.C., Dudley, M.E., Wunderlich, J.R., Somerville, R.P., Hogan, K., Hinrichs, C.S. and Parkhurst, M.R. (2014). Cancer immunotherapy based on mutation-specific CD4⁺ T cells in a patient with epithelial cancer. *Science*, 344(6184), pp.641-645.
 48. Accogli, T., Bruchard, M., & Végran, F. (2021). Modulation of CD4 T Cell Response According to Tumor Cytokine Microenvironment. *Cancers*, 13(3), 373.

49. Tay, R.E., Richardson, E.K. and Toh, H.C. (2021). Revisiting the role of CD4⁺ T cells in cancer immunotherapy—new insights into old paradigms. *Cancer Gene Therapy*, 28(1), pp.5-17.
50. Bos, R., & Sherman, L. A. (2010). CD4⁺ T-cell help in the tumor milieu is required for recruitment and cytolytic function of CD8⁺ T lymphocytes. *Cancer research*, 70(21), 8368-8377.
51. Chowdhury, P. S., Chamoto, K., & Honjo, T. (2018). Combination therapy strategies for improving PD-1 blockade efficacy: a new era in cancer immunotherapy. *Intern Med J*, 283(2), 110-120.
52. Page, D.B., Bear, H., Prabhakaran, S., Gatti-Mays, M.E., Thomas, A., Cobain, E., McArthur, H., Balko, J.M., Gameiro, S.R., Nanda, R. and Gulley, J.L. (2019). Two may be better than one: PD-1/PD-L1 blockade combination approaches in metastatic breast cancer. *NPJ breast cancer*, 5(1), pp.1-9.
53. Zhang, J. Y., Yan, Y. Y., Li, J. J., Adhikari, R., & Fu, L. W. (2020). PD-1/PD-L1 based combinational cancer therapy: Icing on the cake. *Frontiers in Pharmacology*, 11, 722.
54. Park, S.S., Dong, H., Liu, X., Harrington, S.M., Krco, C.J., Grams, M.P., Mansfield, A.S., Furutani, K.M., Olivier, K.R. and Kwon, E.D. (2015). PD-1 restrains radiotherapy-induced abscopal effect. *Cancer immunology research*, 3(6), pp.610-619.
55. Brix, N., Tiefenthaller, A., Anders, H., Belka, C. and Lauber, K. (2017). Abscopal, immunological effects of radiotherapy: narrowing the gap between clinical and preclinical experiences. *Immunological reviews*, 280(1), pp.249-279.
56. Kordbacheh, T., Honeychurch, J., Blackhall, F., Faivre-Finn, C., & Illidge, T. (2018). Radiotherapy and anti-PD-1/PD-L1 combinations in lung cancer: building better translational research platforms. *Annals of Oncology*, 29(2), 301-310.
57. Buchwald, Z.S., Wynne, J., Nasti, T.H., Zhu, S., Mourad, W.F., Yan, W., Gupta, S., Khleif, S.N. and Khan, M.K., 2018. Radiation, immune checkpoint blockade and the abscopal effect: a critical review on timing, dose and fractionation. *Frontiers in oncology*, 8, p.612.
58. Hlavata, Z., Solinas, C., De Silva, P., Porcu, M., Saba, L., Willard-Gallo, K., & Scartozzi, M. (2018). The abscopal effect in the era of cancer immunotherapy: a spontaneous synergism boosting anti-tumor immunity? *Target Oncol*, 1-11.

59. Ngwa, W., Irabor, O. C., Schoenfeld, J. D., Hesser, J., Demaria, S., & Formenti, S. C. (2018). Using immunotherapy to boost the abscopal effect. *Nature Reviews Cancer*, *18*(5), 313-322.
60. Rodríguez-Ruiz, M. E., Vanpouille-Box, C., Melero, I., Formenti, S. C., & Demaria, S. (2018). Immunological mechanisms responsible for radiation-induced abscopal effect. *Trends in immunology*, *39*(8), 644-655.
61. Niwa, H., Yamamura, K. and Miyazaki, J., (1991). Efficient selection for high-expression transformants with a novel eukaryotic vector. *Gene*, *108*, 193–199.
62. Klenow, H., & Henningsen, I. (1970). Selective Elimination of the Exonuclease Activity of the Deoxyribonucleic Acid Polymerase from *Escherichia coli* B by Limited Proteolysis. *Proc Natl Acad Sci USA*, *65*(1), 168–175.
63. Szymczak-Workman, A. L., K. M. Vignali, and D. A. Vignali. (2012). Design and construction of 2A peptide-linked multicistronic vectors. *Cold Spring Harb. Protoc.* (2): 199–204.
64. Kim, J. H., Lee, S. R., Li, L. H., Park, H. J., Park, J. H., Lee, K. Y., Kim, M.K., Shin, B.A. & Choi, S. Y. (2011). High cleavage efficiency of a 2A peptide derived from porcine teschovirus-1 in human cell lines, zebrafish and mice. *PloS one*, *6*(4), e18556.
65. Arber, C., Abhyankar, H., Heslop, H. E., Brenner, M. K., Liu, H., Dotti, G., & Savoldo, B. (2013). The immunogenicity of virus-derived 2A sequences in immunocompetent individuals. *Gene Ther*, *20*(9), 958.
66. Juneja, V. R., McGuire, K. A., Manguso, R. T., LaFleur, M. W., Collins, N., Haining, W. N., ... & Sharpe, A. H. (2017). PD-L1 on tumor cells is sufficient for immune evasion in immunogenic tumors and inhibits CD8 T cell cytotoxicity. *J. Exp. Med.*, *214*(4), 895-904.
67. van den Elsen, P. J., Holling, T. M., van der Stoep, N., & Boss, J. M. (2003). DNA methylation and expression of major histocompatibility complex class I and class II transactivator genes in human developmental tumor cells and in T cell malignancies. *Clinical Immunology*, *109*(1), 46-52.
68. Lau, J., Cheung, J., Navarro, A., Lianoglou, S., Haley, B., Totpal, K., ... & Schmidt, M. (2017). Tumour and host cell PD-L1 is required to mediate suppression of anti-tumour immunity in mice. *Nat. Commun.* *8*(1), 1-11.

69. Ngiow, S.F., Young, A., Jacquelot, N., Yamazaki, T., Enot, D., Zitvogel, L. and Smyth, M.J., 2015. A threshold level of intratumor CD8+ T-cell PD1 expression dictates therapeutic response to anti-PD1. *Cancer research*, 75(18), pp.3800-3811.
70. Grasselly, C., Denis, M., Bourguignon, A., Talhi, N., Mathe, D., Tourette, A., Serre, L., Jordheim, L.P., Matera, E.L. and Dumontet, C. (2018). The antitumor activity of combinations of cytotoxic chemotherapy and immune checkpoint inhibitors is model-dependent. *Frontiers in immunology*, 9, p.2100.
71. Hossain, D.M.S., Javaid, S., Cai, M., Zhang, C., Sawant, A., Hinton, M., Sathe, M., Grein, J., Blumenschein, W., Pinheiro, E.M. and Chackerian, A. (2018). Dinaciclib induces immunogenic cell death and enhances anti-PD1-mediated tumor suppression. *The Journal of clinical investigation*, 128(2), pp.644-654.
72. Moreno, B.H., Zaretsky, J.M., Garcia-Diaz, A., Tsoi, J., Parisi, G., Robert, L., Meeth, K., Ndoye, A., Bosenberg, M., Weeraratna, A.T. and Graeber, T.G., 2016. Response to programmed cell death-1 blockade in a murine melanoma syngeneic model requires costimulation, CD4, and CD8 T cells. *Cancer immunology research*, 4(10), pp.845-857.
73. Kumar, A., Chamoto, K., Chowdhury, P. S., & Honjo, T. (2020). Tumors attenuating the mitochondrial activity in T cells escape from PD-1 blockade therapy. *Elife*, 9, e52330.
74. Anisimov, V. N., Zabezhinski, M. A., Rossolini, G., Zaia, A., Piantanelli, A., Basso, A., & Piantanelli, L. (2001). Long-live euthymic BALB/c-nu mice. II: spontaneous tumors and other pathologies. *Mechanisms of ageing and development*, 122(5), 477-489.
75. Tourdot, S., & Gould, K. G. (2002). Competition between MHC class I alleles for cell surface expression alters CTL responses to influenza A virus. *J Immunol*, 169(10), 5615-5621.
76. Doherty, P. C., Biddison, W. E., Bennink, J. R., & Knowles, B. B. (1978). Cytotoxic T-cell responses in mice infected with influenza and vaccinia viruses vary in magnitude with H-2 genotype. *J. Exp. Med.*, 148(2), 534-543.
77. Bashford, E., J. Murray, and M. Haaland. (1908). Resistance and susceptibility to inoculated cancer. In Third Scientific Report on the Investigations of the Imperial Cancer Research Fund. E. Bashford, ed. Taylor & Francis, London, U.K., p. 359.

78. Kansy, B. A., Concha-Benavente, F., Srivastava, R. M., Jie, H. B., Shayan, G., Lei, Y., ... & Ferris, R. L. (2017). PD-1 status in CD8⁺ T cells associates with survival and anti-PD-1 therapeutic outcomes in head and neck cancer. *Cancer research*, 77(22), 6353-6364.
79. Kumagai, S., Togashi, Y., Kamada, T., Sugiyama, E., Nishinakamura, H., Takeuchi, Y., ... & Nishikawa, H. (2020). The PD-1 expression balance between effector and regulatory T cells predicts the clinical efficacy of PD-1 blockade therapies. *Nature Immunology*, 21(11), 1346-1358.
80. Inoue, H., Park, J.H., Kiyotani, K., Zewde, M., Miyashita, A., Jinnin, M., Kiniwa, Y., Okuyama, R., Tanaka, R., Fujisawa, Y. & Kato, H. (2016). Intratumoral expression levels of PD-L1, GZMA, and HLA-A along with oligoclonal T cell expansion associate with response to nivolumab in metastatic melanoma. *Oncoimmunology*, 5(9), e1204507.
81. Vormehr, M., Reinhard, K., Blatnik, R., Josef, K., Beck, J. D., Salomon, N., ... & Sahin, U. (2019). A non-functional neoepitope specific CD8⁺ T-cell response induced by tumor derived antigen exposure in vivo. *Oncoimmunology*, 8(3), 1553478.
82. Sondak, V. K., Sabel, M. S., & Mule, J. J. (2006). Allogeneic and autologous melanoma vaccines: where have we been and where are we going?. *Clinical cancer research*, 12(7), 2337s-2341s.
83. Kleinman, H. K., & Martin, G. R. (2005). Matrigel: basement membrane matrix with biological activity. In *Seminars in cancer biology* (Vol. 15, No. 5, pp. 378-386). Academic Press.
84. Plautz, G. E., Mukai, S., Cohen, P. A., & Shu, S. (2000). Cross-presentation of tumor antigens to effector T cells is sufficient to mediate effective immunotherapy of established intracranial tumors. *J Immunol*, 165(7), 3656-3662.
85. Gardner, A., & Ruffell, B. (2016). Dendritic cells and cancer immunity. *Trends in immunology*, 37(12), 855-865.
86. Fu, C., & Jiang, A. (2018). Dendritic cells and CD8 T cell immunity in tumor microenvironment. *Frontiers in immunology*, 9, 3059
87. Böttcher, J. P., & e Sousa, C. R. (2018). The role of type 1 conventional dendritic cells in cancer immunity. *Trends in cancer*, 4(11), 784-792.

88. Ferris, S. T., Durai, V., Wu, R., Theisen, D. J., Ward, J. P., Bern, M. D., ... & Murphy, K. M. (2020). cDC1 prime and are licensed by CD4⁺ T cells to induce anti-tumour immunity. *Nature*, *584*(7822), 624-629.
89. Fu, C., Peng, P., Loschko, J., Feng, L., Pham, P., Cui, W., ... & Jiang, A. (2020). Plasmacytoid dendritic cells cross-prime naive CD8 T cells by transferring antigen to conventional dendritic cells through exosomes. *Proceedings of the National Academy of Sciences*, *117*(38), 23730-23741.
90. Su, Y., Tsagkozis, P., Papakonstantinou, A., Tobin, N.P., Gultekin, O., Malmerfelt, A., Ingelshed, K., Neo, S.Y., Lundquist, J., Chaabane, W. and Nisancioglu, M.H. (2021). CD11c-CD8 Spatial Cross Presentation: A Novel Approach to Link Immune Surveillance and Patient Survival in Soft Tissue Sarcoma. *Cancers*, *13*(5), p.1175.